Compliments of the Editor

Physics

SCIENCE OF LIGHT

VOLUME 3 NUMBER 2

March
1955

OHIO STATE
UNIVERSITY
NOV 17 1955
LIBRARY

Gole Memorial Library

Published by the

Institute for Optical Research

Tokyo University of Education

in collaboration with the

Spectroscopical Society of Japan

SCIENCE OF LIGHT

Science of Light contains reports of the Institute for Optical Research and contributions from other science bodies about similar subject.

The editorial staff consists of following members:

Chairman: Prof. Y. Fujioka, *Tokyo University of Education*

Prof. E. Minami, *Tokyo University*

Prof. H. Ootsuka, *Tokyo University of Education*

Prof. M. Seya, *Tokyo University of Education*

Prof. Y. Uchida, *Kyoto University*

Prof. T. Uemura, *Rikkyo University*

All communications should be addressed to the director or to the librarian of the Institute.

The Institute for Optical Research

Tokyo University of Education

400, 4-chome, Hyakunin-machi, Sinjuku-ku, Tokyo, Japan

Printed by
Kokusai Bunken Insatsusha
Chiyoda-ku, Tokyo.

Ruling of a Curved Grating

Yoshimi SAKAYANAGI
Institute for Optical Research, Tokyo University of Education

(Received Dec. 6, 1954)

The writer has recently developed a theory of curved grating[1]. According to this theory the curved grating has the peculiarity stigmatic points appear on the Rowland circle for particular angles of incidence and diffraction. In the present paper a method actually ruling this curved grating and results of its use are described.

1. Introduction

The concave grating which was first constructed by Rowland has the remarkable property of self-focusing, but it also has the defect of large astigmatism. As it was pointed out in the writer's previous paper[1], it is possible to eliminate this defect by means of ruling arc-shaped grooves upon a pherical concave mirror. The outline of the theory is as follows:

Fig. 1 shows the proposed shape of the grooves. ρ_0 is the radius of curvature of the grooves, and the relation between this groove circle and the Rowland circle is shown in Fig. 2. The line joining O′ and O intersects the Rowland

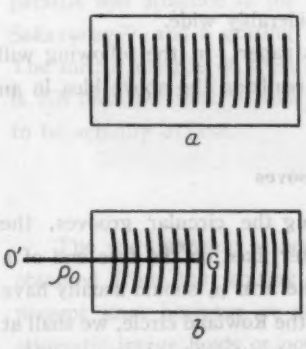

Fig. 1. Shape of the curved grooves, (a) equal curvature (b) concenric circle.

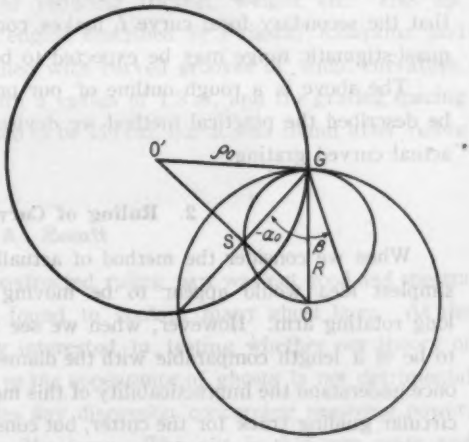

Fig. 2. Geometrical relation between the Rowland circle and the center of the curved groove.

1) Y. Sakayanagi. Science of Light, **3** (1954) 1.

Poole Memorial Library

circle at S. The circlar arc-shaped grooves are ruled on a spherical surface and S comes to be the center of the arcs in 3-dimentional space. The angle of incidence is designated by $-\alpha_0$. The light entering from S makes a vertical focus along the line SO forming a secondary focal line. At the points of intersection of this secondary focal line with the Rowland circle, i.e. S and O, the focus becomes stigmatic.

If we move slit from S to M. i.e. if the angle of incidence changes to $-(\alpha_0+\Delta)$, the secondary focal curve moves along with it. (Fig. 3)

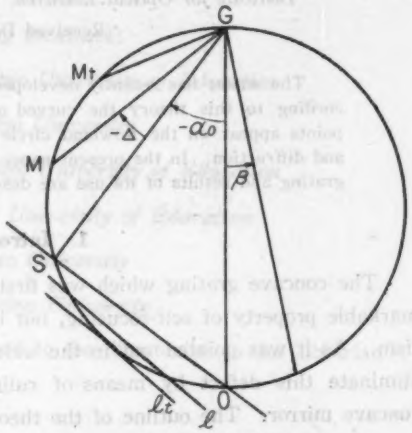

Fig. 3. Relation between angles of incidence and secondary focal curves.

This secondary focal curve is expressed by the formula

$$\frac{r_0}{R\cos\alpha_0} = \frac{1}{\cos(\alpha_0+\beta)-\tan(\alpha_0+\Delta)\sin\Delta}$$

At the points where this curve intersects the Rowland circle, the images are stigmatic and in the vicinity of these points the astigmatism is naturally very small. If the point M is so chosen that the secondary focal curve l_i makes contact with the Rowland circle, the quasi-stigmatic range may be expected to be considerably wide.

The above is a rough outline of our previous paper. In the following will be described the practical method we devised for realizing the above idea in an actual curved grating.

2. Ruling of Curved grooves

When we consider the method of actually ruling the circular grooves, the simplest idea would appear to be moving a cutter fixed on the free end of a long rotating arm. However, when we see that the arm ρ_0 should usually have to be of a length comparable with the diameter of the Rowland circle, we shall at once understand the impracticability of this method. Another idea is to provide a circular guiding track for the cutter, but considerations of the demanded accuracy rule out the consideration of such an apparatus as anything easy to attain.

The method we have adopted is based on the idea shown in Fig. 4. AB is the line of the fixed and slightly inclined axis around which free rotation is provided for the square-shaped main frame. Along the line EF of this main

frame are the pivot points holding the triangular horizontal device shown in the figure, which holds at its apex the cutter D for ruling the grating. The power for operating the cutter is applied to EF to move D back and forth. The

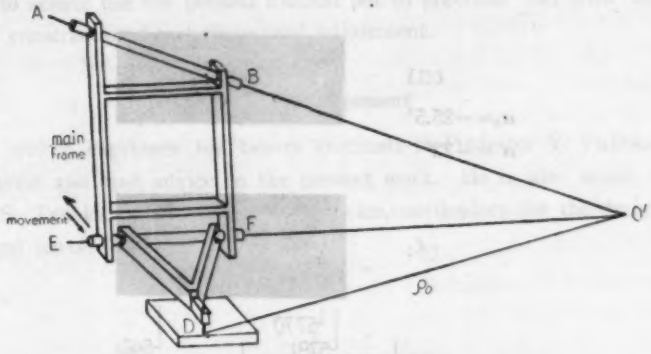

Fig. 4. Ruling device for the curved grooves.

arrangement is so designed as to have the lines AB and EF intersect each other at the point O'. Simple solid geometry will prove that the movement of D will be confined to a spherical surface with the radius ρ_0.

The above is a very schematized description of the principle of the design adopted in the present work. In the actual construction many supplementary devices were used for the purpose of reducing friction, weight etc. This apparatus was attached to the ruling engine described by Fujioka, Kitayama and Sakayanagi[2], and a grating was ruled with curved grooves of equal curvature. The mirror used is of speculum with a radius of 1.5 m, and the grating spacing is 576 lines per mm. ρ_0 was intended to be 150 cm, but it was found after ruling to be actually 315 cm.

3. Result

The workmanship of newly constructed ruling part was not good and spectra obtained from the grating were found to contain many ghost lines. At the present stage however we are only interested in testing whether our theory of stigmatic image holds or not, and so the appearance of ghosts is not detrimental for our purpose, though it precludes any discussion concerning resolving power. Figs. 5 and 6 show results with a Hg lamp. The slit is 0.05 mm wide and 1 mm long.

In both figures (a) shows the spectrum taken with the present curved

2) Y. Fujioka, T. Kitayama, Y. Sakayanagi, Science of Light, **2** (1952) 1.

grating and (b) that taken with the usual concave grating with the same curvature and spacing mounted in the same position as (a). Fig. 5 is mounted for the green region with $\alpha=-22°$ and Fig. 6 for the violet region (2nd) with $\alpha=-26.5°$.

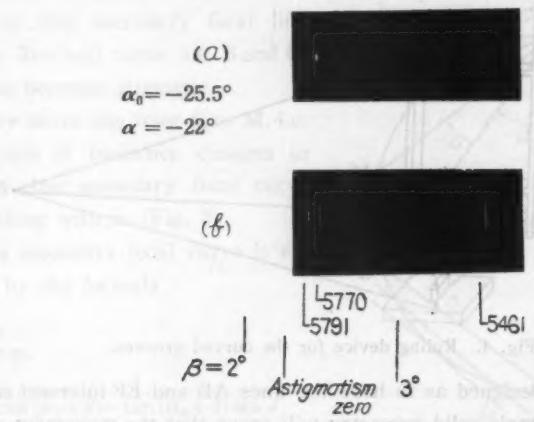

Fig. 5. Spectrum of Hg lamp (1st order) (a) curved grating (b) concave grating.

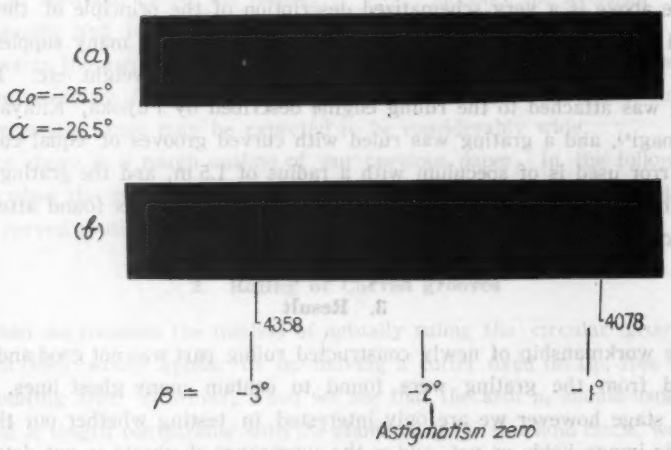

Fig. 6. Spectrum of Hg lamp (2nd order) (a) curved grating (b) concave grating.

In both cases we cannot detect any appreciable astigmatism of the image in the (a) picture apart from the natural elongation due to the difference of distance from the grating to the slit and that to the image. Astigmatic elongation is clearly manifested in the pictures (b) shown for comparison. The anticipation

we held for our grating with respect to stigmatism has been amply proved. It is only too regrettable that the presence of strong ghost prevents any further enlargement of the pictures without risk of spoiling them. The writer is looking forward to seeing use the present method put to practical use, with the application of constractional techniques and adjustment.

Acknowledgement

The writer expresses his hearty gratitude to Professor Y. Fujioka for his deep interest and kind advice on the present work. He is also much indebted to Mr. S. Tanaka for his very useful advice, particulary for the design of the mechanical parts.

A Near Infrared Spectrometer Using a Plane Grating

Yoshimi SAKAYANAGI and Yoshiki SATÔ

Institute for Optical Research, Tokyo University of Education

(Received October 6, 1954)

A near infrared grating spectrometer based on the Littrow mounting is described, in which a PbS cell is used as the detector. The grating has 576 lines/mm and the focal length of the collimating mirror is 60 cm. The amplifier is constructed on the basis of the principle of Wilson's feed-back, with a total gain of 120 db, and the band-width variable from 100 to 5 cps. The source for the synchronous motor for rotating the chopper is supplied by the output of an RC-oscillator.

1. Introduction

In recent years, spectroscopy is playing an important part in the study of molecular structures in the near infrared region. This may be attributed to the fact that the PbS photoconductive cell has excellent qualities as detector for use in this region, which has rendered possible the construction, in combination with plane gratings, of spectrometers with great resolving power. We have studied the design of a near infrared prism spectrometer with a Littrow autocollimating system and featuring the PbS cell. In addition, we have constructed an apparatus based on the Littrow mounting in which a plane grating has been used instead of the prism. We are at present employing this instrument for the study of the molecular structure with good results. In this paper, we shall describe the optical and electrical systems constituting the device and present some of the results obtained.

2. The Optical System

Fig. 1 is the schematic diagram of the optical arrangement used. After passing through the filter F and the chopper C, light from the source L focuses onto the entrance slit S_1, situated on the focal plane of the collimating mirror M_1; upon which it proceeds as a parallel ray into the plane grating PG; the diffracted light then focuses upon the exit slit S_2 after falling on M_1M_2; and from S_2 the ray passes onto M_3M_4 and strikes the receiving area of the detector D.

Generally speaking, the source of radiation should possess the following characters;

1. high brightness,
2. intensity distribution analogous to black body radiation,
3. small fluctuation of radiating power.

Moreover, in the near infrared region even a small fluctuation of the temperature of the source causes a great change in its brightness; accordingly a 100 watt projection lamp was used and lighted by a fixed battery. The character of the glass transmission filter has properties similar to that of the Corning #2540, but is of obscure date of manufacture. M_1 and M_4, both concave spherical mirrors, have 60 cm and 12 cm, respectively and diameters respectively about 13 cm and 12 cm. Both M_2 and M_3 are small plane mirrors. All four mirrors were vacuum aluminized on the surface. The grating is ruled with lines 3 cm long for a width of 5 cm with a spacing of 576 lines/mm, and its reflecting power is a little over 20 percent in the first order. The driving mechanism for the grating is a cam arrangement fitted horizontally inside the spectrometer base, the attached lever being connected by a rod with an arm protruding from the turn table of the grating. The rod pushes the arm forward as the cam rotates, and the grating is thus driven. The cam was so designed that one revolution would correspond to one micron and the dispersion of the grating thus is rendered linear. A 2 rpm, 6 watt synchronous motor was used for operating the cam through a system of spur gears and a worm gear, the latter ratio being 30:1. The gears are made interchangeable so as to produce different scanning rates. The chopper in front of the entrance slit consists of a thin duralumin disk with 36 slots, and the incident light is interrupted at a rate of 1080 cps. The source of the 5 watt synchronous motor used for rotating the chopper will be described later. The sensitivity of the cell[1], constructed by Mr. M. Nakamura at this Institute, is about 1.9×10^{-10} watts at room temperature.

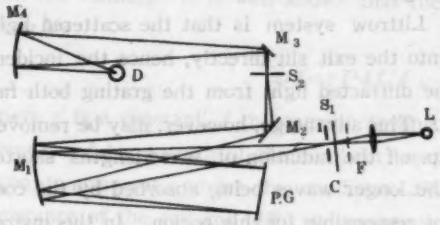

Fig. 1. Schematic diagram of the optical arrangement.

Considered from the point of view that in order to form a perfect image[2] all rays must travel the same distance between the entrance and the exit slits, the Littrow system is inferior to the Ebert system. In addition, in order to obtain a good image with the Littrow system, it is necessary to use an off-axis

1) S. Sasa and M. Nakamura: Science of Light **2** (1953), 104.
2), 3) W. G. Fastie: J. Opt. Soc. Am. **42** (1952), 641.

paraboloidal mirror as the collimator. In the instrument described here, the grating now in use is comparatively small in size and also the slits are short, so that when the optical parts are shaped and arranged with due attention given to assuring that all rays travel sufficiently close to the optical axis, a considerably sharp image can be obtained. Even though M_4 was replaced by an ellipsoidal mirror, since the receiving area of the cell is considerably wide, the resolving power would not become larger.

Another disadvantage[3] of the Littrow system is that the scattered light from the collimating mirror enters into the exit slit directly, hence the incident light from the entrance slit and the diffracted light from the grating both fall upon the same portion of this mirror. This advantage, however, may be removed to a great extent, since the filter cuts off the radiation of wave-lengths shorter than those of the desired region, the longer waves being absorbed by the condensing lens while the detector is not responsible for this region. In this instrument therefore, the effect of the so-called "stray light" is hardly perceptible.

3. The Electrical System

(a) Amplifier

Noise which occurs in a certain electronic component is always proportional to the band-width of the amplifier used in its measurement. Consequently, in order to obtain optimum performance of the spectrometer, the band-width of the amplifier must be sufficiently narrow, particularly when it is used with the PbS

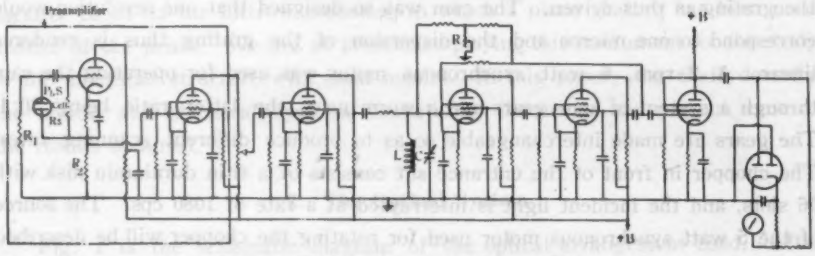

Fig. 2. Wiring diagram of the amplifier.

detector because of its extremely large amount of noise. A narrow band-width, in general, is obtained through the use of either a tuning circuit or a twin-T circuit. However the required conditions will not be satisfied unless the circuits are inserted in the system at more than two points. Therefore, the amplifier employed was constructed on the principle of the feed-back, first designed by Wilson[4], this form being comparatively easy to construct. The schematic dia-

4) G. P. Kuiper, W. Wilson, and R. J. Cashman, Astrophys. J. **106** (1943), 243.

gram of the amplifier circuit is shown in Fig. 2. As R is advanced, positive feed-back is increased and the band-width can be varied between 100 and 5 cps. The preamplifier was laied close to the detector, since the in-put signal is lowered when the impedance of the preamplifier and cable is large.

In the PbS cell, the excess-current noise[5] is so large as compared to the Johnson noise or thermal noise that the latter may be neglected in comparison with the former. It is well known that the excess-current noise $\overline{\Delta i_e^2}$ is roughly given by

$$\overline{\Delta i_e^2}=\gamma I^2 \Delta f/f \ ,$$

where γ is a constant, I the current flowing into the cell, f and Δf the frequency and band-width of the amplifier, respectively. Now, let us calculate the signal-to-noise ratio under the condition $\Delta R_s \ll R_s$, in which R_s represents the resistance of the cell and ΔR_s its variation resulting from the incident light, the value of which then becomes $(1/\gamma \cdot f/\Delta f)^{1/2} \cdot \Delta R_s/R_s+R_1+R_2$. Accordingly, the signal-to-noise ratio is not concerned explicitly with the voltage developed across the cell. Indeed, although there are a few reports[6] that maintain that ΔR_s is somewhat affected by the voltage, it is hardly perceptible for the cell in use. A tention of about 10 volts was applied on the cell. In addition, it can be seen that the voltage sensitivity has a maximum value when the resistance of the matching load is equal to that of the cell, while the signal-to-noise ratio becomes rather large when the values of the former are small in comparison to that of the latter. This conclusion is compatible with the condition for repressing fluctuation of the voltage developed across the cell as caused by the signal, that is to say, which lowers the external impedance viewed from the both ends of the cell[7].

As seen above, the excess-current noise is roughly inversely proportional to the frequency, while the sensitivity of the cell decreases with increasing frequency: the optimum frequency for the amplifier with the cell in use appears to be near 1000 cps.

As the inductance L and capacity C in the tuning circuit, a 30 H low-frequency choke and 860 pf variable air condenser were respectively used, whereby the frequency of the amplifier can be adjusted so as to match with the interrupting frequency of the chopper. A change in the amplitude of the in-put signal causes a fluctuation of the gain and band-width of the amplifier, since the "B–μ" curve

5) See any book on noise.
6) See, for example H. Kubota, J. Appli. Phys. Soc. Japan. **21** (1952), 208.
7) E. Rittner, Rev. Sci. Inst. **18** (1947), 36.

of a silicon steel is non-linear. Hence, a coil consisting of a dust core with high permeability should be the best to use. The low-frequency choke also has an another disadvantage that the Q-value is very small, but it is still available in the view of the fact that the frequency of the chopper source, described below, is not necessarily perfectly stable. The total gain of the amplifier is about 120 db. The A, and B sources have both been obtained by eliminator circuits using the 2A3 tube, and the arrangement has proved satisfactory.

(b) Constant Frequency Source

As described above, since the band-width of the amplifier is sufficiently narrow, the number of revolutions of the chopper must be held at a constant value corresponding to the former. A synchronous or induction motor connected to the A.C. mains could not be expected to satisfy the above requirement. An ideal power source should be a synchronous motor connected to the out-put of a tuning-fork oscillator, particularly if provided with a constant temperature device. An RC-oscillator was used as a substitute. Its out-put is about 30 watts. The frequency ω is given by

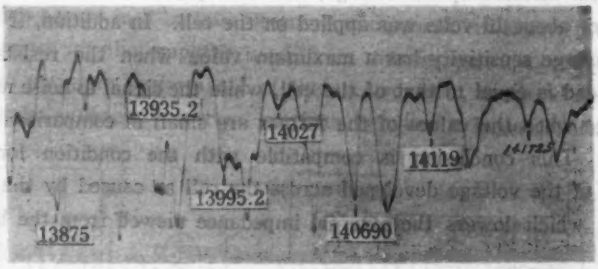

Fig. 3. Absorption Spectrum of the Combination Band $\nu_1+\nu_3$ of H_2O at 1.38 μ.

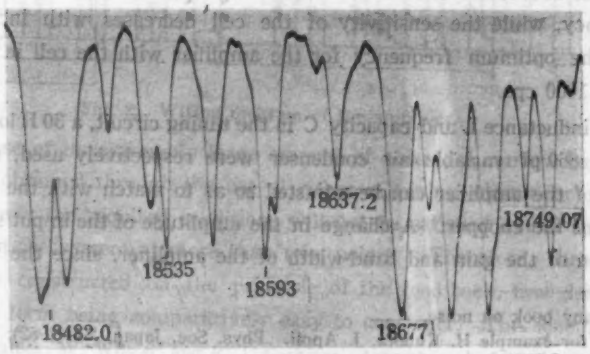

Fig. 4. Absorption Spectrum of the Combination Band $\nu_2+\nu_3$ of H_2O at 1.88 μ.

$$\omega = 1/\sqrt{C_1 C_2 R_1 R_2}\ ,$$

where the R's and C's represent the resistance and capacity of the retarding circuit respectively. Trouble is envisaged when this frequency equals that of the line voltage, so 60 cps was employed. The stability of the frequency was tested in the following manner: over a period of the several hours, the reading of an electrochronograph driven from the out-put of this oscillator was compared at frequency intervals to those of an accurate stopwatch. The readings corresponded satisfactory well with each other.

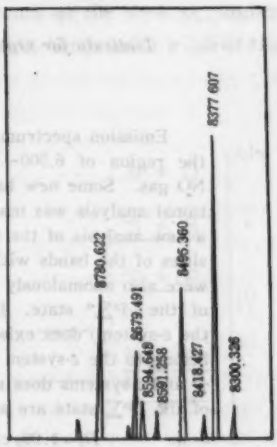

Fig. 5. Emission spectrum of Neon.

Results

Typical spectra obtained with the use of the present spectrometer are shown in Figs. 3–5. Figs. 3 and 4 show a portion of the 13.8 μ and 18.3 μ bands of atmospheric water by means of a galvanometer, the spot of light being made to fall on a continuously moving photographic film to give a continuous spectral recording. Fig. 5 is an emission spectrum of Neon by a recorder.

Acknowledgements

The authors take pleasure in mentioning their deep gratitude to Professor Yoshio Fujioka, Director of the Institute, for his encouragement and much valuable advice, and to Dr. Ryumyo Onaka for his deep interest and many valuable discussions offered throughout the present work. The authors also wish to express their appreciations of the valuable help offered by Mr. Keiei Kudo. They are indebted to Mr. Masatoshi Nakamura for his generous provision of the PbS cell.

Finally, they wish to record their gratitude to the Department of Education for financial support.

On the Emission Spectra of the β-, γ- and ε-systems of Nitric Oxide

Masaru OGAWA

Institute for Optical Research, Tokyo University of Education.

(Received May 20, 1954)

Emission spectrum of the nitric oxide molecule was photographed in the region of 6,500~1,950A, using direct electrical excitation of flowing NO gas. Some new bands of the β- and γ-systems were observed. A rotational analysis was made of the nineteen bands of the γ-system, including a new analysis of the (1-6), (2-6), (2-7), (2-8), and (5-5) bands. The intensities of the bands with $v' \geqq 4$ of the γ-system were anomalously strong as were also anomalously large the rotational constants of $v=4$ and 5 levels of the $A^2\sum^+$ state. It was concluded that the $D^2\sum$ state (upper state of the ε-system) does exist and that the observed emission bands with $v' \geqq 4$ belong to the ε-system and that Herzberg and Mundie's assumption for the γ- and ε-systems does not apply. The rotational and vibrational constants of the $D^2\sum$ state are as follows;

$$B_0 = 1.99_0\ \mathrm{cm^{-1}},\ B_1 = 1.97_2\ \mathrm{cm^{-1}},\ B_e = 1.99_9\ \mathrm{cm^{-1}},$$
$$\alpha = 0.01_8\ \mathrm{cm^{-1}},\ r_e = 1.06_3 \times 10^{-8}\ \mathrm{cm},\ \omega_e = 2327\ \mathrm{cm^{-1}},$$
$$\omega_e x_e = 24\ \mathrm{cm^{-1}} \quad \text{and} \quad \nu_e(D^2\sum - X^2\Pi) = 53{,}083\ \mathrm{cm^{-1}}.$$

The Λ-type doubling of the $X^2\Pi_{3/2}$ state was negligibly small and that of the $X^2\Pi_{1/2}$ state small but not negligible and increased linearly with the rotational quantum number, showing qualitative agreement with theoretical results. The coupling constant A of the $X^2\Pi$ state decreases with the vibrational quantum number. In the visible region, the bands with $v'=5$ and 6 of the β-system were observed but a clear decrease of their intensities, expected from Kaplan's suggestion, was not observed.

1. Introduction

The NO molecule has the well-known four band systems, β, γ, δ and ε[1], and their lower states are commonly the $X^2\Pi$ ground state. As shown in the energy diagram of Fig. 1, their upper states (A, B, C and D) are situated close

1) References for other systems:
Y. Tanaka: Sci. Pap. Inst. Phys. Chem. Res. (Tokyo), **39** (1942), 456.
M. W. Feast: Canadian Jour. Res., **28** (1950), 488.
Y. Tanaka, M. Seya & K. Mori: Science of Light, (Tokyo), **1** (1951), 80, J. Chem. Phys., **19** (1951), 979.
P. Baer & E. Miescher: Helv. Phys. Acta., **24** (1951), 331.
M. Ogawa: Science of Light (Tokyo), **2** (1953), 87.
L. H. Sutcliffe & A. D. Warsh: Proc. Phys. Soc., **66** (1953), 209.
Y. Tanaka: J. Chem. Phys., **21** (1953), 788.
M. Ogawa: Science of Light (Tokyo), **3** (1954), 39.

together and are slightly higher than the dissociation limit of the $X^3\Pi$ ground state (5.29 eV). Therefore, if any unstable electronic state which might perturb these four states does exist, it may be expected that the predissociation will occur to some extent in the vibrational states of the observed bands.

J. Kaplan[2] suggested that the predissociation occurs at the $v=4$ or higher levels of the $B^3\Pi$ state on the ground that the emission bands with $v' \geqq 5$ of the β-bands had not been observed.

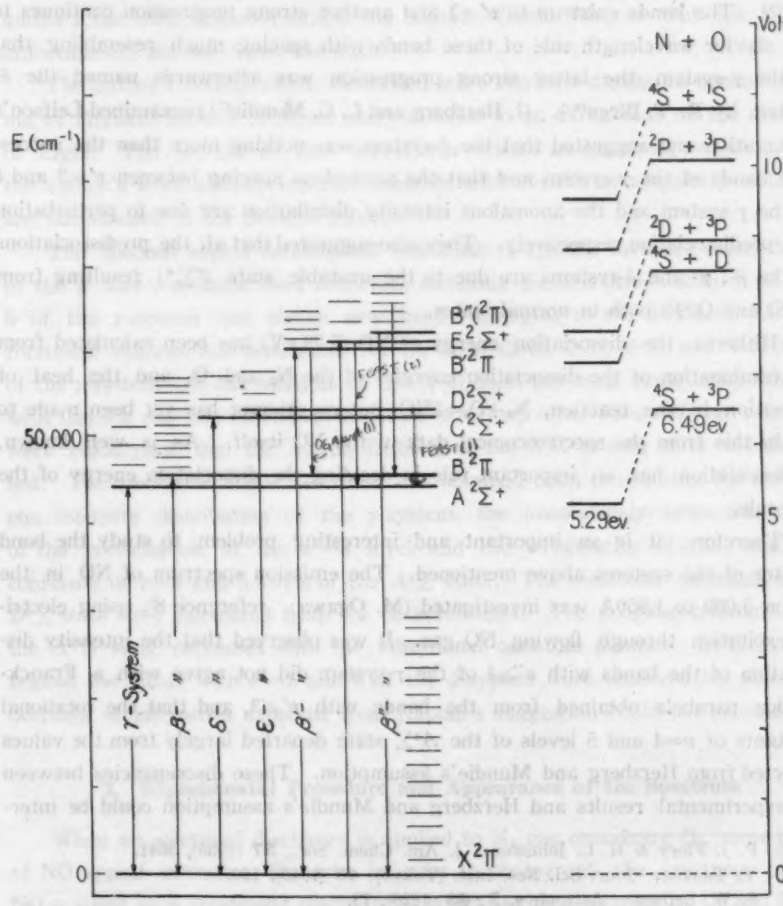

Fig. 1. Energy level Diagram of the NO Molecule.

2) J. Kaplan: Phys. Rev., **37** (1931), 1404.

P. J. Flory and H. L. Johnston[3] observed that the NO molecule was dissociated by irradiation of light corresponding to the (1–0) and (2–0) bands of the δ-system. From this, they concluded that the predissociation occurs with $v \geqq 1$ in the $C^1\Sigma$ state (upper state of the δ-system). Y. Tanaka[4] supported this conclusion from his results: in the absorption spectrum of the NO in the extreme ultraviolet region, (1–0) and (2–0) bands of the δ-system have anomalously strong intensities and the bands with $v' \geqq 3$ are not observed.

The absorption spectrum of the γ-system was first observed by S. W. Leifson[5]. The bands exist up to $v'=3$ and another strong progression continues to the shorter wavelength side of these bands with spacing much resembling that of the γ-system (the latter strong progression was afterwards named the ε-system by R. T. Birge[6]). G. Herzberg and L. G. Mundie[7] reexamined Leifson's observation and suggested that the ε-system was nothing more than the successive bands of the γ-system and that the anomalous spacing between $v'=3$ and 4 of the γ-system and the anomalous intensity distribution are due to perturbation and predissociation respectively. They also suggested that all the predissociations of the β-, γ- and δ-systems are due to the unstable state ($^2\Sigma^+$) resulting from N(^4S) and O(^3P) both in normal states.

Hitherto, the dissociation energy of NO (5.29 eV) has been calculated from the combination of the dissociation energies of the N_2 and O_2 and the heat of formation in the reaction, $N_2+O_2=2NO$, but no attempt has yet been made to obtain this from the spectroscopical data of the NO itself. As is well known, predissociation has an important role in deciding the dissociation energy of the molecule.

Therefore, it is an important and interesting problem to study the band spectra of the systems above mentioned. The emission spectrum of NO in the region 5,000 to 1,950A was investigated (M. Ogawa: reference 8), using electrical excitation through flowing NO gas. It was observed that the intensity distribution of the bands with $v' \geqq 4$ of the γ-system did not agree with a Franck-Condon parabola obtained from the bands with $v' \leqq 3$, and that the rotational constants of $v=4$ and 5 levels of the $A^2\Sigma$ state departed largely from the values expected from Herzberg and Mundie's assumption. These discrepancies between the experimental results and Herzberg and Mundie's assumption could be inter-

3) P. J. Flory & H. L. Johnston: J. Am. Chem. Soc., **57** (1935), 3641.
4) Y. Tanaka: Jour. Sci. Res. Inst. (Tokyo), **43** (1949), 160.
5) S. W. Leifson: Astrophys. J., **63** (1926), 73.
6) R. T. Birge: Trans. Frad. Soc., **25** (1929), 707.
7) G. Herzberg & L. G. Mundie: J. Chem. Phys., **8** (1940), 263.
8) M. Ogawa: Science of Light (Tokyo), **1** (1951), 19.

preted however, by assuming that the $D^2\sum$ state actually does exist. Therefore, it was concluded that the $D^2\sum$ state does exist and that the observed emission bands with $v' \geqq 4$ do not belong to the γ-system but to the ε-system.

A. G. Gaydon[9] investigated the emission spectrum of NO, using various forms of electrical excitation of N_2 with a small portion of O_2 gas. He has also reported the same conclusion on the basis of almost the same experimental results as the author's and proposed a new value of the dissociation energy of the NO, namely, 6.49 eV. His reports were published several years before author's but they appeared during the Second World War, so that the author unfortunately did not know his work.

The author's results above mentioned were reported during an annual meeting of Physical Society of Japan and published in an early issue of the Science of Light. The journal at that period was written in Japanese, and therefore, the author's work already reported together with results subsequently obtained are summarized in the present paper.

The spectral region investigated was 6,500 to 1,950A, in which many bands of the β- and γ-systems were observed, including six new bands with $v'=5$ and 6 of the γ-system and eleven new bands belonging to the β-system. A new rotational analysis has been made for the (1–6), (2–6), (2–7), (2–8), and (5–5) bands of the γ-system and the analysis of the (4–4) band has been made independently with Gaydon and the rotational structure of fifteen other bands of the γ-system were reanalysed, and the Λ-type doubling of the $X^2\Pi$ ground state was discussed. The conclusion above described was obtained upon considering the anomalous intensity distribution of the γ-system, the anomalously large magnitude of the perturbation at the $v'=4$ level and the irregularity of the rotational constants of $v=4$ and 5 levels of the $A^2\sum$ state. The molecular constants of the $D^2\sum$ state were calculated from the observed data. The coupling constant A of the $X^2\Pi$ state decreases with the vibrational quantum number. In the visible region, the bands with $v'=5$ and 6 of the β-system were observed but the clear decrease of intensities expected from Kaplan's suggestion could not be observed.

2. Experimental Procedure and Appearance of the Spectrum

When an electrical discharge is applied to N_2 gas containing O_2, some bands of NO appear strongly. Hitherto, in order to photograph the spectrum of the NO a silent or a condensed discharge was applied to a mixture of O_2 and N_2 or

9) A. G. Gaydon: Proc. Phys. Soc., **56** (1944), 95.
A. G. Gaydon: Proc. Phys. Soc., **56** (1944), 160.

their compound, mostly NO_2. The bands of N_2 (the first and the second positive groups) and NO_2 appear in the same region as those of the NO bands, so in the present case the NO gas itself was used.

In order to ascertain the existence of the predissociation of the $B^3\Pi$ state, we must investigate the intensity distribution or the rotational structure of the bands with $v'=4$ or 5. If the predissociation occurs at the $v=4$ level of the $B^3\Pi$ state as suggested by J. Kaplan, we may expect that the bands with $v'=5$ or the rotational lines with high energy of the band with $v'=4$ must be weak in the emission spectrum. To confirm these surmises, it is desirable to photograph the β-bands in the visible region or in the extreme ultraviolet region. Since the Franck-Condon parabola of the β-system has a large width, bands with $v'\geqq 4$ should appear in these regions. In the present experiment, the visible region was taken. The β-system appears strongly in the active nitrogen afterglow which is produced when the discharge is applied to the mixture of N_2 with a small portion of O_2. Thus far, only this method has been used to investigate the β-system, and the spectrum appears up to $v'=4$. A discussion on predissociation on the basis of the results obtained with this particular excitation will involve doubtful points unless the excitation mechanism of the β-system in the active nitrogen afterglow is clarified. Therefore, direct electrical excitation of flowing NO itself was used in the present work, with a pressure of 2~5 mmHg.

The method of preparation and purification of the NO gas was the same as that described in the previous paper[10]. One of the two discharge tubes used was the same as the one described in the paper and the other was a water cooled type which was used mainly to photograph the weak bands or the bands for rotational analysis. In order to excite the fresh NO gas in the vicinity of the window of the slit side, the gas was passed continuously through the discharge tube from the gas inlet near the slit of the spectrograph.

Two transformers of 20 KV, 1 KW and 30 KV, 300 W were used, the former only for the water cooled type discharge tube. The gas was passed through the discharge tube under various pressures and the silent electrical discharge was applied to it. Below one mm Hg, the spectrum in the visible region showed fairly strong nitrogen bands (the first and the second positive groups) together with a weak continuous background (air afterglow), and in the ultraviolet region the second positive group of N_2 appeared predominantly, the γ- and weak β-bands of NO were also being observed. When the pressure was slowly increased, the N_2 bands gradually lost their intensity and finally at a pressure of about

10) Y. Tanaka & M. Ogawa: Jour. Sci. Res. Inst. (Tokyo), **44** (1949), 1.

5 mm Hg they disappeared almost completely leaving only the NO bands. The γ-bands appeared most strongly at a pressure of 1 mm Hg but its intensity decreased with increase above this level, while in spite of this the intensity of the β-bands still increased.

When the β-bands in the visible region were photographed, a sector in front of the slit of the spectrograph was used to avoid superposition of the continuous spectrum of the air afterglow and to reduce the intensity of the N_2 bands produced by the decomposition of the NO gas. The sector was synchronized to open the slit simultaneously with the main discharge, which was repeated with a period of 6 cycles per second, each flash lasting about 1/30 seconds. By this method the N_2 bands were excluded almost completely.

The spectrum in the visible region was photographed by a glass spectrograph composed of three 60° glass prisms of 6 cm base. The focal length of the camera lens was 50 cm. The dispersion was about 46 A/mm at 6,000 A. The spectrum in the region 1,950 to 5,000A was photographed by a Hilger E_2 quartz spectrograph. The spectrum of the γ-bands to analyse the rotational structure was photographed by a Hilger E_1 quartz spectrograph, the dispersion of which was about 1.7 A/mm at 2,200A. The photographic plates used were Fuji process plate for the ultraviolet region and Oriental hyperpanchromatic plate for the visible region. In the region below 2,300A, the sensitivity of the plate dropped, and so machine oil was coated on the process plate. The oil had good sensitivity and did not perceptibly lower the sharpness of the spectral line but was rather volatile.

The exposure times were 2~4 hours in the case of the glass spectrograph, 10~60 minutes in the case of the E_2. When the E_1 was used, exposure times of from 30 minutes to 4 hours were necessary to photograph the bands in the region of $\lambda \geqq 2{,}300$A, and in the region of $\lambda \leqq 2{,}300$A the necessary exposure times ranged from 30 minutes to 15 hours.

The spectra of the γ-system photographed by the E_2 with pressures of 0.5 mm and 5 mm Hg are shown in Fig. 2a. In this figure the (1–0) and (2–0) bands have completely disappeared by the self-absorption of NO in the case of 5 mm Hg. The (0–0) band is also weak though it is not shown in this figure.

In order to determine the existence of the ε-system, the analysis not only of the rotational structure of $v=4$ of the $A^3\Sigma$ state but that of $v=5$ are also recommended. Unfortunately, the strong (1–0) band of the γ-system partly overlape the (5–5) band, so that the above mentioned self-absorption of the (1–0) band was utilized to photograph the (5–5) band, for which, the pressure was increased to about 1.5 mm Hg or more but the (1–0) band could not be satisfactorily

Table 1. Deslandres table of the γ- and ε-systems. Show-

v' \ v''		0		1		2		3		4
$D^2\Sigma$	$A^2\Sigma$	*44076.9*	*1875.8*	*42201.1*	*1847.1*	*40354.0*	*1819.7*	*38534.3*	*1791.2*	*36743.1*
		44201.0	*1876.0*	*42325.0*	*1847.5*	*40477.5*	*1820.0*	*38657.5*	*1791.6*	*36865.9*
	0	2269.3		2370.2		2478.4		2595.3		2721.9
		2268.0		2369.0		2477.0		2593.9		2720.5
		2262.6		2363.6		2470.9		2587.0		2713.4
		2261.8		2362.3		2469.8		2586.1		2711.7
		2341.8		*2341.9*						
		2341.8		*2341.8*						*2341.4*
		46418.7	*1875.7*	*44543.0*						
		46542.8	*1876.0*	*44666.8*						*29207.3*
	1	2155.3		2245.9				2447.3		2558.6
		2154.0		2244.7				2445.5		2557.3
				2239.7				2439.5		2550.6
				2238.6				2438.3		2549.8
						45004.2	*1819.1*	*43185.1*		
						45127.7	*1819.5*	*43308.2*		
	2	2053.1		2135.2		2222.8		2316.5		
		2051.9		2134.2		2221.7		2315.5		
				2129.9		2216.7		2310.0		
		2047.8		2128.7		2215.7		2308.9		
										43670.1
										43792.7
	3			2036.4		2115.7		2200.4		2290.7
				2035·2		2114.7		2199.4		2289.5
				2031.2		2110.3		2194.4		2284.2
				2030.2		2109.2		2193.4		.....
										2164.2
										2164.3
										45834.3
										45957.0
0	4					2023.0		2100.2		2182.3
						2022.2		2099.2		2181.3
						2018.0		2094.8		2176.6
						2017.3		2094.0		2175.6
								2004.5		2078.8
1	5							2003.7		2078.0
								1999.6		2073.6
								1998.9		2072.9
										1986.2
2	6									1985.3
										1581.8
										1980.6

ing the band origin in cm^{-1} unit and the band head in A.

5		6		7		8		9
1764.1	*34979.0*							
1764.5	*35101.4*							
	2859.3	3008.7						
	2857.9	3006.7						
	2849.6	2997.4						
	.....	.....						
	3341.5							
	2341.9							
	37320.5	*1735.8*	*35584.7*					
1764.0	*37443.3*	*1736.0*	*35707.3*					
	2679.6		2810.5		2952.0		3106.1	3274.3
	2678.6		2809.2		2950.5		.....	
	2671.4		2801.2		2941.6		.....	
	2669.8		2799.9		2940.5		3092.9	
			2308.6					
			2308.6					
			27893.3	*1707.2*	*36186.1*	*1679.8*	*34506.3*	
			38015.9	*1707.4*	*36308.5*	*1680.2*	*34628.3*	
	3523.2		2638.9		2763.6		2898.3	3043.7
	2522.2		2637.8		2762.4		2896.9	.....
	2515.6		2631.1		2754.7		2888.4	3032.5
	.....		2629.5		2753.2		.....	3031.2
	2386.1							
	2385.6*							
	2379.8*							
	2378.8*							
	46349.8							
	46472.2							
	2158.0		2242.2		2331.1		2426.4	
	2157.1		2241.0		.....		2425.7	
	2152.4		2235.9		2324.8		2419.3*	
	2151.3		.....		2323.8		2418.0*	
	over-		2135.2				.....	
	lapped		2134.2				2300.5*	
	with		2629.6				2295.0	
	δ(0—2)		2128.7				2294.4	

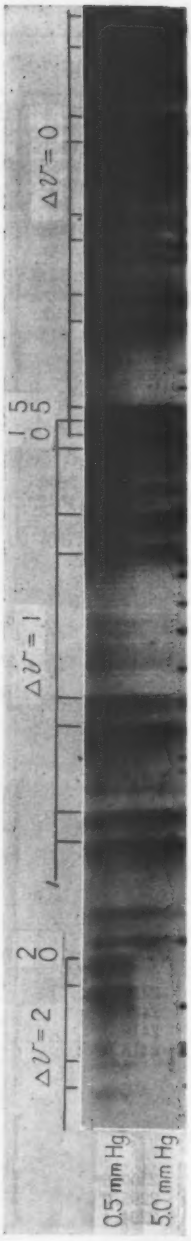

Fig. 2a. Spectrum of the γ-system.

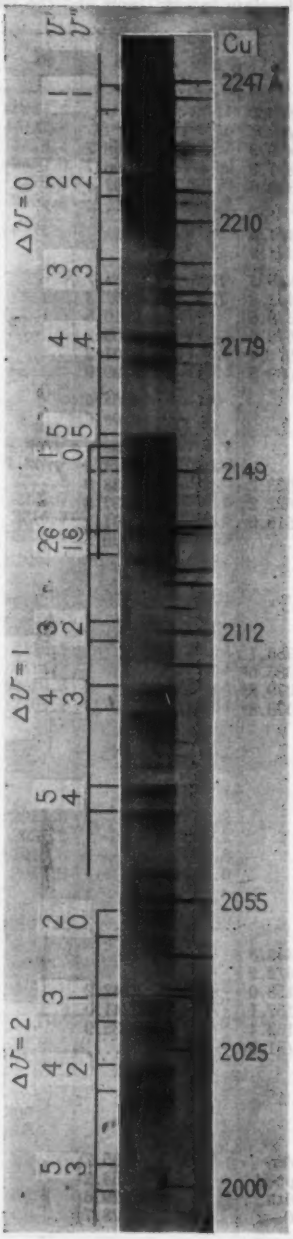

Fig. 2b. Spectrum of the γ-system.

removed. Better results were anticipated with the use of higher pressure but it was found that the intensity of the γ-system decreased and even with 1.5 mm Hg exposure times of 10 to 15 hours were necessary. The use of higher pressures was therefore abandoned. To remove the (1–0) band completely, an absorption tube with quartz windows was placed between the slit of the E_1 and the discharge tube and NO gas at various pressures was passed through it, but the light emerging from the discharge tube was reduced by the reflection from the windows and a plate with suitable blackness could not be obtained by this method.

3. Vibrational Analysis of the γ-system

The band spectra of the γ-system photographed by the E_2 spectrograph are shown in Figs. 2a and 2b. Since the γ-system arises from the transition of $^2\Sigma - ^2\Pi$, the band should have twelve branches. Among these branches those of the four groups (P_2, $^PQ_{12}$), Q_2, $^QR_{12}$), ($^QP_{21}$, Q_1) and ($^RQ_{21}$, R_1) do not split into two branches because of the small spin doubling of the $A^2\Sigma$ state. The $^QP_{12}$, (P_2, $^PQ_{12}$), P_1 and ($^QP_{21}$, Q_1) branches constitute four heads in this order, counting from the longer wavelength side. In Table 1, are listed the wavelengths of these four heads. The bands newly observed are (5–6), (5–7), (5–8), (6–4), and (6–8), all these bands belong to the ε-system as mentioned in a later section of this paper. The (6–6) band overlaps the (2–1) band, so that assignment of the (6–6) band may not be made with confidence prior to an investigation with a spectrograph of high resolving power.

The intensity distribution of the bands with $v' \leqq 3$ agrees with the Franck-Condon parabola obtained by R. Schmid[11] but not so the bands with $v' \geqq 4$. As seen in Fig. 2b the bands with $v' \geqq 4$ are much stronger than that of the bands with $v' \leqq 3$ in the $\Delta v =$ constant sequences. The (5–3) band is weaker than the (3–1) band but the (5–3) band is situated on the shortest wavelength side and the sensitivity of the plate and the transparency of the spectrograph drop sharply in this region, so that to compare the intensities of the (5–3) to that of the (3–1) band is meaningless. The anomalous intensity distribution above mentioned cannot be explained by the predissociation suggested by Herzberg and Mundie. This is because if the predissociation occurs at the $v' \geqq 4$ levels, the NO molecules at such levels should have the chance of dissociating without radiation, and the intensities of the emission bands should thus be weakened.

11) R. Schmid: Zeits. f. Phys., **64** (1930), 84.

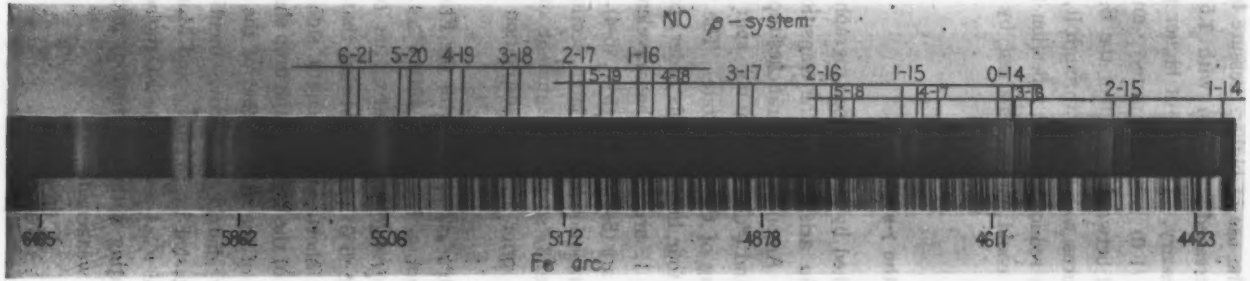

Fig. 3a. Spectrum of NO in the Visible Region. (silent discharge)

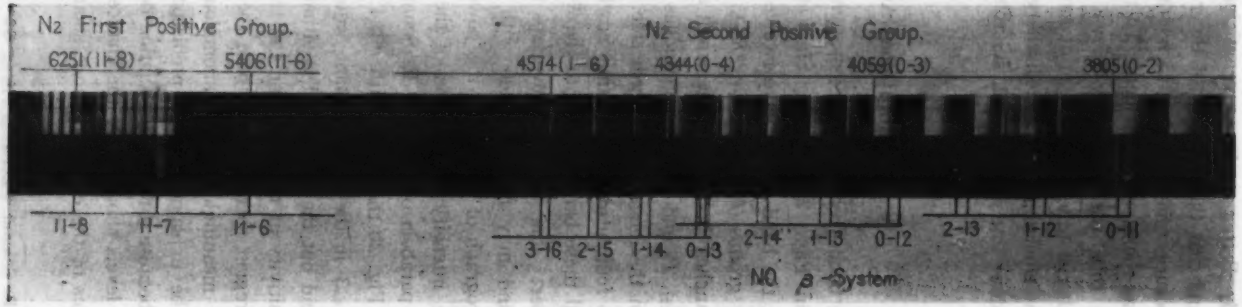

Fig. 3b. Spectrum of NO in the Visible Region. (in the active nitrogen afterglow)

Table 2. Wavelengths and Wavenumbers of the β-system.

$v'-v''$	Present Measurement				Pearse & Gaydon's* Table		$v'-v''$	Present Measurement				Pearse & Gaydon's* Table	
	$\lambda_{obs.}$	$\nu_{obs.}$		I	λ	I		$\lambda_{obs.}$	$\nu_{obs.}$		I	λ	I
6–21	5614.1 5572.8	17869 17939	*70*	2			2–16	4810.6 2792.1	20782 20862	*80*	4	4810.0 4791.4	1
5–20	5488.4 5466.4	18215 18289	*74*	2			5–18	4780.1 4762.8	20914 20990	*76*	2		
4–19	5481.8 5359.6	18578 18653	*75*	3			1–15	4709.9 4691.7	21226 21308	*82*	5		
3–18	5273.4 5251.6	18957 19037	*80*	3	5270.1 5252.7	0	4–17	4685.8 4667.1	21335 21421	*76*	3		
2–17	5163.0 5141.4	19363 19445	*82*	2			0–14**	4608.8 4591.9	21691 21771	*80*	2		
5–19	5115.1 5095.2	19545 19621	*76*	2			3–16	4589.7 4573.0	21778 21861	*83*	5	4590.8 4574.0	5
1–16	5056.9 5035.4	19770 19854	*84*	1			2–15	4496.2 4480.3	22235 22314	*79*	5	4496.2 4479.8	3
4–18	5013.0 4993.6	19943 20020	*77*	3			1–14	4401.6 4386.5	22713 22791	*78*	4	4401.5 4385.7	2
3–17	4911.9 4892.2	20353 20435	*82*	4	4912.1 4892.1	2							

* R. W. B. Pearce and A. G. Gaydon: The Identification of Molecular Spectra, (1950) p. 180.

** Masked by (3–16) band.

4. Vibrational Analysis of the β-system

The bands of the β-system in the visible region were photographed as described in Section 2. The spectrum is shown in Fig. 3a, and for comparison with this the spectrum obtained with the afterglow of N_2 containing a trace of O_2 is also shown in Fig. 3b. In this latter figure only the β-system and characteristic N_2 first positive group are revealed but in Fig. 3a other NO bands are revealed as well as the β-system. From a comparison of two figures, we can recognize the clear effect of the excitation method which influences the appearance of the band spectrum.

The bands of the β-system newly observed are the (6–21), (5–20), (4–19), (2–17), (5–19), (1–16), (4–18), (5–18), (1–15), (4–17), and (0–14) bands, and the wavelengths and their wavenumbers are listed in Table 2. Other known bands in this region are the Feast-band ($E^3\Sigma - A^3\Sigma$), the $B'-B^3\Pi$ band and the $B''-B^3\Pi$ band. Some farther unknown bands are also seen and their investigation is now in progress.

5. Rotational Analysis of the γ-system

Rotational analysis was made for the (0–0), (0–1), (0–2), (0–3), (0–4), (0–5), (1–0), (1–1), (1–4), (1–5), (1–6), (2–2), (2–3), (2–6), (2–7), (2–8), (3–4), (4–4), and (5–5) bands. Most of these had already been analysed by R. Schmid[12] or W. R. Guillery[13], but a new analysis was conducted since older attempt did not make use of modern spectroscopical notation and quantum numbers. Table 3 shows, as examples of the results obtained, the observed wavenumbers of the rotational lines of the (0–1) band. The (1–6), (2–6), (2–7), (2–8) and (5–5) bands are those analysed for first time, and the wavenumbers of their rotational lines observed

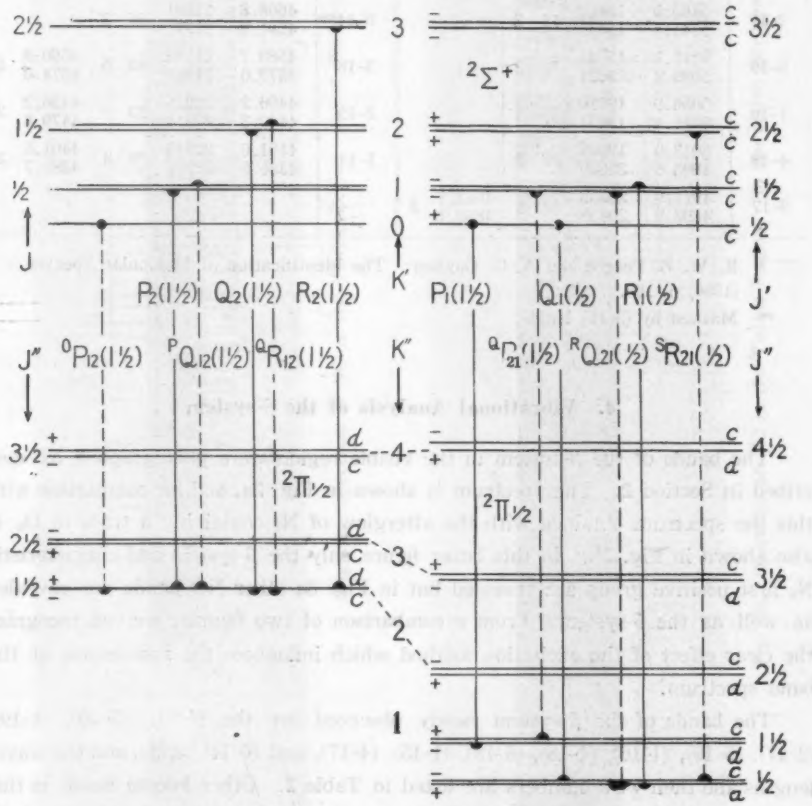

Fig. 4. Rotational energy level diagram.

12) R. Schmid: Zeits. f. Phys., **49** (1928), 428.
13) W. R. Guillery: Zeits. f. Phys., **42** (1927), 121.

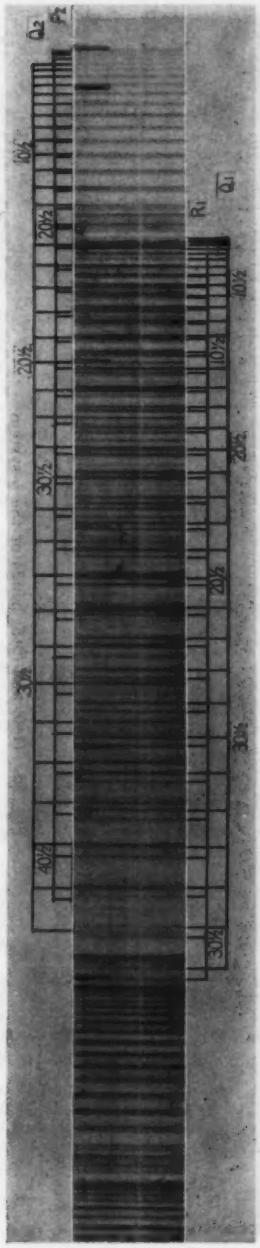

Fig. 5a. (0–4) band of the γ-system.

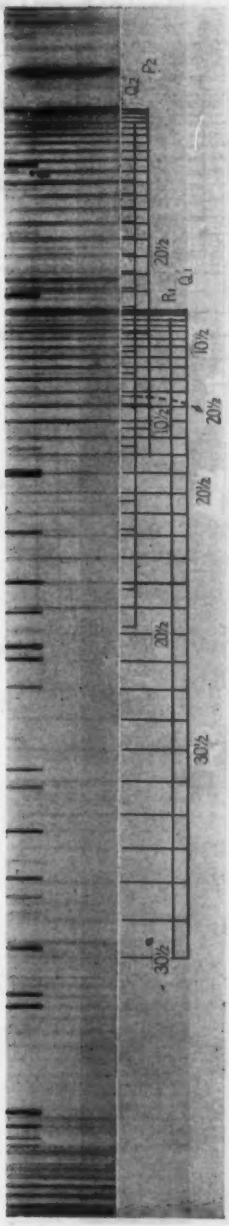

Fig. 5b. (2–3) band of the γ-system.

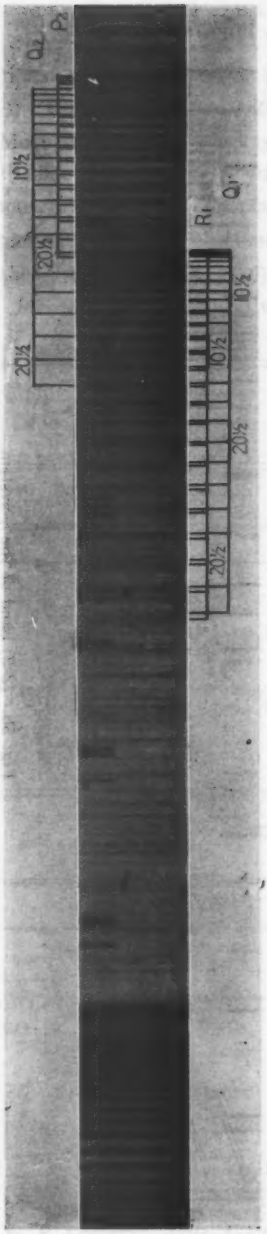

Fig. 5c. (2–6) band of the γ-system.

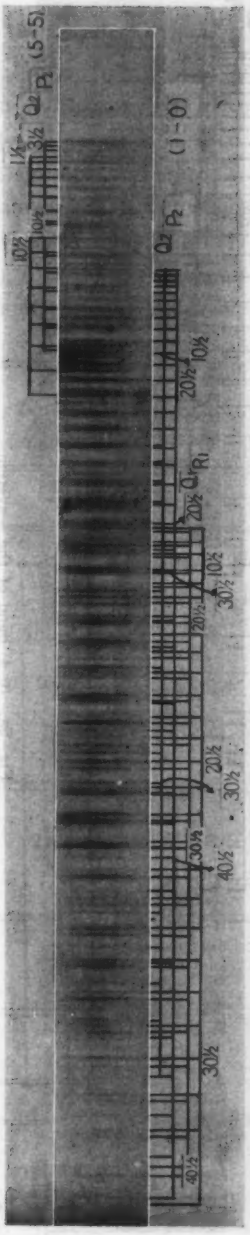

Fig. 5d. (1–0) and (5–5) bands of the γ-system

Table 3. Wavenumbers of the Rotational Lines of (0–1) γ-Band.

	$A^2\Sigma - X^2\Pi_{3/2}$ transition				$A^2\Sigma - X^2\Pi_{1/2}$ transition			
J	R_2	Q_2, $^QR_{12}$	P_2, $^PQ_{12}$	$^OP_{12}$	$^SR_{21}$	R_1, $^RQ_{21}$	Q_1, $^QP_{21}$	P_1
$^1/_2$						42327.3		
$1^1/_2$		42210.6			42343.3	30.7		
$2^1/_2$		14.0			49.5	33.7		
$3^1/_2$		18.1	42202.2	42190.6	57.9	38.4		
$4^1/_2$	42246.4	22.5		87.2	66.6	43.3		
$5^1/_2$		27.7	04.0	84.4		49.1	42325.1	42305.6
$6^1/_2$	65.5	33.4	05.8	82.1	87.0	55.2	27.3	03.8
$7^1/_2$	75.5	39.8	08.0	80.7		62.2	30.7	02.7
$8^1/_2$	86.5	46.4	10.9	78.9	42409.1	69.8	33.7	
$9^1/_2$	97.9	54.1	14.3	78.9	21.7	78.0	38.4	02.7
$10^1/_2$	42309.9	62.0	18.4	78.9	34.3	87.0	43.3	03.8
$1^1/_2$	22.1	70.4	22.7	78.9	48.0	96.5	49.1	05.6
$2^1/_2$	35.1	79.7	28.2	80.7	62.3	42406.6	55.2	07.7
$3^1/_2$	48.8	89.3	33.9	82.3	76.9	17.7	62.2	10.6
$4^1/_2$	62.6	99.7	40.4	84.4	91.9	28.8	69.8	14.4
$5^1/_2$	78.0	42310.6	47.0	87.6	42508.3	41.0	78.0	18.7
$6^1/_2$	93.3	22.1	54.6	91.2		54.2	86.5	23.2
$7^1/_2$	42409.1	33.3	62.5	95.1	43.2	67.9	96.5	28.9
$8^1/_2$	25.7	46.5	71.0	42200.0	60.6	81.8	42406.6	35.1
$9^1/_2$	42.6	59.8	80.4	05.8	80.2	96.5	17.4	42.0
$20^1/_2$	60.5	73.2	89.8	10.6	98.9	42511.9	28.6	49.2
$1^1/_2$	78.8	87.5	42300.4			28.0	40.7	57.9
$2^1/_2$		42402.7	11.3		42639.4	44.9	53.4	66.6
$3^1/_2$	42516.6	18.0	23.2		60.9	62.2	67.0	75.4
$4^1/_2$	37.1	34.3	35.1	39.8	82.5	80.2	81.0	86.5
$5^1/_2$	57.5	50.9	48.8	49.3	42705.3	98.9	95.7	96.9
$6^1/_2$	78.6	67.9	61.9	58.6	28.5	42618.1	42511.0	42409.1
$7^1/_2$	42600.5	86.1	75.4	68.4		37.8	27.1	20.5
$8^1/_2$	22.9	42504.5	89.9	79.7		58.3	43.6	32.9
$9^1/_2$	45.8	23.5	42405.0	89.8		79.4	60.6	46.4
$30^1/_2$	69·4	43.2	20.5			42701.5	78.6	60.5
$1^1/_2$	93.5	63.5	36.9	42314.4		28.3	97.1	74.9
$2^1/_2$	42718.0	84.2	53.7	27.3		46.8	42616.1	89.7
$3^1/_2$	44.0	42606.0	71.3	42.0		70.3	35.9	42505.9
$4^1/_2$	70.0	27.6	89.7	55.2		94.7	56.1	
$5^1/_2$	96.0	50.1	42508.3	69.8		42819.8	77.2	39.8
$6^1/_2$	42823.1	73.4	27.1			45.1	99.3	57.5
$7^1/_2$	50.6	97.4	47.4			71.2	42721.6	75.8
$8^1/_2$	79.0	42721.6	68.0			98.3	44.0	94.9
$9^1/_2$	42907.8	47.0	88.9			42925.7	67.8	42614.7
$40^1/_2$		72.2				53.6	92.1	35.6
$1^1/_2$							42816.9	56.1
$2^1/_2$							42.2	
$3^1/_2$							68.3	
$4^1/_2$							95.1	
$5^1/_2$							42922.0	
$6^1/_2$							50.1	

are listed in Tables 4 and 5. One of the principal purposes of our present study was to analyse the (4–4) and the (5–5), since their rotational structures were seen to hold the key in determining the existence of the ε-system. At the period when this report was published first in the early issue of Science of Light, the rotational analysis of (4–4) band had been made independently by Gaydon, and so the observed wavenumbers of its rotational lines are removed from

Table 4. Wavenumbers of the Rotational Lines of (1–6) γ-Band

	$A^2\Sigma - X^2\Pi_{3/2}$ transition				$A^2\Sigma - X^2\Pi_{1/2}$ transition			
J	R_2	Q_2, $^QR_{12}$	P_2, $^PQ_{12}$	$^OP_{12}$	$^SR_{21}$	R_1, $^RQ_{21}$	Q_1, $^QP_{21}$	P_1
$^1/_2$						35708.9		
$1^1/_2$						11.0		
$2^1/_2$	35612.9	35597.6				16.0		
$3^1/_2$		35601.8	35585.7			20.9	35704.4	
$4^1/_2$	30.6	07.1	87.4			26.4	06.5	
$5^1/_2$		12.9	89.4	35570.0	35760.1	32.9	08.9	35689.1
$6^1/_2$	50.4	19.6	92.1		70.5	39.9	11.0	
$7^1/_2$	63.1	26.8	95.4	67.9	82.6	48.0	16.0	
$8^1/_2$	74.1	34.7	99.5	67.9	95.6	56.7	20.9	35689.1
$9^1/_2$	85.8	43.5	35604.0		35809.8	66.3	26.4	
$10^1/_2$	35700.9	53.0	09.8	70.0	22.8	76.6	32.9	
$1^1/_2$		63.1	16.0		37.8	87.5	39.9	
$2^1/_2$	28.8	74.1	23.0	75.8	55.0	99.5	48.0	35700.9
$3^1/_2$	44.6	85.8	30.6	79.5	70.7	35812.0	56.7	06.5
$4^1/_2$	60.1	97.9	39.1	83.4	90.0	25.7	66.3	11.0
$5^1/_2$	76.6	35711.0	48.1	89.4	35908.3	40.5	76.6	18.2
$6^1/_2$	95.6	24.7	58.1	95.2		55.0	87.5	24.4
$7^1/_2$	35813.9	39.3	68.6	35601.8	46.5	70.7	99.5	32.9
$8^1/_2$	32.8	54.4	79.7	09.8		87.7	35812.0	42.2
$9^1/_2$	52.4	70.5	91.6		86.8	35904.8	25.7	51.7
$20^1/_2$	73.3	87.5	35704.4	26.4	36008.6	23.3	40.5	62.2
$1^1/_2$	94.5	35804.3	18.1	34.7	34.0	42.0	55.0	
$2^1/_2$	35916.6	22.8	32.8	45.7	55.8	62.1	70.7	84.8
$3^1/_2$	39.4	40.5	48.0	58.1		82.3	87.7	95.6
$4^1/_2$	62.1	60.9	62.2	68.6		36003.5	35904.8	
$5^1/_2$	86.8	81.1	79.2	79.7		25.6	23.3	35825.7
$6^1/_2$	36011.4	35902.1	95.6	93.8		48.5	42.0	
$7^1/_2$	37.5	23.3	35813.9			72.0	62.1	55.0
$8^1/_2$	63.5	46.5	32.8	35724.4		96.7	82.3	73.3
$9^1/_2$	91.1	69.8	52.4	39.3		36121.6	36003.5	90.0
$30^1/_2$		93.5	73.3	56.7		47.5	25.6	35908.3
$1^1/_2$	36147.5	36018.0	92.5			74.0	48.5	
$2^1/_2$		43.7	35914.1				72.0	46.5
$3^1/_2$		69.7					96.7	
$4^1/_2$		96.7					36121.6	
$5^1/_2$							47.5	
$6^1/_2$							74.0	

Table 5.

The upper state of the γ-system is $^2\Sigma$, and its rotational energy is given by the following formulae,

$$F_1(K)=B_v K(K+1)-D_v K^2(K+1)^2+\cdots\cdots+\gamma/2\cdot K$$
$$J=K+1/2\,, \qquad (1)$$
$$F_2(K)=B_v K(K+1)-D_v K^2(K+1)^2+\cdots\cdots-\gamma/2(K+1)$$
$$J=K-1/2\,, \qquad (2)$$
$$B_v=B_e-\alpha(v+1/2)+\cdots\cdots,$$
$$D_v=D_e-\beta(v+1/2)+\cdots\cdots, \qquad (3)$$
$$B_e=h/8\pi^2 c\mu r_e^2\,,$$

where γ, α, and β are constants. The rotational energy of the $X^3\Pi$ ground state is given by the following formulae, in the Hund coupling case a,

$$F(J)=B_v[J(J+1)-\Omega^2+S(S+1)-\Sigma^2]-D_v J^2(J+1)^2+\cdots\cdots. \qquad (4)$$

As shown in Fig. 4 the twelve branches $^0P_{12}$, P_2, $^PQ_{12}$, Q_2, $^QR_{12}$, R_2, P_1, $^QP_{21}$, Q_1, $^RQ_{21}$, R_1, and $^SR_{21}$ appear according to the selection rule, $K=0, \pm1$, and $J=0, \pm1$. Spin doubling of the $A^3\Sigma$ state is very small and the group of (P_2, $^PQ_{12}$), (Q_2, $^QR_{12}$), (Q_1, $^QP_{21}$), and (R_1, $^RQ_{21}$) branches do not split into two but have stronger intensity than others and are distinct, while the other four branches are hardly observed in the weak bands. The four former groups were therefore used for the rotational analysis. The relation between the notations used by Schmid and Guillery and those adopted in the present analysis is:

Present Notation	Schmid's and Guillery's Notation
$^0P_{12}(2^1/_2)$	$P_1(2)$
$P_2(2^1/_2)$, $^PQ_{12}(2^1/_2)$	$Q_1(3)$
$Q_2(2^1/_2)$, $^QR_{12}(2^1/_2)$	$R_1(4)$
$R_2(2^1/_2)$	$R_1'(5)$
$P_1(2^1/_2)$	$P_2(2)$
$Q_1(2^1/_2)$, $^QP_{21}(2^1/_2)$	$Q_2(3)$
$R_1(2^1/_2)$, $^RQ_{21}(2^1/_2)$	$R_2(4)$
$^SR_{21}(2^1/_2)$	$R_2'(5)$

If the spliting due to the Λ-type doubling of the $X^3\Pi$ state is small and could be neglected as an approximation, the B_v and D_v values of the $A^3\Sigma$ and $X^3\Pi$ states could be calculated by using the following combination relations,

$$\Delta_1F(K)=\Delta_1F(J-1/2)=R_1(J)-Q_1(J)=^RQ_{21}(J)-^QP_{21}(J)$$
$$=Q_2(J)-P_2(J)=^QR_{12}(J)-^PQ_{12}(J)$$
$$=2B_v(K+1)-4D_v(K+1)^3+\cdots,\ K=J-1/2 \qquad (^3\Sigma \text{ state}) \quad (5)$$
$$\Delta_1F(K)/K+1=2B_v-4D_v(K+1)^2+\cdots \qquad (^3\Sigma \text{ state}) \quad (6)$$

$$\Delta_1 F_1(J)=R_1(J)-Q_1(J+1)={}^{R}Q_{21}(J)-{}^{Q}P_{21}(J+1)$$
$$=2B_v(J+1)-4D_v(J+1)^3+\cdots\cdots, \quad (X^2\Pi_{1/2}\text{ state}) \quad (7)$$
$$\Delta_1 F_2(J)=Q_2(J)-P_2(J+1)={}^{Q}R_{12}(J)-{}^{P}Q_{12}(J+1)$$
$$=2B_v(J+1)-4D_v(J+1)^3+\cdots\cdots, \quad (X^2\Pi_{3/2}\text{ state}) \quad (8)$$
$$\Delta_1 F(J)/J+1=2B_v-4D_v(J+1)^3+\cdots\cdots, \quad (X^2\Pi\text{ state}) \quad (9)$$

where $F_1(J)$ and $F_2(J)$ are the rotational energies of the $X^2\Pi_{1/2}$ and the $X^2\Pi_{3/2}$

Table 5. Wavenumbers of the Rotational

	(2-6)				(2-7)		
J	Q_2, ${}^{Q}R_{12}$	P_2, ${}^{P}Q_{12}$	R_1, ${}^{R}Q_{21}$	Q_1, ${}^{Q}P_{21}$	Q_2, ${}^{Q}R_{12}$	P_2, ${}^{P}Q_{12}$	R_1, ${}^{R}Q_{21}$
$1/_2$	——		38017.6		——		36310.1
$1^1/_2$	37903.3		20.4		36194.6		13.3
$2^1/_2$	06.9	37894.1	23.9	38012.4	98.5		17.3
$3^1/_2$	11.3		28.7		36203.4	86.9	22.3
$4^1/_2$	15.2		34.2	15.1	08.7	88.4	27.8
$5^1/_2$	20.7	97.4	40.1	17.6	14.1	90.8	34.0
$6^1/_2$	27.1	37900.1	46.6	20.4	20.5	93.4	40.9
$7^1/_2$	34.2	03.3	54.9	23.9	27.6	96.7	48.8
$8^1/_2$	42.0	06.9	63.7	28.7	35.8	36200.9	57.8
$9^1/_2$	50.2	11.5	73.2	34.2	44.6	05.7	67.3
$10^1/_2$	59.5	16.8	83.0	40.1	54.0	11.2	77.8
$1^1/_2$	69.2	22.5	93.5	46.6	64.0	17.5	88.5
$2^1/_2$	79.3	29.2	38104.9	53.9	75.1	24.2	36400.3
$3^1/_2$	90.3	36.4	17.0	62.0	86.7	32.1	13.2
$4^1/_2$		44.1	30.1	71.3	98.8	40.6	26.8
$5^1/_2$	15.1	52.8	43.9	81.0	36311.7	49.6	41.2
$6^1/_2$	28.7	61.8	58.2	91.4	25.4	59.4	55.6
$7^1/_2$	41.6	72.1	73.0	38102.9	40.9	69.8	71.3
$8^1/_2$	55.9	82.5	89.2	15.3	55.2	81.4	88.0
$9^1/_2$	71.3	93.6	38205.9	27.6	71.6	93.3	36505.6
$20^1/_2$	87.2			41.3	88.5	36305.7	23.7
$1^1/_2$		38017.6		55.3	36404.7	19.6	42.5
$2^1/_2$				70.6	23.6	34.0	62.0
$3^1/_2$					42.2	48.8	82.5
$4^1/_2$					61.6	64.0	
$5^1/_2$					81.4		
$6^1/_2$					36502.8		
$7^1/_2$					23.7		
$8^1/_2$							
$9^1/_2$							
$30^1/_2$							
$1^1/_2$							
$2^1/_2$							
$3^1/_2$							
$4^1/_2$							
$5^1/_2$							

* This band is (1-5) band of the ε-system.

states respectively. The $\Delta_1 F$ values obtained are listed in Tables 6, 7 and 8.

In the rotational analysis above described the Λ-type doubling of the $X^2\Pi$ state has thus far been neglected, but this doubling should be considered for deriving accurate rotational constants. If the splitting due to the Λ-type doubling is designated as $z(J)$ and the rotational energy having no Λ-type doubling as $F(J)$, the rotational energies of the $X^2\Pi$ state are given by the formulae,

Lines of (2–6), (2–7), (2–8) and (5–5)* γ-Bands.

	(2–8)				(5–5)	
Q_1, $^QP_{21}$	Q_2, $^QR_{12}$	P_2, $^PQ_{12}$	R_1, $^RQ_{21}$	Q_1, $^QP_{21}$	Q_2, $^QR_{12}$	P_2, $^PQ_{12}$
	——		34630.2		——	
	34515.1		34.3		46359.0	
	18.6		38.3		62.6	
36305.3	23.4		42.6		66.7	56350.4
07.9	29.6		47.9	34628.3	71.9	
10.1	35.7	34512.0	54.1	30.8	77.2	53.8
13.3	42.2	15.1	61.4	34.3	83.3	56.0
17.3	49.8	18.6	69.8	38.3	90.1	59.0
22.3	58.2	23.2	79.1	43.9	98.3	63.0
27.8	67.2	28.3	88.8	49.5	46406.7	67.1
34.0	76.9	34.1	99.3	56.4	15.8	72.7
40.9	87.6	40.7	34710.9	64.0	25.5	78.1
48.8	98.9	47.6	23.2	72.5	36.0	85.2
57.8	34610.5	56.1	35.9	81.7	47.9	92.3
67.3	23.3	64.8	49.9	91.7	59.7	46400.7
77.8	37.1	74.7	64.7	34702.5	71.7	09.7
88.5	51.6	85.1	80.3	13.9	85.3	18.1
36400.3	66.7	96.2	96.6	26.5	99.5	28.5
13.2	82·2	34608.3	34813.9	39.9		28.6
26.8	99.2	20.8	31.8	53.8		38.6
41.2	34716.2	34.3	50.7	69.0		49.6
55.6	53.7	48.2	70.2	84.5		
71.3	72.8	64.0	89.4	34801.2		
88.0		79.1		18.6		
36505.6		96.5		36.7		
23.7		34713.8		55.8		
42.5		31.4		75.9		
62.0		49.9				
82.5		69.0				

Table 6. $\Delta_1 F$ values of the $X\Pi_{3/2}$ State*.

J \ v	0	1	2	3	4	5	6	7	8
$^1/_2$									
$1^1/_2$									
$2^1/_2$			11.6			12.2		11.6	
$3^1/_2$			15.6			15.6		15.0	
$4^1/_2$	19.2	18.5	18.4	18.4	18.2	18.1	17.8	17.9	17.6
$5^1/_2$	22.4	22.0	21.8	21.7	21.5	21.2	20.8	20.7	20.5
$6^1/_2$	25.9	25.6	25.3	25.1	24.7	24.4	24.0	23.8	23.6
$7^1/_2$	29.2	28.9	28.6	28.5	28.2	27.5	27.3	26.7	26.6
$8^1/_2$	32.9	32.2	31.8	31.6	31.3	31.1	30.6	30.1	29.9
$9^1/_2$	36.2	35.8	35.5	34.9	34.5	34.1	33.6	33.4	33.7
$10^1/_2$	39.6	39.1	38.5	38.5	37.9	37.3	37.0	36.5	36.2
$1^1/_2$	43.0	42.4	42.2	41.8	41.1	40.4	40.1	39.8	40.0
$2^1/_2$	46.3	45.9	45.6	45.0	44.1	43.8	43.2	43.0	42.8
$3^1/_2$	49.9	49.0	48.7	48.3	47.5	47.2	46.5	46.1	45.7
$4^1/_2$	53.3	52.6	52.1	51.6	51.0	50.4	49.8	49.2	48.6
$5^1/_2$	56.6	56.0	55.7	54.9	54.2	53.6	53.1	52.3	52.0
$6^1/_2$	59.8	59.5	58.8	58.3	57.4	57.1	56.4	55.6	55.4
$7^1/_2$	63.3	62.7	62·2	61.6	60.9	60.9	59.4	59.5	58.4
$8^1/_2$	66.6	66.2	65.3	64.7	64.0	63.4	62.6	61.9	61.4
$9^1/_2$	70.0	70.1	69.0	68.1	67.0	66.4	66.1	65.9	64.9
$20^1/_2$	73.8	73.7	72.2	71.4	70.4	70.0	69.4	68.9	68.0
$1^1/_2$	77.2	76.2	75.8	74.8	73.6	....	71.5	70.7	....
$2^1/_2$	80.6	79.5	78.7	78.1	77.0	75.6	74.8	74.8	74.6
$3^1/_2$	83.7	82.9	81.7	80.9	80.2	79.2	78.3	78.2	76.3
$4^1/_2$	87.5	85.9	85.3	84.3	83.9	82.2	81.7		
$5^1/_2$	90.4	89.5	88.5	87.3	86.5	85.8	85.5		
$6^1/_2$	94.0	92.9	92.2	90.9	89.9	88.7	88.2		
$7^1/_2$	97.3	96.2	95.2	95.4	93.1	92.4	91.4		
$8^1/_2$	100.7	99.5	98.9	98.3	96.0	95.4	94.9		
$9^1/_2$	104.0	103.0	101.8	100.8	99.0	98.0	97.7		
$30^1/_2$	107.3	106.3	105.2		102.5	101.3	101.4		
$1^1/_2$	111.3	109.8	108.1		105.7	104.7	103.9		
$2^1/_2$	114.4	112.9	112.0		108.9	107.9			
$3^1/_2$	117.3	116.3	115.1						
$4^1/_2$	121.1	119.3	118.1						
$5^1/_2$	124.5	123.0	121.2						
$6^1/_2$	127.6	126.0							
$7^1/_2$	130.5	129.4							
$8^1/_2$	134.8	132.7							
$9^1/_2$									
$40^1/_2$									

* This $\Delta_1 F(J)$ means $\Delta_1 F(J)+[z_2(J+1)+z_2(J)]/2$.

Table 7. Δ_1F values of the $X^2\Pi_{1/2}$ State**.

J	0	1	2	3	4	5	6	7*	8
$^1/_2$									
$1^1/_2$									
$2^1/_2$				11.3		11.2	11.6	11.6	
$3^1/_2$				14.8		13.8	14.4	14.4	14.1
$4^1/_2$		18.2	18.5	18.3	17.5	16.8	17.1	17.7	17.1
$5^1/_2$		21.8	21.4	21.4	20.9	20.9	21.2	20.7	19.7
$6^1/_2$		24.8	24.6	24.6	24.0	24.0	23.9	23.6	22.7
$7^1/_2$	28.3	28.4	27.9	27.8	27.5	26.8	27.1	26.5	25.8
$8^1/_2$	32.1	31.4	31.3	30.8	30.7	30.3	30.0	30.0	29.6
$9^1/_2$	....	34.8	34.5	34.1	33.6	33.3	33.3	33.3	32.3
$10^1/_2$	38.7	38.0	37.7	37.6	37.2	36.6	36.5	36.9	35.2
$1^1/_2$	41.9	41.3	41.1	40.6	40.3	40.2	39.6	39.7	38.2
$2^1/_2$	44.6	44.8	44.5	43.9	43.3	42.9	42.9	42.5	41.2
$3^1/_2$	48.7	48.2	47.6	47.2	46.7	46.1	45.7	45.9	44.1
$4^1/_2$	51.9	51.4	50.9	50.4	49.9	49.3	49.1	49.0	47.4
$5^1/_2$	55.3	54.7	54.2	53.7	53.2	52.5	52.8	52.7	50.9
$6^1/_2$	58.5	57.9	57.4	56.9	56.2	55.8	55.4	55.3	53.9
$7^1/_2$	62.0	61.3	60.7	60.3	59.7	59.0	58.3	58.1	56.7
$8^1/_2$	65.2	64.6	64.0	63.2	62.7	62.0	61.8	61.2	60.1
$9^1/_2$	68.7	67.9	67.0	66.5	65.8	65.2	64.3	64.4	62.8
$20^1/_2$	71.6	71.2	70.9	69.7	69.2	68.4	68.3	68.1	66.2
$1^1/_2$	75.4	74.6	73.7	73.0	72.3	71.4	71.3	71.2	69.0
$2^1/_2$	78.8	77.9	77.2	76.1	75.6	74.6	74.4	74.0	
$3^1/_2$	82.1	81.1	80.2	79.4	78.8	77.8	77.5	76.9	
$4^1/_2$	85.4	84.5	83.6	82.5	81.8	80.7	80.2		
$5^1/_2$	88.8	87.9	86.8	85.7	84.8	84.1	83.6		
$6^1/_2$	92.1	91.0	90.2	89.0	88.0	87.0	86.4		
$7^1/_2$	95.6	94.2	93.6	92.1	91.4	90.4	89.7		
$8^1/_2$	98.7	97.7	96.8	95.5	94.4	93.4	93.2		
$9^1/_2$	102.1	100.8	99.9	98.9	97.7	96.7	95.9		
$30^1/_2$	105.4	104.4	103.0		100.7	99.8	99.0		
$1^1/_2$	108.9	107.7	106.0		103.7		102.0		
$2^1/_2$	111.8	110.9	109.2						
$3^1/_2$	115.2	114.2	112.9						
$4^1/_2$	118.3	117.5	115.7						
$5^1/_2$	121.5	120.5							
$6^1/_2$	124.5	123.5							
$7^1/_2$		127.2							
$8^1/_2$		130.5							
$9^1/_2$		133.6							
$40^1/_2$		163.7							

* R_1 branch overlap to Q_1 branch and so this Δ_1F value calculated from them has no good accuracy.

** This $\Delta_1F(J)$ means $\Delta_1F(J)+[z_1(J+1)+z_1(J)]/2$.

Table 8. Δ_1F values of the $D^2\Sigma$ and $A^2\Sigma$ States.

K \ v	0	1	2	3	4(0)*	5(1)*	K \ v	0	1	2	3	4(0)*	5(1)*
0							21	87.3	86.5	85.6	84.6	86.6	
							2	91.4	90.5	89.5		90.0	
1							3	95.2	94.3	93.1		95.4	
2							4	99.1	98.2	96.9			
3	15.8	16.0	15.8			16.3	5	103.0	102.1	100.5			
4	20.0	19.8	19.6										
5	23.9	23.6	23.5		23.9	23.4	6	106.9	105.8	104.5			
							7	111.0	109.8	107.8			
6	27.7	27.6	27.3	27.1	27.7	27.3	8	114.9	113.7				
7	31.8	31.6	31.3	31.0	31.8	31.3	9	118.8	117.6				
8	35.8	35.5	35.1	34.9	35.8	35.4	30	122.5	121.4				
9	39.7	39.5	39.0	38.6	40.4	39.6							
10	43.7	43.3	42.8	42.4	43.9	43.1	1	126.4	125.4				
							2	130.5	129.2				
1	47.7	47.2	46.8	46.6	48.2	47.4	3	134.5	133.0				
2	51.7	51.2	50.8	50.4	51.8	50.8	4	138.3					
3	55.7	55.1	54.7	54.2	55.7	55.6	5	142.1					
4	59.6	59.0	58.5	58.2	59.6	59.0							
5	63.6	63.0	62.4	61.6	63.7	62.5	6	145.7					
6	67.7	66.9	66.4	65.5	67.6	67.0							
7	71.5	70.8	70.1	69.3	71.8	71.0							
8	75.3	74.7	73.9	73.3	76.2	75.0							
9	79.4	78.6	77.9	79.6	79.6								
20	83.5	82.6	81.7	81.1	82.8								

* Vibrational quantum number of $D^2\Sigma$ state.

$$F(J)=B_v[J(J+1)-\Omega^2+S(S+1)-\Sigma^2]-D_vJ^2(J+1)^2+\cdots\cdots \tag{10}$$

$$F_e(J)=F(J)+\Phi_e(J), \qquad F_d(J)=F(J)+\Phi_d(J) \tag{11}$$

$$z_1(J)=\Phi_{1e}-\Phi_{1d} \qquad \text{for } X^2\Pi_{1/2} \text{ state}$$

$$z_2(J)=\Phi_{2d}-\Phi_{2e} \qquad \text{for } X^2\Pi_{3/2} \text{ state} \tag{12}$$

where $\Phi(J)$ is the shift due to Λ-type doubling. We can let

$$z(J+1)+z(J-1)\fallingdotseq 2z(J)\,. \tag{13}$$

The Δ_1F values of the upper and the lower states can be obtained from the following combination relations;

for upper $A^2\Sigma$ state,

$$\Delta_1F(K)+z_1(J)=R_1(J)-Q_1(J)={}^RQ_{21}(J)-{}^QP_{21}(J) \tag{14}$$

$$\Delta_1F(K)-z_1(J-1)={}^SR_{21}(J-1)-{}^RQ_{21}(J-1) \tag{15}$$

$$\Delta_1F(K)-z_1(J+1)=Q_1(J+1)-P_1(J+1) \tag{16}$$

$$\Delta_1F(K)+z_2(J)=Q_2(J)-P_2(J)={}^QR_{12}(J)-{}^PQ_{12}(J) \qquad K=J-1/2 \tag{17}$$

$$\Delta_1F(K)-z_2(J-1)=R_2(J-1)-Q_2(J-1) \tag{18}$$

$$\Delta_1F(K)-z_2(J+1)={}^PQ_{12}(J+1)-{}^OP_{12}(J+1) \tag{19}$$

$$\Delta_1F(K)=2B_v(K+1)-4D_v(K+1)^3 \tag{20}$$

for lower $X^2\Pi$ state

$$\Delta_1F_1(J)+\Phi_{1e}(J+1)-\Phi_{1d}(J)=R_1(J)-Q_1(J+1)={}^RQ_{21}(J)-{}^QP_{21}(J+1)$$
$$\fallingdotseq\Delta_1F_1(J)+[z_1(J+1)+z_1(J)]/2 \quad (21)$$

$$\Delta_1F_1(J)+\Phi_{1d}(J+1)-\Phi_{1e}(J)={}^QE_{21}(J)-{}^RQ_{21}(J+1)=Q_1(J)-P_1(J+1)$$
$$\fallingdotseq\Delta_1F_1(J)-[z_1(J+1)+z_1(J)]/2 \quad (22)$$

$$\Delta_1F_2(J)+\Phi_{2d}(J+1)-\Phi_{2e}(J)=Q_2(J)-P_2(J+1)={}^QR_{12}(J)-{}^PQ_{12}(J+1)$$
$$\fallingdotseq\Delta_1F_2(J)+[z_2(J+1)+z_2(J)]/2 \quad (23)$$

$$\Delta_1F_2(J)+\Phi_{2e}(J+1)-\Phi_{2d}(J)=R_2(J)-Q_2(J+1)={}^PQ_{21}(J)-{}^QP_{12}(J+1)$$
$$\fallingdotseq\Delta_1F_2(J)-[z_2(J+1)+z_2(J)]/2 \quad (24)$$

$\Delta_1F(K)\pm z_1(J)$ and $\Delta_1F(K)\pm z_2(J)$ of the $A^3\Sigma$ state and $\Delta_1F(J)\pm[z(J+1)+z(J)]/2$ of the $X^2\Pi$ state obtained according to above combination relation are shown in Tables 6, 7, 9, 10 and 11.

The spliting due to the Λ-type doubling could be obtained from the above combination defects, for example,

$$z_1(J+1)+z_1(J)=[R_1(J)-Q_1(J+1)]-[Q_1(J)-P_1(J+1)] \quad (25)$$
$$z_2(J+1)+z_2(J)=[Q_2(J)-P_2(J+1)]-[R_2(J)-Q_2(J+1)]\,. \quad (26)$$

The upper state is $^2\Sigma^+$ or $^2\Sigma^-$ according to whether the sign of these defects are positive or negative. According to these relation the Λ-type doubling of the $X^2\Pi$ state was calculated from the values of Tables 6, 7 and 11, in which the $\Delta_1F(J)\pm[z(J+1)+z(J)]/2$ values of the $X^2\Pi$ state are listed. Thus, it was recognized that (a) the sign of the defect was positive as expected and (b) the Λ-type doubling of the $X^2\Pi_{3/2}$ state is smaller than that of the $X^2\Pi_{1/2}$, but the experimental error was too large for obtaining smooth curves from them. Therefore, to obtain good results, the $\Delta_1F(K)\pm z$ values of the $v=0$ level of the $A^3\Sigma$ state was taken, since a large number of the band due to transition from this level were observed, and moreover these bands were well developed. The bands used were the (0-0), (0-1), (0-2), (0-3), (0-4), and (0-5) bands. The values of $\Delta_1F(K)+z(J)$, $\Delta_1F(K)-z_1(J)$ and $\Delta_1F(K)-z_2(J)$ of these band are listed in Tables 12, 13 and 14 respectively. The average values of them obtained under the assumption that in the present experimental accuracy the Λ-type doubling does not vary with the vibrational quantum number are shown in the last column of each Table. They together with $z(J)$ and $\Delta_1F(K)$ values obtained from them are summarized in Table 15. It would be recognized from Table 15 or Fig. 6 that the Λ-type doubling of the $X^2\Pi_{3/2}$ state is negligibly small but that of the $X^2\Pi_{1/2}$ state, though also small, is not negligible, the magnitude increasing almost linearly with the rotational quantum number. These facts agree qualitatively with the theoretical results in the Hund case a, the Λ-type doubling of the $^2\Pi_{1/2}$ component varying linearly with J, whereas for the $^2\Pi_{3/2}$ component it

varies with the third power of J and for small J is very small compared to that of $^2\Pi_{1/2}$.

To calculate the $\Delta_1F(K)$ values of the $A^2\Sigma$ state or the $\Delta_1F(J)$ values of the $X^2\Pi$ state, the average values between $[\Delta_1F(K)+z(J)]$ and $[\Delta_1F(K)-z(J)]$ or $\{\Delta_1F(J)+[z(J+1)+z(J)]/2\}$ and $\{\Delta_1F(J)-[z(J+1)+z(J)]/2\}$ have been taken and these values are shown in Tables 16 and 17. In the case of the $A^2\Sigma$ state, these values obtained from the sub-bands corresponding to the $A^2\Sigma-X^2\Pi_{3/2}$ and the $A^2\Sigma-X^2\Pi_{1/2}$ transitions should be equal. In the last column of Table 15, their difference in the $v=0$ level are shown and these show that the two average values coinside in experimental errors.

The rotational constants B_v and D_v were obtained from the Δ_1F values in Tables 16 and 17, using the graphical method[14], and the values are listed in Table 18. In the case of B_4', B_5', B_7'' and B_6'', the values of Δ_1F listed in Tables 6, 7 and 8 were used. In this case, the error which comes from the Λ-type doubling might be negligibly small, because the above Δ_1F values had not been obtained for high rotational quantum number, and the error entering into Δ_1F only corresponded to $z_1/2$ in the case of the $A^2\Sigma$ state.

Even the Λ-type doubling of the high rotational lines of the $X^2\Pi_{1/2}$ state amount to only a small value of 0.5 cm^{-1}, so that it might safely be said that the rotational constants can be calculated in good approximation from the Δ_1F values in Tables 6, 7 and 8 obtained by combinations of $(R_1, {}^RQ_{21})$ and $(Q_1, {}^QP_{21})$ or $(Q_2, {}^QR_{12})$ and $(P_2, {}^PQ_{12})$.

The orthodox method to calculate the rotational constant of the $A^2\Sigma$ state is to use the following combination relations;

$$\Delta_2F(K)={}^SR_{21}(J)-{}^QP_{21}(J)=R_2(J)-P_2(J)=4B_v(K+1/2)-8D_v(K+1/2)^3 \quad K=J+1/2\,, \tag{27}$$

$$\Delta_2F(K)=R_1(J)-P_1(J)={}^QR_{12}(J)-{}^OP_{12}(J)=4B_v(K+1/2)-8D_v(K+1/2)^3 \quad K=J-1/2\,. \tag{28}$$

These Δ_2F relations were used in the case of the $v=0$ level, as an example, and the Δ_2F values are listed in the last column of Table 16. The B_0 and D_0 values obtained from those are 1.98_8 cm^{-1} and 6×10^{-6} cm^{-1}, and the latter value is smaller by 1×10^{-6} cm^{-1} than that obtained from the Δ_1F values but such difference may be considered as experimental error.

The wavenumbers of the band origins (not to $J=0$ but $F(J)=0$) are listed in Table 1.

The vibrational energies $G(v)$ and $\Delta G_{v+1/2}$ are given by the following formulae,

14) G. Herzberg: Molecular Spectra and Molecular Structure, vol. 1 (1950), p. 168.

Table 9. $\Delta_1F(K)\pm z_2(J)$* Values of $A^3\Sigma$ State.

	$\Delta_1F(K)+z_2(J)$						$\Delta_1F(K)-z_2(J)$			
v / K	0	1	2	3	4(0)	5(1)	0	1	2	3
0										
1										
2							11.9			
3	15.8	16.1	16.5			16.3	15.7	15.3		
4		20.1	19.9				19.8	19.4		
5	23.8	24.0	23.5			23.4	23.7	23.6	23.1	
6	27.7	27.5	27.1	27.1	27.8	27.3	27.6	27.3	27.2	27.1
7	31.7	31.6	31.2	30.7	31.9	31.3	31.8	31.4	31.0	29.8
8	35.7	35.3	35.0	34.7	36.1	35.4	35.7	35.5	34.9	34.7
9	39.8	39.5	38.9	38.4	40.3	39.6	39.6	39.5	39.0	38.9
10	43.6	43.2	42.7	42.4	44.2	43.1	43.6	42.9	42.9	42.7
1	47.8	47.0	46.7	46.5	48.0	47.4	47.8	47.1	46.6	47.0
2	51.6	51.1	50.7	50.3	51.4	50.8	51.7	51.3	50.8	50.0
3	55.5	55.0	54.6	53.7	55.5	55.6	55.4	55.0	54.3	53.6
4	59.5	59.0	58.4	57.8	59.5	59.0	59.6	58.8	57.7	60.4
5	63.5	62.9	62.4	61.4	63.5	62.5	63.6	62.8	62.3	
6	67.5	66.8	66.2	65.3	67.6	67.0	67.4	66.9	65.9	
7	71.1	70.7	70.2	69.0	71.8	71.0	71.2	70.5	70.1	69.6
8	75.2	74.5	73.8	73.0	76.3	75.0	75.3	74.6		72.1
9	79.3	78.7	78.0	76.3	79.7		79.3	78.5	78.1	76.9
20	83.4	82.8	81.6		82.7		83.3	82.1	81.6	80.4
1	87.2	86.6	85.3		86.6		87.0	86.5	85.5	
2	91.4	90.5	89.5		90.7		91.3	90.4		
3	95.1	94.1	93.2		95.4		95.1	93.8		
4	99.1	98.3	97.3				98.9	98.5		
5	102.8	102.1	100.3				103.0	102.1		
6	106.6	105.9	104.3				106.7	105.6		
7	110.9	109.4					110.7	109.3		
8	114.8	113.4					114.8	113.3		
9	118.7	117.6					118.5	117.4		
30	122.4	121.6					122.4	121.4		
1	126.4	125.3					126.4	124.5		
2	130.4	130.0					130.2	129.1		
3	134.6	132.5					134.2	132.4		
4	138.1	137.0					138.3	136.3		
5	141.9	140.8					141.9	140.4		
6	146.0						145.8			
7	150.0						149.7			
8	153.6						153.2			
9	158.1						157.4			
40							160.8			

* $z_2(J)$ means the Λ-type spliting of the $X^3\Pi_{3/2}$ state.

Table 10. $\Delta_1 F(K)\pm z_1(J)$* Values of $A^2\Sigma$ State.

	$\Delta_1 F(K)+z_1(J)$					$\Delta_1 F(K)-z_1(J)$			
K \ v	0	1	2	3	4(0)	0	1	2	3
0									
1									
2						12.4			
3	16.9	16.1	15.8			15.7	15.7	15.4	
4	20.4	19.6	19.5			20.0	19.8	19.6	
5	23.7	23.7	23.4		23.9	23.7	23.5	23.1	
6	27.8	27.7	27.3		27.5	27.6	27.6	27.2	26.6
7	31.8	31.6	31.2	31.3	31.9	31.8	31.5	31.3	30.2
8	35.9	35.7	35.1	35.0	35.8	35.5	35.5	34.9	34.8
9	39.8	39.5	39.2	38.8	40.4	39.5	39.3	39.2	
10	43.7	43.3	43.0	42.4	43.6	43.5	43.4	42.9	
1	47.7	47.4	46.9	46.7	48.3	47.4	47.0	46.5	46.4
2	51.7	51.2	50.9	50.4	52.2	51.7	50.7	50.5	
3	55.7	55.2	54.8	54.6	56.0	55.6	55.0	54.5	
4	59.7	59.2	58.3	58.5	59.8	59.3	58.9	57.9	57.2
5	63.6	63.2	62.6	62.0	64.1	63.3	63.2	62.7	61.8
6	67.8	66.9	66.5	65.9	69.0	67.6	66.8	66.1	65.1
7	71.7	70.9	70.1	69.7	72.0	71.3	70.5	69.8	69.2
8	75.5	75.0	74.0	73.8	76.1	75.0	74.7	73.6	72.8
9	79.6	78.7	77.6	77.4		79.1	78.6	77.4	77.1
20	83.6	82.5	81.7	81.1		82.9	82.4	81.6	80.8
1	87.4	86.6	85.7	85.4		87.0	86.2	85.2	
2	91.4	90.6	89.6	89.5		91.0	90.2		89.0
3	95.2	94.4	93.2	92.9		94.8	94.1	93.7	93.3
4	99.2	98.2	97.0	96.6		98.7	97.5		
5	103.0	102.2	100.8			102.7	102.0	100.6	98.8
6	107.0	106.0	105.0			106.5	105.4	103.8	102.8
7	111.0	110.1	107.8			110.5	109.4	107.0	
8	114.8	113.9	112.2			114.4	113.4		110.8
9	119.1	117.8				118.1	117.3		
30	122.7	121.6				122.1	120.9		
1	126.6	125.8				126.1	125.1		
2	130.6	129.1				130·4	128.4		
3	134.6	132.8				133.9	132.5		
4	138.4					137.6	136.6		
5	142.5					141.5	139.9		
6	145.8					145.8	144.0		
7	149.6					149.1	148.8		
8	154.3					153.1	152.6		
9	157.9					156.2			
40	161.5					160.8			

* $z_1(J)$ means the A-type spliting of the $X^2\Pi_{1/2}$ state.

Table 11. $\Delta_1F(J)-[x(J+1)+x(J)]/2$ Values of $X^3\Pi$ State.

$\Delta_1F_2(J)-[z_2(J+1)-z_2(J)]/2$ ($X^3\Pi_{3/2}$)								$\Delta_1F_1(J)-[z_1(J+1)+z_1)J)]/2$ ($X^3\Pi_{1/2}$)							
J \ v	0	1	2	3	4	5	6	J \ v	0	1	2	3	4	5	6
								1/2							
1 1/2				8.5				1 1/2		9.6					
2 1/2							11.1	2 1/2		11.1					
3 1/2		15.0	15.3	15.1				3 1/2		14.6	14.4	14.5	13.1	13.8	
4 1/2	18.5	18.5	18.2	18.1	18.0	18.0	17.6	4 1/2	18.2	17.5	18.0	17.8		16.8	17.4
5 1/2	22.0	21.9	21.7	21.3	21.3	21.1		5 1/2	21.3	21.5	21.4	20.8	20.8	20.6	20.2
6 1/2	26.0	25.6	25.4	24.8	24.8	24.3	23.7	6 1/2	24.8	24.6		24.3	24.0	23.5	22.5
7 1/2	28.8	28.7	28.8	28.1	28.0	27.4	27.1	7 1/2		27.8	27.7	27.4	26.9	26.9	26.4
8 1/2	32.8	32.2	31.8	31.4	31.2	31.1	30.6	8 1/2	31.8	31.2	31.0	30.8	30.4	29.9	29.5
9 1/2	36.0	35.6	35.3	34.9	34.5	34.1	33.4	9 1/2	33.9	34.7	34.2	33.9	33.3	32.9	33.1
10 1/2	39.5	39.2	38.1	38.4	37.9	37.6	36.6	10 1/2	39.0	37.9	37.5	37.3	37.2	36.4	
1 1/2	43.1	42.4	42.5	41.7	41.0	40.4	40.2	1 1/2	41.9	41.5	40.8	40.5	40.0	39.5	38.8
2 1/2	46.4	45.9	45.2	44.7	44.1	43.9	43.3	2 1/2	44.5	44.6	44.2	43.4	42.8	42.9	41.5
3 1/2	49.9	49.3	48.3	48.0	47.5	46.8	46.7	3 1/2	48.3	48.0	47.4	46.9	46.2	45.3	45.4
4 1/2	53.1	52.6	52.1	51.6	50.9	49.7	49.4	4 1/2	51.5	51.0	50.9	50.3	49.4	48.7	48.8
5 1/2	56.7	56.0	55.3	54.9	54.6	53.1	52.9	5 1/2	55.1	54.6	54.1	53.5	53.1	52.3	52.6
6 1/2	59.9	59.4	58.9	57.9	57.0	56.9	56.3	6 1/2	58.2	57.6	56.9	57.1	55.8	55.2	54.6
7 1/2	63.4	62.7	62.0		60.4	60.5	59.1	7 1/2	61.9	61.3	60.2	59.8	59.2	58.9	57.6
8 1/2	66.5	65.8	65.8	65.0	63.9	63.3	62.3	8 1/2	64.9	64.3	63.5	62.5	62.3	61.4	60.9
9 1/2	70.1	69.3	69.0	68.0	66.9	66.3	65.2	9 1/2	68.6	68.0	66.6	66.1	65.5	64.6	63.6
20 1/2	73.4	73.0	71.9	71.3	70.2	69.6	68.9	20 1/2	71.5	70.8	70.4	69.3	69.1	68.2	
1 1/2	77.1	76.1	75.7	74.5	74.0	72.5	71.7	1 1/2	75.2	74.1	73.2	72.7	72.1	71.4	71.1
2 1/2	80.6	79.2	78.7	77.8	77.2	75.8	74.7	2 1/2	78.6	77.6	76.8	75.5	75.1	74.2	73.5
3 1/2	83.9	82.7	82.1	81.0	79.9	79.5	78.5	3 1/2	81.6	80.6	80.3	79.2	78.4	77.7	
4 1/2	87.2	86.0	85.5	84.4			81.7	4 1/2	84.9	84.3	82.3	82.3	81.4		79.1
5 1/2	90.3	89.8	88.5	87.7		85.5	85.1	5 1/2	88.3	87.3	86.5	85.5	84.4	84.0	
6 1/2	93.7	92.5		90.5			88.1	6 1/2	91.4	90.7	89.7	88.7	87.5	86.7	
7 1/2	97.5	95.9	94.8	94.1		92.1	91.2	7 1/2	95.0	94.2		91.9	90.8	89.8	88.8
8 1/2	100.6	99.4	98.4	97.3		95.0	93.7	8 1/2	98.0	97.2	95.7	95.2	94.0	93.0	92.3
9 1/2	103.7	102.6	101.4			98.2	97.6	9 1/2	101.5	100.1		98.4	97.4		95.2
30 1/2	107.3	106.0	105.2	104.4		101.2		30 1/2	105.1	103.7	103.0	101.4		99.5	
1 1/2	110.8	109.4		107.4		104.7	103.8	1 1/2	107.7	107.4	105.6	104.5			
2 1/2	114.2	111.9	111.6	110.5				2 1/2	111.3	110.2	109.1	108.4		105.2	
3 1/2	117.3	116.3	115.7	113.8				3 1/2	114.6			111.1		108.8	
4 1/2	120.6		117.9	116.6				4 1/2	118.0	116.3	115.2	114.1			
5 1/2		122.6	121.2	120.1				5 1/2	121.5	119.7		117.3			
6 1/2		125.7						6 1/2		123.5					
7 1/2		129.0						7 1/2		126.5					
8 1/2		132.0						8 1/2		129.3					
9 1/2		135.6						9 1/2		132.2					
40 1/2								40 1/2		136.0					

Table 12. $\Delta_1F(K)+z_2(J)$ Values of the $v=0$ Level of $A^2\Sigma$ State.

	$\Delta_1F(K)+z_2(J)$							$\Delta_1F(K)+z_1(J)$						
$v'-v''$ / K	0–0	0–1	0–2	0–3	0–4	0–5	aver-age	0–0	0–1	0–2	0–3	0–4	0–5	aver-age
0														
1														
2														
3		15.9	15.8			15.8	15.8			17.2*	16.7		16.7	16.7
4										21.0	19.9		20.2	20.4
5	24.3	23.7	23.8	23.9	23.5	23.7	23.8		24.0	24.0	23.1		23.8	23.7
6	27.8	27.6	27.7	27.8	27.6	27.4	27.7	27.6	27.9	28.2	27.5	26.9	28.4	27.8
7	31.7	31.8	31.7	31.7	31.5	31.9	31.7		31.5	31.9	31.9			31.8
8	36.0	35.5	35.6	36.0	35.7	35.6	35.7	36.0	36.1	36.0	35.7	35.7	36.1	35.9
9	79.7	39.8	40.5	39.5	39.6	39.4	39.8	40.1*	39.6	39.9	40.0	39.8	40.0	39.8
10	43.8	43.6	43.2	43.9	43.6	43.3	43.6	43.3	43.7	43.7	43.6	44.1	43.8	43.7
1	47.9	47.7	47.7	47.8	48.1	47.5	47.8	46.4*	47.4	47.8	47.8	47.8	47.6	47.7
2	51.6	51.5	51.6	51.9	51.5	51.7	51.6	51.3	51.4	51.6	52.2	51.8	52.2*	51.7
3	55.3	55.4	55.7	55.8	55.4	55.6	55.5	55.6	55.5	55.7	55.8	55.7	55.6	55.7
4	59.9	59.3	59.5	59.7	59.6	59.5	59.6	59.6	59.0	59.7	59.8	59.5	59.7	59.7
5	63.2	63.6	63.5	63.7	63.7		63.5	63.9	63.0	63.5	63.4	63.9	64·0	63.6
6	67.2	67.5	67.5	67.6	67.5		67.5	68.1	67.7	67.9	67.9	67.4	67.9	67.8
7	70.2	71.2	71.5	71.6	71.0		71.1	71.4	71.4	71.8	71.4	72.0	71.9	71.7
8	75.1	75.5	75.3		75.0	75.1	75.2	75.6	75.2	75.4	75.5	75.7	65.6	75.5
9	78.9	79.4	79.4	79.7	78.9	79.4	79.3	79.6	79.1	79.6	79.4	79.4	79.5	79.6
20	83.6	83·4	83.3	83.5	83.3	83.5	83.4	83.6	83.3	83.7	83.5	83.1	83.7	83.5
1	87.0	87.1	87.3	87.4	87.1	87.4	87.2	87.3	87.3	87.4	87.5	87.5	87.4	87.4
2	91.3	91.4	91.5	91.5	91.2	91.5	91.4	91.7	91.5	91.4	91.2	91.6	91.0	91.4
3	95.1	94.8	95.0	95.2	95.3		95.1	95.4	95.2	95.0	95.3	95.2	95.1	95.2
4	99.1	99.2	98.6		99.3		99.1	99.4	99.2	98.9	99.2	99.2	99.1	99.2
5	103.1	102.0	102.8	103.1	103.0		102.8	103.2	103.2	103.1	103.0	102.9	102.6	103.0
6	106.7	106.0	106.9		106.7		106.6	107.2	107.1	106.9	107.2	106.9	106.5	107.0
7	110.9	110.7	111.0	111.1	110.6		110.9	111.3	110.7	111.3	110.9	110.9	110.7	111.0
8	115.0	114.6	114.9	114.6	114.8		114.8	115.0	114.7	115.1	114.7	114.8	114.8	114.8
9	118.8	118.5	118.9	119·3	117.9		118.7	118.7	118.8	118.8	118.9	118.7	120.5	119.1
30	122.5	122.7	122.5	122.4	122.1		122.4	122.7	122.9	122.8	122.3	122.6	122.6	122.7
1	126.8	126.6	126.1	126.2	126.2		126.4	126.9	126.7	126.2		126.4		126.6
2	130.8	130.5	130.5	129.8	130.3		130.4	130.8	130.7	130.3	130.9	130.2		130.6
3	134.4	134.7	134.6	134.5			134.6	134.9	134.4	134.4	134.4	135.0		134.6
4	138.5	137.9	138.1	138.2			138.1	138.3	138.6	138.2				138.4
5		141.8	141.9	142.0			141.9	142.4	142.6		142.4			142.5
6		146.3	145.7				146.0		145.8					145.8
7		150.0					150.0		149.6					149.6
8		153.6					153.6		154.3					154.3
9		158.1					158.1		157.9					157.9
40									161.5					161.5

Table 13. $\Delta_1F(K)-z_1(J)$ Values of the $v=0$ Level of $A^3\Sigma$ State.

$v'-v''$ / K	0-0		0-1		0-2		0-3		0-4		0-5		
	$^sR_{21}-R_1$	Q_1-P_1	$^sR_{21}-R_1$	Q_1-P_1	$^sR_{21}-R_1$	Q_1-P_1	$^sR_{21}-R_1$	Q_1-P_1	$^sR_{21}-R_1$	Q_1-P_1	$^sR_{21}-R_1$	Q_1-P_1	average
0													
1													
2			12.6				12.2						12.4
3			15.8		15.6*	16.9*	16.0		15.4				15.7
4			19.5	19.5	20.0	19.5	20.5		20.7		19.3*	20.0	20.0
5			23.3	23.5	23.6	24.1*	24.0		24.0			22.9*	23.7
6				28.0	27.9	27.5*	27.4	27.7		27.2			27.6
7	31.0		31.8	31.0*	33.0*	31.6		31.9		31.7		32.1	31.8
8	34.8			35.7	35.9	36.2	35.0	35.4				35.2	35.5
9	39.0		39.3	39.5		39.5	40.1	39.4		39.7	39.6	39.1	39.5
10	43.5		43.7	43.5	44.2	43.4	42.9	43.1		43.6	43.9	43.8	43.5
1	47.2		47.3	47.5	47.3	48.8*	48.1	47.1			46.6*		47.4
2	52.1	51.2	51.5	51.6	51.4	51.5	51.9	51.5			52.7	50.8*	51.7
3	55.4	55.3	55.7	55.4	55.4	55.6	55.3			56.2	55.8	54.7*	55.6
4	58.9	59.1	59.2	59.3	60.4*	59.4	59.6	59.8		59.2	59.1	58.7*	59.3
5	63.0	63.4	63.1	63.3	63.2	63.5	63.2	63.7	63.2	63.2	64.5*	63.3	63.3
6	67.2	66.9*	67.3	67.6	67.6	68.0	67.1	68.2	67.3	67.6	67.6	67.2*	67.6
7	70.9	71.3		71.5	71.0	72.8*	71.7	71.3	71.3	70.8*		72.5*	71.3
8	74.9	74.8	75.3	75.4	75.1	74.7	74.9	74.7*	74.7	74.7	75.5		75.0
9	79.0	79.0	78.8	79.4	79.1	79.7	78.3*	79.2	79.2	79.8		78.8	79.1
20		82.9	83.7	82.8	82.8	83.7		82.9	82.5	82.6	82.6		82.9
1		86.7	87.0	86.8	86.4	86.9	86.9	87.0		87.4	87.2	87.8	87.0
2		91.0		91.6		91.1	90.7	90.3		91.4	90.7	91.4*	91.0
3		94.4	94.5	94.5		95.3	94.9	95.0		95.1		95.3*	94.8
4	98.6	98·8	98.7	98.8		97.7*	98.8	98.6		98.9			98.7
5	103.3	102.6	102.3	101.9		102.5	102.6	102.5		102.8			102.7
6		106.3	106.4	106.6		107.0	106.7	106.6		106.4			106.5
7	110.4	110.8	110.4	110.7		112.4*	110.3	110.4		110.5			110.5
8				114.2		114.0	114.5	114.8		114.5			114.4
9		118.2		118.1			118.1	118.1		118.0			118.1
30	122.2	122.4		122.2		122.8	122.0	121.9		121.5			122.1
1		125.8		126.4		125.8	126.2	126.4					126.1
2		130.0		130.0		130.2		131.2					130.4
3		134.2				134.0	133.9	113.6					133.9
4		138.0		137.4		137.7		138.1					137.6
5				141.8		141.1							141.5
6				145.8									145.8
7				149.1									149.1
8				153.1									153.1
9				156.2									156.2
40				160.8									160.8

Table 14. $\Delta_1F(K)-z_2(J)$ Values of the $v=0$ Level of $A^3\Sigma$ State.

$v'-v''$ / K	0-0		0-1		0-2		0-3		0-4		0-5		
	R_2-Q_2	$P_{2^-}{}_{P_{12}}$	R_2-Q_2	$P_{2^-}{}_{P_{12}}$	R_2-Q_2	$P_{2^-}{}_{P_{12}}$	R_2 Q_2	$P_{2^-}{}_{P_{12}}$	R_2-Q_2	$P_{2^-}{}_{P_{12}}$	R_2-Q_2	$P_{2^-}{}_{P_{12}}$	average
0													
1													
2				11.6		12.2	12.0						11.9
3						16.1	15.2*		15.3				15.7
4		19.9		19.6		19.6	19.8			20.0			19.8
5	23.6	23.9	23.9	23.7		23.6	24.7*		23.3	23.9	23.3	23.7	23.7
6	27.4	27.9		27.3	27.4	27.9		28.1*	27.3	27.8		26.6*	27.6
7	32.0	32.5*	32.1	32.0	31.9	32.4	31.2	31.5	32.0	31.8	31.4		31.8
8	35.9	35.6	35.7	35.4	36.6*	35.5	35.9	35.9	35.1*	35.8	36.4	35.1	35.7
9	39.9	39.1	40.1	39.5	39.8	39.8	39.4		39.9		39.6		39.6
10	43.5	43.2	43.8	43.8	43.5		43.7		43.4		42.3*	44.0	43.6
1	47.8	48.0	47.9	47.7	49.6*	48.1	47.8	47.6	47.9	47.5	47.7	47.7	47.8
2	51.3	51.5	51.7	51.8	52.0	52.0	52.1	51.4	51.8	51.8	52.5*	51.7	51.7
3	56.1*	54.8	55.4	56.0	55.3	55.6	55.7	55.3	55.1*	55.3			55.4
4	59.4	59.3	59.5	59.4	60.3	58.7*	59.5	59.5	59.2	59.9	59.3	58.6*	59.6
5	63.1	63.3	62.6*	63.8	63.6	63.5	64.4	63.7	63.6	64.0		62.9	63.6
6	67.7	67.2	67.4	67.4	66.9	67.6	66.6*	67.6	68.4*	68.4*		66.9*	67.4
7	71.9*	70.7	71.2	71.0	71.9	71.2	71.1		71.0	71.1		72.5*	71.2
8		75.3	75.4	75.6	75.3	75.4	74.6	75.6				75.5	75.3
9	78.7	79.2	79.2	79.2	80.1	79.8			79.6	79.3	78.3		79.3
20	83.5	83.1	82.8		83.2	83.7	83.0	83.4		83.6		83.0	83.3
1	86.5	87.3*	87.3		87.1		87.5		87.0	87.5	86.3		87.0
2	91.3	91.4	91.3		91.4		91.1	91.1	91.3		90.5*		91.3
3	95.2	94.8	94.4*	95.3	95.0		95.0		95.4	95.0			95.1
4	99.5	98.6	98.6	99.5	99.0		99.0	98.2	98.9				98.9
5	102.8	102.8	102.8	103.3	103.0		102.9		103.6*	103.3			103.0
6	106.5	106.2	106.6	107.0	106.9		106.5	107.0	106.4*				106.7
7	110.9		110.7	110.2*			110.4		110.9				110.7
8	115.6*	114.7	114.4	115.2	114.5		114.3		114.8				114.8
9	118.6	118.1	118.4	117.8*	118.4		118.7		118.3		118.6		118.5
30	122.7	122.8*	122.3	122.5	122.1				122.5				122.4
1	125.4	126.4	125.2	126.4	126.1		126.4		126.6				126.4
2	130.4	130.9*	130.0	129.3			130.9						130.2
3	134.0	134.7*	133.8	134.5	134.2		134.5						134.2
4	138.2	137.6*	138.0	138.5	138.7		138.3						138.3
5			142.4		141.7		141.5						141.9
6			145.9		145.7		145.8						145.8
7			149.7				149.7						149.7
8			153.2										153.2
9			157.4										157.4
40			160.8										160.8

Table 15. Λ-type Doubling of $X^2\Pi$ State and $\Delta_1F(K)$ Values of the $v=0$ Level of $A^2\Sigma$ State.

	$A^2\Sigma - X^2\Pi_{3/2}$				$A^2\Sigma - X^2\Pi_{1/2}$				
K	Δ_1F+z_2	Δ_1F-z_2	$2z_2$	A_1*	Δ_1F+z_1	Δ_1F-z_1	$2z_1$	A_2*	A_1-A_2
0									
1									
2		11.9		11.9		12.4		12.4	
3	15.8	15.7	0.1	15.8	16.9	15.7	1.2	16.4	−0.6
4		19.8		19.8	20.4	20.0	0.4	20.2	−0.4
5	23.8	23.7	0.1	23.8	23.7	23.7	0.0	23.7	0.1
6	27.7	27.6	0.1	27.7	27.8	27.6	0.2	27.7	0.0
7	31.7	31.8	−0.1	31.8	31.8	31.8	0.0	31.8	0.0
8	35.7	35.7	0.0	35.7	35.9	35.5	0.4	35.7	0.0
9	39.8	39.6	0.2	39.7	39.8	39.5	0.3	39.7	0.0
10	43.6	43.6	0.0	43.6	43.7	43.5	0.2	43.6	0.0
1	47.8	47.8	0.0	47.8	47.7	47.4	0.3	47.6	0.2
2	51.6	51.7	−0.1	51.7	51.7	51.7	0.0	51.7	0.0
3	55.5	55.4	0.1	55.5	55.7	55.6	0.1	55.7	−0.2
4	59.5	59.6	−0.1	59.6	59.7	59.3	0.4	59.5	0.1
5	63.5	63.6	−0.1	63.6	63.6	63.3	0.3	63.5	0.1
6	67.5	67.4	0.1	67.5	67.8	67.6	0.2	67.7	−0.2
7	71.1	71.2	−0.1	71.2	71.7	71.3	0.4	71.5	−0.3
8	75.2	75.3	−0.1	75.3	75.5	75.0	0.5	75.3	0.0
9	79.3	79.3	0.0	79.3	79.6	79.1	0.5	79.4	−0.1
20	83.4	83.3	0.1	83.4	83.5	82.9	0.6	83.2	0.2
1	87.2	87.0	0.2	87.1	87.4	87.0	0.4	87.2	−0.1
2	91.4	91.3	0.1	91.4	91.4	91.0	0.4	91.2	0.2
3	95.1	95.1	0.0	95.1	95.2	94.8	0.4	95.0	0.1
4	99.1	98.9	0.2	99.0	99.2	98.7	0.5	99.0	0.0
5	102.8	103.0	−0.2	102.9	103.0	102.7	0.3	102.9	0.0
6	106.6	106.7	−0.1	106.7	107.0	106.5	0.5	106.8	−0.1
7	110.9	110.7	0.2	110.8	111.0	110.5	0.5	110.8	0.0
8	114.8	114.8	0.0	114.8	114.8	114.4	0.4	114.6	0.2
9	118.7	118.5	0.2	118.6	119.1	118.1	1.0	118.6	0.0
30	122.4	122.4	0.0	122.4	122.7	122.1	0.6	122.4	0.0
1	126.4	126.4	0.0	126.4	126.6	126.1	0.5	126.4	0.0
2	130.4	130.2	0.2	130.3	130.6	130.4	0.2	130.5	−0.2
3	134.6	134.2	0.4	134.4	134.6	133.9	0.7	134.3	0.1
4	138.1	138.3	−0.2	138.2	138.4	137.6	0.8	138.0	0.2
5	141.9	141.9	0.0	141.9	142.5	141.5	1.0	142.0	−0.1
6	146.0	145.8	0.2	145.9	145.8	145.8	0.0	145.8	0.1
7	150.0	149.7	0.3	149.9	149.6	149.1	0.5	149.4	0.5
8	153.6	153.2	0.4	153.4	154.3	153.1	1.2	153.7	−0.3
9	158.1	157.4	0.7	157.8	157.9	156.2	1.7	157.1	0.7
40		160.8		160.8	161.5	160.8	0.7	161.2	−0.4

* A being the average of Δ_1F+z and Δ_1F-z.

Table 16. Δ_1F and Δ_2F Values of $A^3\Sigma$ State.

K \ v	Δ_1F 0	1	2	3	Δ_2F 0	K \ v	Δ_1F 0	1	2	3	Δ_2F 0
0						21	87.2	86.5	85.4		170.4
						2	91.3	90.4	89.5	89.3	178.4
1					11.5	3	95.1	94.1	93.2	93.1	186.4
2	11.9				19.4	4	99.0	98.1	97.1		194.0
3	15.7	15.6	15.6		28.0	5	102.9	102.1	100.7		201.8
4	20.0	19.7	19.5		35.7						
5	23.7	23.7	23.3		43.7	6	106.7	105.7	104.4		209.7
						7	110.8	109.6	107.8		217.5
6	27.7	27.5	27.2	27.1	51.5	8	114.7	113.5			225.5
7	31.8	31.5	31.2	31.0	59.6	9	118.6	117.5			233.4
8	35.7	35.5	35.0	34.8	67.6	30	122.4	121.4			240.8
9	39.7	39.5	39.1	38.7	75.5						
10	43.6	43.2	42.9	42.5	83.3	1	126.4	125.4			248.8
						2	130.4	129.1			256.8
1	47.7	47.1	46.7	46.5	91.3	3	134.3	132.6			264.6
2	51.7	51.1	50.7	50.2	99.4	4	138.1	136.7			272.6
3	55.6	55.0	54.5	53.7	107.3	5	142.0	140.6			280.0
4	59.5	59.0	58.3	57.8	115.1						
5	63.5	63.0	62.5	61.9	122.9	6	145.8				287.7
						7	149.7				295.7
6	67.6	66.9	66.2	65.5	130.8	8	153.5				303.3
7	71.4	70.6	70.0	69.4	139.1	9	157.4				311.0
8	75.3	74.7	73.8	73.2	146.6	40	161.0				318.9
9	79.4	78.6	77.8	76.9	154.5						
20	83.3	82.5	81.7	81.0	162.6						

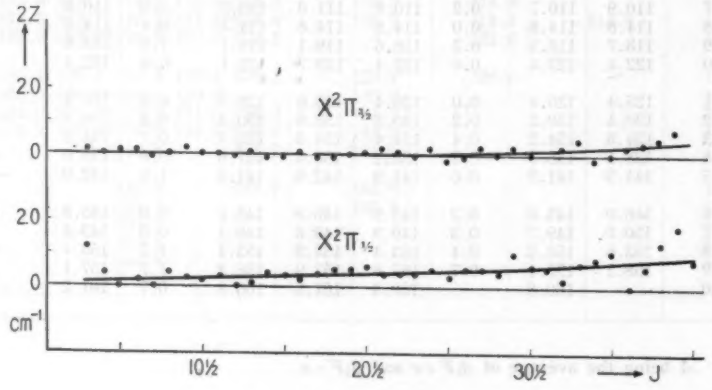

Fig. 6. A-type doubling of $X^3\Pi$ state.

Table 17. $\Delta_1 F$ Values of $X\,^3\Pi$ State.

	$^3\Pi_{3/2}$							$^3\Pi_{1/2}$							
J \ v	0	1	2	3	4	5	6	J \ v	0	1	2	3	4	5	6
								1/2							
1 1/2				8.5				1 1/2		9.6					
2 1/2			11.6			12.2	11.1	2 1/2		11.1		11.3		11.2	
3 1/2		15.0	15.4	15.1		15.6		3 1/2		14.6	14.4	14.6	13.1	13.8	
4 1/2	18.8	18.5	18.3	18.3	18.1	18.0	17.7	4 1/2	18.2	17.9	18.2	18.1	17.5	16.8	17.3
5 1/2	22.2	22.0	21.8	21.5	21.4	21.2	20.8	5 1/2	21.3	21.7	21.4	21.1	20.9	20.7	20.7
6 1/2	25.9	25.6	25.3	25.0	24.7	24.3	23.9	6 1/2	24.8	24.7	24.6	24.5	24.0	23.7	23.2
7 1/2	29.0	28.8	28.7	28.3	28.1	27·5	27.2	7 1/2	28.3	28.1	27.8	27.6	27.2	26.9	26.7
8 1/2	32.8	32.2	31.8	31.5	31.1	31.1	30.6	8 1/2	32.0	31.3	31.2	30.8	30.6	30.1	29.7
9 1/2	36.1	35.7	35.4	34.9	34.5	34.1	33.5	9 1/2	34.9	34.7	34.4	34.0	33.5	33.1	33.2
10 1/2	39.6	39.2	38.3	38.4	37.9	37.4	36.8	10 1/2	38.9	38.0	37.6	37.5	37.2	36.5	
1 1/2	43.0	42.4	42.3	41.7	41.1	40.4	40.1	1 1/2	41.9	41.4	41.0	40.6	40.2	39.8	39.2
2 1/2	46.4	45.9	45.4	44.8	44.1	43.8	43.3	2 1/2	44.6	44.5	44.3	43.7	43.1	42.9	42.2
3 1/2	49.6	49.2	48.5	48.1	47.5	47.2	46.6	3 1/2	48.5	48.1	47.5	47.1	46.4	45.7	45.5
4 1/2	53.2	52.6	52.1	51.6	51.0	50.1	49.6	4 1/2	51.7	51.2	50.9	50.4	49.7	49.0	48.9
5 1/2	56.7	56.0	55.5	54.9	54.4	53.3	53.0	5 1/2	55.2	54.7	54.2	53.6	53.1	52.4	52.7
6 1/2	59.9	59.5	58.8	58.1	57.2	57.0	56.3	6 1/2	58.4	57.8	57.2	57.2	56.0	55.5	55.0
7 1/2	63.4	62.7	62.1	61.6	60.7	60.5	59.3	7 1/2	62.0	61.3	60.4	60.1	59.4	58.9	58.0
8 1/2	66.6	66.0	65.4	64.9	64.0	63.4	62.4	8 1/2	65.1	64.5	63.8	63.2	62.5	61.7	61.4
9 1/2	69.9	69.7	69.0	68.1	67.0	66.4	65.8	9 1/2	68.7	67.9	66.8	66.6	65.6	64.9	64.0
20 1/2	73.6	73.4	72.0	71.4	70.3	69.8	69.2	20 1/2	71.6	71.0	70.6	69.5	69.2	68.3	
1 1/2	77.2	76.2	75.7	74.7	73.8	72.5	71.6	1 1/2	75.3	74.4	73.5	72.9	72.2	71.4	71.2
2 1/2	80.6	79.4	78·7	77.9	77.1	75.7	74.8	2 1/2	78.7	77.8	77.0	75.8	75.4	74.4	74.3
3 1/2	83.6	82.8	81.9	81.0		79.3	78.4	3 1/2	81.8	80.9	80.3	79.3	78.6	77.7	
4 1/2	87.4	86.0	85.4	84.4		82.2	81.7	4 1/2	85.2	84.4	83.6	82.4	81.6		79.7
5 1/2	90.4	89.7	88.5	87.5		85.6	85.3	5 1/2	88.6	87.6	86.7	85.6	84.6	84.0	
6 1/2	93.9	92.7	92.2	90.7		88.7	88.2	6 1/2	91.8	90.9	90.0	88.9	87.7	86.9	89.3
7 1/2	97.4	96.1	95.0	94.7		92.3	91.3	7 1/2	95.3	94.2	93.6	92.0	91.1	90.1	92.8
8 1/2	100.7	99.5	98.7	97.8		95.2	94.3	8 1/2	98.4	97.5	96.8	95.3	94.2	93.2	95.5
9 1/2	103.9	102.8	101.6	100.8		98.3	97.6	9 1/2	101.8	100.5	99.9	98.6	97.6		
30 1/2	107.3	106.2	105.2	104.3		101.3		30 1/2	105.3	104.1	103.0			49.7	
1 1/2	111.1	109.6	108.1	107.4		104.7	103.9	1 1/2	108.3	107.6	105.8				
2 1/2	114.3	112.4	111.8	110.5		107.9		2 1/2	111.6	110.6	109.2				
3 1/2	117.3	116.3	115.4	113.8				3 1/2	114.9	114.2	112.9				
4 1/2	120.8	119.3	118.0	116.6				4 1/2	118.1	116.8	115.5				
5 1/2	124.5	122.8	121.2	120.1				5 1/2	121.5	120.1					
6 1/2	127.6	125.9						6 1/2	124.5	123.5					
7 1/2	130.5	129.2						7 1/2		127.0					
8 1/2	134.8	132.4						8 1/2		129.9					
9 1/2		135.6						9 1/2		132.9					
40 1/2								40 1/2		136.4					

Table 18. B_v and D_v Values of $A^3\Sigma$ and $X^3\Pi$ States.

		0	1	2	3	4	5	6	7	8
$A^3\Sigma$	B_v	1.988	1.971	1.953	1.937	1.99_0*	1.97_2*			
	D_v	7×10^{-6}	7×10^{-6}	10×10^{-6}	15×10^{-6}					
$X^3\Pi_{3/2}$	B_v	1.719	1.700	1.681	1.664	1.645	1.625	1.607	1.59_0	1.57_3
	D_v	6.5×10^{-6}	8×10^{-6}	6×10^{-6}	6×10^{-6}	8×10^{-6}	7×10^{-6}	5×10^{-6}		
$X^3\Pi_{1/2}$	B_v	1.676	1.659	1.641	1.624	1.607	1.588	1.573		1.53_4
	D_v	4.5×10^{-6}	4.5×10^{-6}	4×10^{-6}	4×10^{-6}	4×10^{-6}	4×10^{-6}	4×10^{-6}		

* These B_4 and B_5 values are B_0 and B_1 values of the $D^3\Sigma$ state, respectively.

Table 19. Vibrational and Rotational Constants of $D^3\Sigma$, $A^3\Sigma$ and $X^3\Pi$ States.

	ω_e	$\omega_e x_e$	B_e	I_e (10^{-40} gm cm^2)	r_e (10^{-8} cm)	α		ν_e	ν_{00}
$D^3\Sigma$	2327.	24.	1.99_9	14.0_0	1.06_3	0.018	ε: $D^3\Sigma-X^3\Pi$	53083.	53168.1 53292.1
$A^3\Sigma$	2374.6_6	16.4_5	1.99_6	14.0_2	1.06_3	0.017_1	γ: $A^3\Sigma-X^3\Pi$	43966.3	44076.9 44201.0
$X^3\Pi_{3/2}$	1903.5_5	13.9_9	1.72_8	16.1_9	1.14_3	0.018_5			
$X^3\Pi_{1/2}$	1903.9_9	14.0_1	1.68_6	16.6_0	1.15_7	0.017_6			

$$G(v)=\omega_e(v+{}^1/_2)-\omega_e x_e(v+{}^1/_2)^2+\cdots\cdots, \tag{29}$$

$$\Delta G_{v+1/2}=\omega_e-2\omega_e x_e(v+1)+\cdots\cdots. \tag{30}$$

The vibrational constants ω_e and $\omega_e x_e$ were obtained by using the wavenumbers of the band origins, and the values are listed in Table 19 together with the other molecular constants, B_e, I_e, r_e, α and ν_e. In the calculation of these molecular constants, the bands with $v'\geqq4$ and $v'\leqq3$ were regarded as belonging to the ε-system and the γ-system respectively, the reason for this will be dis-

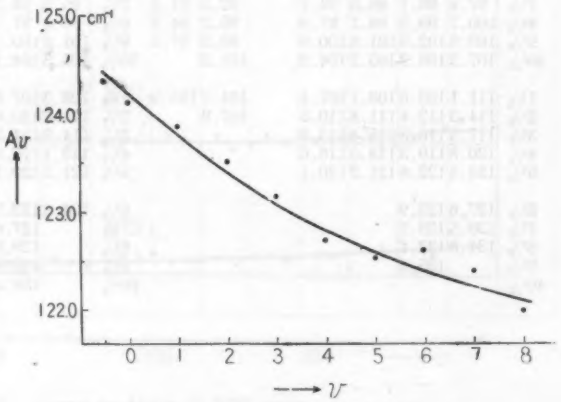

Fig. 7. Coupling constant A of $X^3\Pi$ state.

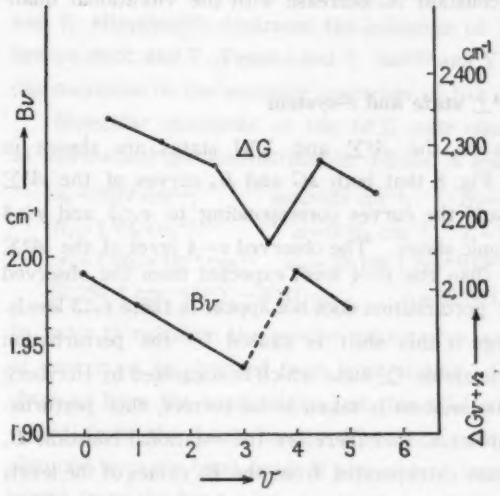

Fig. 8. B_v and ΔG curves of the $A^2\Sigma$ state.

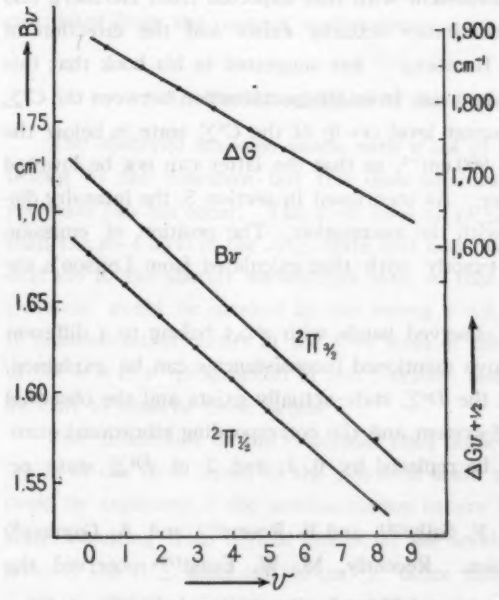

Fig. 9. B_v and ΔG curves of $X^2\Pi$ state.

cussed in a later section.

The $X^2\Pi$ state is considered to belong approximately to the Hund coupling case a and the electronic energy T_e is given by the following formula,

$$T_e = T_0 + A\Lambda\Sigma\,, \qquad (31)$$

where T_0 is the term value when the spin is neglected and A is a coupling constant. In the $^2\Pi$ state, Λ equals unity and Σ equals $\pm 1/2$, so the coupling constant A can be calculated by the relation,

$$\begin{aligned} A\Lambda\Sigma(^2\Pi_{3/2}) - A\Lambda\Sigma(^2\Pi_{1/2}) = A \\ = \nu_e(A^2\Sigma - X^2\Pi_{1/2}) \\ - \nu_e(A^2\Sigma - X^2\Pi_{3/2}) \\ = 43{,}966.3 - 43{,}842.0 \\ = 124.3\ \mathrm{cm}^{-1}, \qquad (32) \end{aligned}$$

if the electronic energy difference between the $A^2\Sigma$ state and the $X^2\Pi_{3/2}$ is represented by $\nu_e(A^2\Sigma - X^2\Pi_{3/2})$.

In the direction of the internuclear axis, the upper $A^2\Sigma$ state does not posses a magnetic field due to the electron orbital motion and so the energy difference of each band origin will give the magnetic interaction energy (A_v) between the magnetic field produced by the electron orbital motion and the magnetic moment of electron spin in the given vibrational level of the $X^2\Pi$ state. The differences obtained are graphically shown in Fig. 7. This shows clearly

that the values of the coupling constant A_v decrease with the vibrational quantum number.

6. $D^2\Sigma$ state and $\mathcal{E}$-system

$\Delta G_{v+1/2}:v$ and $B_v:v$ curves of the $A^2\Sigma$ and $X^2\Pi$ states are shown in Figs. 8 and 9. It is clear from Fig. 8 that both ΔG and B_v curves of the $A^2\Sigma$ state are discontinuous at $v=4$ and the curves corresponding to $v\leqq 3$ and $v\geqq 4$ seem to belong to different electronic states. The observed $v=4$ level of the $A^2\Sigma$ state is lower by about 80 cm^{-1} than the $v=4$ level expected from the observed $v\leqq 3$ levels, while the particular perturbation does not appear in these $v\leqq 3$ levels. This value seems to be very large if this shift is caused by the perturbation between the $v=4$ level and the unstable $^2\Sigma$ state which is suggested by Herzberg and Mundie. However, if the assumption is taken to be correct, this perturbation must be a vibrational perturbation, and therefore the rotational constant B_4 and B_5 should be the same as that extraporated from the B_v values of the levels with $v\leqq 3$. Consequently the discontinuity of the B_v curve cannot occur. Thus the observed phenomena are inconsistent with that expected from Herzberg and and Mundie's assumption: discontinuity actually exists and the direction of shift of $v=4$ level is opposite. Herzberg[15] has suggested in his book that this deviation of the $v=4$ level may be arise from the perturbation between the $C^2\Sigma$ state and this level. But the nearest level ($v=0$) of the $C^2\Sigma$ state is below the $v=4$ of the $A^2\Sigma$ state by about 900 cm^{-1}, so that the latter can not be lowered by the perturbation of the former. As mentioned in section 3, the intensity distribution also does not coincide with the assumption. The position of emission bands observed agrees almost exactly with that calculated from Leifson's absorption bands.

If it is assumed that the observed bands with $v'\geqq 4$ belong to a different system, the $\mathcal{E}$-system, all the above mentioned inconsistencies can be explained. Therefore, it might be said that the $D^2\Sigma$ state actually exists and the observed bands with $v'\geqq 4$ belong to the $\mathcal{E}$-system and the corresponding vibrational quantum numbers 4′, 5′ and 6′ must be replaced by 0, 1, and 2 of $D^2\Sigma$ state respectively.

L. Gerö, R. Schmid and K. F. Szily[16], and B. Rosen[17] and A. Gaydon[9] have reported the same conclusion. Recently, M. W. Feast[18] observed the

15) G. Herzberg: Molecular Spectra and Molecular Structure, vol. 1 (1950), p. 559.
16) L. Gerö, R. Schmid & K. F. Szily: Physica, **9** (1944), 144.
17) B. Rosen: Phys. Rev., **68** (1945), 124.
18) M. W. Feast: Canadian Jour. Res., **28** (1950), 488.

emission spectrum due to the $D^1\Sigma \rightarrow A^1\Sigma$ transition in the near infrared region and E. Miecsher[19] confirmed the existence of the $D^1\Sigma$ state from vibrational isotope shift, and Y. Tanaka and T. Sai[20] and Y. Tanaka[21] observed the bands of the ε-system in the emission spectrum of NO in the extreme ultraviolet region.

Molecular constants of the $D^1\Sigma$ state obtained under above conclusion are as follows and are summarized in Tables 18 and 19.

$\omega_e = 2327\ \mathrm{cm^{-1}}$, $\omega_e x_e = 24\ \mathrm{cm^{-1}}$, $B_0 = 1.99_0\ \mathrm{cm^{-1}}$, $B_1 = 1.97_2\ \mathrm{cm^{-1}}$, $B_e = 1.99_9\ \mathrm{cm^{-1}}$. $\alpha = 0.01_8\ \mathrm{cm^{-1}}$, $I_e = 14.0_9 \times 10^{-40}\ \mathrm{gm.\ cm^2}$ $r_e = 1.06_3 \times 10^{-8}\ \mathrm{cm^{-1}}$, $\nu_{00} = 53{,}168.1\ \mathrm{cm^{-1}}(D^1\Sigma - X\Pi_{3/2})$ and $53{,}292.1\ \mathrm{cm^{-1}}(D^1\Sigma - X^1\Pi_{1/2})$, $\nu_e = 53{,}083\ \mathrm{cm^{-1}}$.

In order to calculate the precise values of ω_e and $\omega_e x_e$, those of $\Delta G_{1/2}$ and $\Delta G_{3/2}$ at least must be obtained from band origins. Unfortunately only $\Delta G_{1/2}$ has been obtained from the band origins but this $\Delta G_{1/2}$ almost the same as the $\Delta G_{1/2}$ obtained from the band heads. Therefore, under the assumption that the $\Delta G_{3/2}$ obtained from the band heads is also almost same as the $\Delta G_{3/2}$ which would be obtained from the band origins, ω_e and $\omega_e x_e$ were calculated with $\Delta G_{1/2} = 2{,}280\ \mathrm{cm^{-1}}$ and $\Delta G_{3/2} = 2{,}234\ \mathrm{cm^{-1}}$ obtained from the band heads. ν_{00} of the ε-system was calculated from the relation $\nu_{00}(\varepsilon\text{-system}) = \nu_{04}(\varepsilon) - \nu_{04}(\gamma) + \nu_{00}(\gamma)$.

8. Predissociations of the β- and the γ-systems

The observed emission bands with $v' \geqq 4$ of the γ-system are considered to belong to the ε-system but this does not mean that the predissociation of the γ-system can not occur. The $v=0$ level of $D^1\Sigma$ state is lower by about $80\ \mathrm{cm^{-1}}$ than the $v=4$ level of the $A^1\Sigma$ state and both bands of the ε- and the γ-systems degrade to the shorter wavelength side, so that the $v'=4$, v''-progression of the γ-system would be masked by the strong $v'=0$, v''-progression of the ε-system. If predissociation occurs at the $v=4$ level of the $A^1\Sigma$ state, the emission bands of the $v'=4$, v''-progression of the γ-system become weak and it should be more difficult to observe those bands.

The intensities of the rotational lines higher than $P_2(21^1/_2)$, $Q_2(20^1/_2)$, and $R_1(20^1/_2)$ of the (2–3) bands of the γ-system seem to drop sharply (Fig. 5b). This could be explained if the predissociation occurs by interaction of the unstable $^1\Sigma$ state, resulting from normal atoms, at the levels higher than the $v=2$, $K=21$ level of the $A^1\Sigma$ state ($49{,}750\ \mathrm{cm^{-1}}$). Since many rotational lines of other bands

19) E. Miescher: Nature, **169** (1952), 581.
20) Y. Tanaka & T. Sai: Science of Light (Tokyo), **1** (1951), 85.
21) Y. Tanaka: J. Chem. Phys., **21** (1953), 788.

of the $v'=2$ v''-progression overlapped other lines of the β- and the γ-systems, such intensity distribution resembling that of (2-3) band could not be observed. As Gaydon pointed out, the electronic states in the same species perturb each other strongly and cannot cross in general. Therefore, unless a more precise measurement is made it is impossible to discuss the predissociation of the γ-system.

Some β-bands with $v'=5$ and 6 were observed in the visible region. The bands of the $\Delta v=-15$ sequence are clearly revealed and the intensity drop expected by Kaplan's suggestion is not seen. The same phenomena have been observed by Gaydon[9] in the ultraviolet region.

The author wishes to express his sincere thanks to Professor Yoshio Fujioka, Director of the Institute, for his valuable discussion upon the present work. He is also much indebted to Professor Yoshio Tanaka for his encouragement and valuable advice in the course of this work and to Professor G. Herzberg and to Professor A. G. Gaydon for their kind provision of reference papers on this work, and to Miss Midori Ueda for her kind assistance upon the vibrational analysis of the β-system.

On the Emission Intensities of the O_2 Atmospheric Bands ($b^1\Sigma_g^+ \rightarrow X^3\Sigma_g^-$)

Mitsuyoshi SHIMAZU

Industrial Research Institute of Kanagawa Prefecture

(Received October 23, 1954)

Abstract

The relative intensities of the (0–0) and (1–1) bands of the atmospheric oxygen bands obtained in electric discharge were measured, and the procedure of measurement are described. Vibrational and rotational temperatures were measured, and showed good agreement. Assuming the thermal distribution of the excited molecules, the relative intensities of many bands belonging to this system were calculated for the temperature range of 400°~5,000°K. Results of several experiments on the emission of the atmospheric bands reported up to the present time are discussed on the basis of the present results.

I. Introduction

The atmospheric oxygen bands which appear between the red and near infrared region are known to result from a forbidden transition $b^1\Sigma_g^+ - X^3\Sigma_g^-$. In recent years cases have come to be described in which these bands are observed in the laboratory not only as absorption spectra but also as emission spectra. The author has previously obtained these emission bands both in the direct discharge and in the afterglow in the so-called Wood tube discharge, and has described the details of the experiment and suggested some probable emission processes[1]. While only the (0–1) band of this system is observed both in airglow and in aurora, several other bands have been obtained in laboratory emission experiments. Much discussion has been made in connection with this fact[2]. The spectroscopic study of the airglow and the aurora is very important for the understanding of phenomena in the upper atmosphere, and laboratory studies of the O_2 atmospheric emission bands might provide some useful suggestions to serve in the first-mentioned investigations.

To discuss emission mechanisms data concerning intensity distributions are

1) M. Shimazu: Science of Light **2** (1953) 95.

2) J. W. Chamberlain: Astrophys. J. **119** (1954) 328.

in general necessary, and therefore the present paper will deal mainly with this intensity distribution. The results obtained by the author in previous experiments were carefully reexamined, and the intensity ratio of the (0–0) and (1–1) bands were measured. Then, in order to obtain some information on the emission mechanism of the atmospheric bands, the vibrational temperature was measured using the theoretical values of the overlap integrals corresponding to these transitions. The vibrational temperature thus obtained was compared with the rotational temperature which had been independently obtained.

II. Relative Intensities of the (1–1) and (0–0) Bands

In previous experiments the author observed the (0–0), (0–1) and (1–1) bands under direct discharge, and the (0–0) and (0–1) bands in the afterglow. No attempt was then made to measure the relative intensities. The intensity measurement of the (0–0) and (1–1) bands based on previous data is the subject of this report, and the method and the results thereof will first be described. For details of the experimental conditions and the apparatus used, readers are referred to the previous paper[3].

1. Intensity of the Vibrational Band

It is well known that the emission intensity of a vibrational band of a diatomic molecule is given by[4]

$$I^{v'v''} \sim N_{v'} \nu^4 \left[\int \psi_{v'} \psi_{v''} dr\right]^2 \qquad (1)$$

where v' and v'' represent the vibrational quantum numbers of the upper and the lower electronic states respectively, $N_{v'}$ the number of molecules in the upper vibrational level, $\psi_{v'}$, $\psi_{v''}$, the vibrational eigenfunctions of the two states and $\left[\int \psi_{v'} \psi_{v''} dr\right]$ the so-called overlap integral, proportional to the vibrational transition probability. Then the relative intensities of respective bands will be determined if the overlap integrals are known.

If we assume the thermal distribution.

$$N_{v'} \sim \exp\left[-\frac{hc}{kT} E(v')\right],$$

the intensity becomes

3) M. Shimazu: loc. cit.

4) G. Herzberg: Spectra of Diatomic Molecules (2nd ed.; New York, Toronto and London; D. Van Nostrand Co., 1951) p. 200.

$$I^{v'v''} \sim \nu^4 \left[\int \psi_{v'} \psi_{v''} dr\right]^2 \exp\left[-\frac{hc}{kT} E(v')\right]. \quad (2)$$

The intensity ratio of the two bands, for example, the (0–0) and (1–1) will be given by

$$\frac{I^{(0-0)}}{I^{(1-1)}} \sim \left(\frac{\nu_{0-0}}{\nu_{1-1}}\right)^4 \frac{\left[\int \psi_0' \psi_0'' dr\right]^2}{\left[\int \psi_1' \psi_1'' dr\right]^2} \exp\left[-\frac{hc}{kT}\{E'(0)-E'(1)\}\right]. \quad (3)$$

2. Measurement of the intensity ratio of the (1–1) and (0–0) bands

When the photographic method is used to measure the intensities of spectral lines, plate is ordinarily calibrated with the use of intensity marks. This photographic spectrophotometry however is very tedious to carry out, and even the application of great skill and labor cannot always eliminate a considerable amount of error being involved. The difficulties are increased when this is attempted in the infrared region since it necessitates corrections for the spectral intensity distribution of the standard lamp, measurement of transmission in the infrared region of the step filters used in making the intensity marks etc.

Fortunately in the present case as will be explained below, the relative intensities of the (0–0) and the (1–1) bands of the atmospheric system could under certain assumptions be estimated easily by a simple method.

(1) *The rotational intensity distribution in the P-type branch of the (0–0) bands.*

In Fig. 1, is reproduced the spectrogram obtained by a replica grating spectrograph. The resolving power of the spectrograph is not sufficient because the spectrograph is small, and also since we adopted rather wide slit in order to avoid much longer exposure times, and consequently, the *R*-type branch was not resolved. The *P*-type branch was, but since the atmospheric bands result from the transition ${}^1\Sigma_g^+ - {}^3\Sigma_g^-$, and therefore the bands should be composed of the 4 branches[5] R, ${}^RQ$, P and ${}^PQ$, it will be seen from Fig. 1. that the P and ${}^PQ$ branches still remain unresolved. We will discuss the intensity distribution of this unresolved *P*-type branch.

In the first place the rotational temperature will be examined, because this will be found to be necessary in the ensuing discussions.

As is well known, several methods[6] are used to determine the temperature from the intensity distribution of the rotational lines.

Two methods were adopted here:

(i) Determination from the J-value corresponding to the maximum intensity.

5) G. Herzberg: loc. cit. p. 278.
6) G. Herzberg: loc. cit. p. 465.

(ii) Determination from the slope of the $\log(I/i)\sim J(J+1)$ diagram when it assumes a straight line.

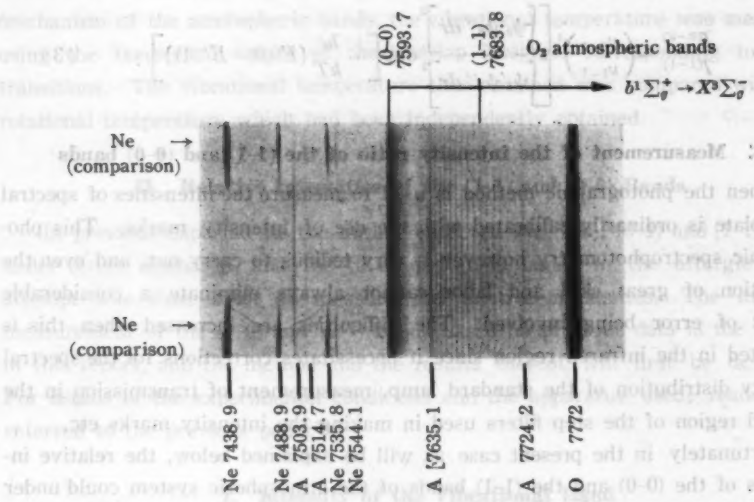

Fig. 1. O_2 atmospheric bands photographed by a replica grating spectrograph.

Strictly speaking, as stated already, the P-type branch is composed of the ${}^rQ$ and the P branches, but for the sake of simplicity, the P branch only was considered in the previous paper for the measurement of rotational temperature. The resulting error however was not very large, as will be seen later. Here, we will determine the rotational temperature by considering the P-type branch to be composed of the P and the ${}^rQ$ branches, but having been observed as superimposed upon each other.

According to Schlapp[7] the intensity factors for the P and ${}^rQ$ branches of the ${}^1\Sigma-{}^3\Sigma$ bands are given by

$$i(P)=\frac{1}{2}(J+2)$$

and

7) R. J. Schlapp: Phys. Rev., **39** (1932) 806.

$$i(^rQ)=\frac{1}{2}J$$

respectively. Strictly speaking these are the intensity factors for electric quadrupole radiation, but as they may be applied also to magnetic dipole transition without involving much error, we will adopt these for the O_2 atmospheric system which is believed to result from a magnetic dipole transition[8]. As has been noted, since the P and the ^rQ branches were not resolved, considering the P and ^rQ branches to have been observed together, we adopt the intensity factor

$$i(P+{}^rQ)=i(P)+i(^rQ)$$
$$=\frac{1}{2}(2J+2)=J+1\,.$$

The intensities of the unresolved $P+{}^rQ$ rotational lines are then given by

$$I(P+{}^rQ)\sim(J+1)\exp[-B_vJ(J+1)hc/kT]\,,$$

and therefore the temperature is given by

$$T=1.987\,(J_m+1)\,(2J_m+1)\,,$$

where J_m corresponds to the line for maximum intensity. In the present case as $J_m\sim13$, we have

$$T=752°K\,.$$

For the determination of temperature by the method (ii), the relative intensities of each rotational line must be obtained, and the resulting $\log_{10}(I/i)\sim J(J+1)$ relation must assume a straight line.

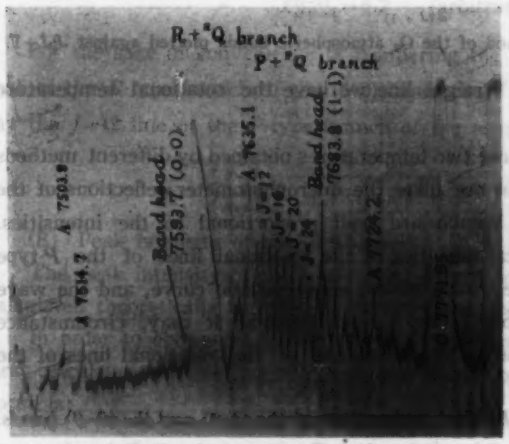

Fig. 2. Microphotometer curve of the O_2 atmospheric bands.

In our experiment we did not resort to photometry with intensity marks for each rotational lines, and instead the following method was adopted to determine the relative intensities.

In Fig. 2. is reproduced the microphotometer curve. Here we assume that the deflection of the microphotometer is proportional to the line intensity I, based on which the quantity I/i was calculated for each line. This

8) G. Herzberg: loc. cit. p. 278.

assumption is supported by the following facts.

The relation log $I/i \sim J(J+1)$ becomes a straight line as seen in Fig. 3, from which it will be seen that the observed points are well on the straight line up to the point $J=24$, but that they deviate from this line beyond $J=26$. This deviation may be explained as due to the overlapping of the (1-1) band at this

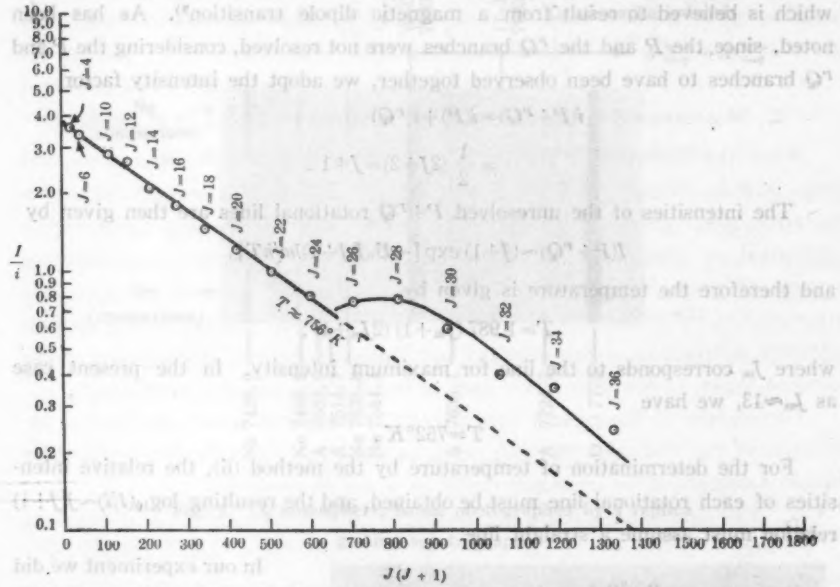

Fig. 3. log (I/i) for the (0-0) band of the O_2 atmospheric bands plotted against $J(J+1)$

point. From the slope of the straight line we have the rotational temperature $T=756 \pm 20°K$.

The good agreement of these two temperatures obtained by different methods is a witness of the fact that in our plate the microphotometer deflections of the rotational lines of the P-type branch are well proportional to the intensities. This must be due to the optical densities of the rotational lines of the P-type branch lying in a favourable range of the characteristic curve, and the wave length range in question not being very large. Be it as it may, circumstance is most convenient for intensity measurements of the rotational lines of the P-type branch.

(2) ***Comparison between the peak intensities of the (1-1) and the (0-0) bands.***

In the next place, the intensity ratio of the (1-1) and the (0-0) bands must be determined. We will refer to the peak intensity of the bands, as is generally used in the measurement of unresolved bands.

In the present case the (1–1) band only makes a very weak appearance, and only the *R*-type branch can be observed, forming the head of the band.

Therefore the peak intensity of the *R*-type branch of the (1–1) band and the corresponding branch of the (0–0) band must be compared. Unfortunately, a straightforward comparison of the respective microphotometer deflections does not give their correct relative intensities, because as may be seen from Fig. 1, in the case of the *R*-type branch of the (0–0) band, the blackness on the photographic plate of this band forming the head is disproportionately intense considering the characteristics of the plate, and the deflection of the microphotometer cannot therefore be considered to be proportional to the intensities.

Accordingly the peak intensity has been compared with the peak of the *R*-type branch of the (0–0) band as calculated theoretically, using as intermediary the intensity of a given rotational line of the *P*-type branch.

(A) Peak intensity of the (1–1) band.

As noted under **2**(1), the deflection of the microphotometer record of the rotational lines of the *P*-type branch of the (0-0) band was found to be proportional to their respective intensities, and on this basis the relative intensities of the rotational lines were plotted against their wave length. (Fig. 4.)

Using this figure, the peak intensity of the *R*-type branch of the (1-1) band, $I^{(1-1)}_{R\,\mathrm{peak}}$ is obtained by subtracting the intensities of the overlapping lines of *P*-type branch of the (0–0) band, thus,

$$I^{(1-1)}_{R\,\mathrm{peak}}=6.2 \qquad \text{(arbitrary scale)}.$$

For the sake of convenience of comparing the intensity of the $I^{(1-1)}_{R\,\mathrm{peak}}$ with that of the *R*-type branch of the (0–0) band, the $I^{(0-0)}_{R\,\mathrm{peak}}$ is first compared with say the $J=12$ line of the *P*-type branch of the same band, namely $I^{(0-0)}_{J=12}$:

$$\frac{I^{(0-0)}_{J=12}}{I^{(1-1)}_{R\,\mathrm{peak}}}=\frac{34.1}{6.2} \quad \text{or} \quad I^{(0-0)}_{J=12}=5.5\, I^{(1-1)}_{R\,\mathrm{peak}}. \qquad (4)$$

(B) Peak intensity of the (0–0) bands

The peak intensity of the unresolved *R*-type branch of the (0–0) band was calculated theoretically for the reason described above.

In order to obtain the profile of the *R*-type branch of the (0–0) band, we first calculated the line intensities of the *R*-type branch by using the following formula;

$$I(R+{}^{R}Q)\sim\{i(R)+i({}^{R}Q)\}\exp\left[-\frac{hc}{kT}B_v J(J+1)\right]\sim J\exp\left[-\frac{hc}{kT}B_v J(J+1)\right],$$

where the temperature T was assumed to be 756°K.

Next the intensity of each line calculated by the above formula was drawn against its wave-length. Since the true slit width is finite, correction must be made for the fact that the spectral lines are not actually infinitely narrow.

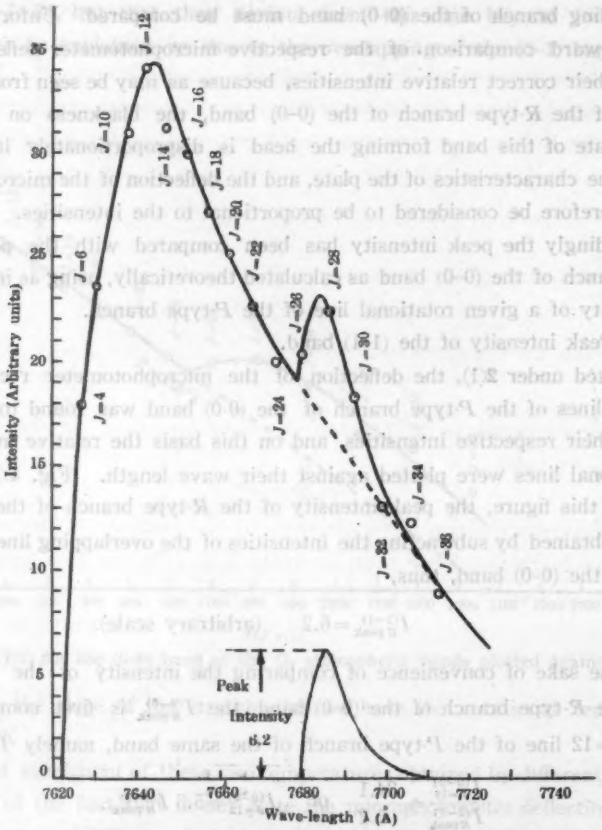

Fig. 4. The observed relative intensities of the rotatinal lines plotted against their wave length.

Estimating the effective slit width expressed in equivalent wave-length to be =3Å, based on results of microphotometer tracing, we now substitute the lines by the rectangles having a width of 3Å, and to which heights equivalent to the aggregate intensities are given at the overlapping portions, and thus we obtain the diagram shown in Fig. 5. This diagram may then be idealised by rounding out the corners of the rectangles. This method of finding the profiles is described in detail in a paper by Swings and Nicholet[9].

9) P. Swings and M. Nicholet: Astrophys J. **88** (1938) 173.

Thus we have established that the peak intensity of the *R*-type branch of the (0–0) band

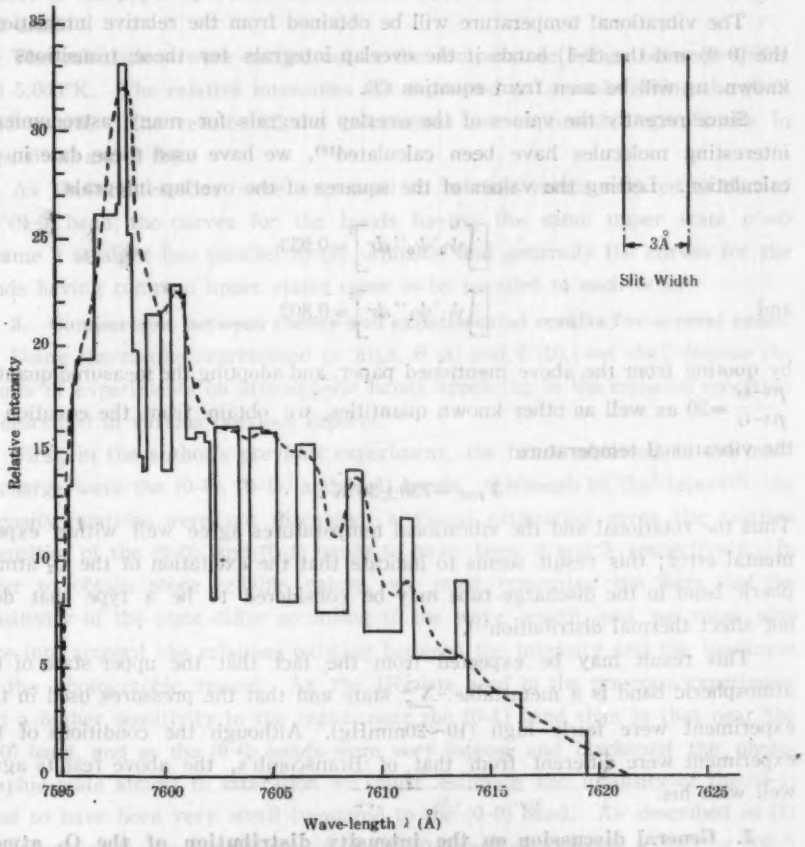

Fig. 5. The calculated profile of the *R*-type branch of the (0–0) band (dotted line).

$$I^{(0-0)}_{R\,\mathrm{peak}} = 32. \qquad (5)$$

Finally, the relative intensities of the (0–0) and (1–1) bands are given by

$$\frac{I^{(0-0)}_{R\,\mathrm{peak}}}{I^{(1-1)}_{R\,\mathrm{peak}}} = \frac{I^{(0-0)}_{R\,\mathrm{peak}}}{I^{(0-0)}_{P(J=12)}} \cdot \frac{I^{(0-0)}_{P(J=12)}}{I^{(1-1)}_{R\,\mathrm{peak}}} = \frac{32}{8.6} \times 5.5 \approx 20 \qquad (6)$$

where

$$\frac{I^{(0-0)}_{R\,\mathrm{peak}}}{I^{(0-0)}_{P(J=12)}} = \frac{32}{8.6}$$

is the theoretically computed value.

III. Discussion

1. Considerations on the relative intensities of the (0–0) and (1–1) bands.

The vibrational temperature will be obtained from the relative intensities of the (0–0) and the (1–1) bands if the overlap integrals for these transitions are known, as will be seen from equation (3).

Since recently the values of the overlap integrals for many astronomically interesting molecules have been calculated[10], we have used these date in our calculation. Letting the values of the squares of the overlap integrals

$$\left[\int \psi_0' \psi_0'' \, d\tau\right]^2 = 0.933$$

and

$$\left[\int \psi_1' \psi_1'' \, d\tau\right]^2 = 0.802$$

by quoting from the above mentioned paper, and adopting the measured quantity $\frac{I^{(0-0)}}{I^{(1-1)}} \approx 20$ as well as other known quantities, we obtain from the equation (3) the vibrational temperature

$$T_{\text{vibr.}} = 730 \pm 30°\text{K} .$$

Thus the rotational and the vibrational temperatures agree well within experimental error; this result seems to indicate that the excitation of the O_2 atmospheric band in the discharge tube may be considered to be a type that does not affect thermal distribution[11].

This result may be expected from the fact that the upper state of the atmospheric band is a metastable $^1\Sigma_g^+$ state and that the pressures used in this experiment were fairly high (10~20mmHg). Although the conditions of the experiment were different from that of Branscomb's, the above results agree well with his.

2. General discussion on the intensity distribution of the O_2 atmospheric bands appearing in the emission spectrum.

As was shown under 1. of this section, it seems very probable that the thermal distribution is attained in the discharge tube before the excited O_2 molecule emit the atmospheric bands.

It is therefore of interest for the discussion of the emission mechanism, to calculate the intensity distributions of the vibrational bands at various temperatures based on the above stated assumption.

10) R. A. Fraser, W. R. Jarmain and R. W. Nicholls: Astrophys. J. **119** (1954) 286.
11) G. Herzberg: loc. cit. p. 466.

In order to calculate the vibrational intensity distribution, the values of the overlap integrals are of course necessary, and in the following calculations the results of the paper by P. A. Fraser, W. R. Jarmain and R. W. Nicholls[12] were also used.

The calculations were carried out in the temperature range between 400°K and 5,000°K. The relative intensities are expressed on a scale giving the (0–0) band as 100. The results of the calculations are represented graphically in Figs. 6 (a) and 6 (b).

As these intensities were expressed in relative values referred to that of the (0–0) band, the curves for the bands having the same upper state $v'=0$ became a straight line parallel to the ordinate, and generally the curves for the bands having common upper states come to be paralled to each other.

3. Comparison between theory and experimental results for several cases.

Using the results represented in Figs. 6 (a) and 6 (b), we shall discuss the results of experiments on atmospheric bands appearing in the emission spectrum as described in various previous reports.

First, in the author's previous experiment, the bands obtained in the main discharge were the (0–0), (0–1), and (1–1) bands. Although in the report[13] the intensity relations were not discussed, a visual estimation gives the relative intensities of the (0–0), and (0–1) bands to have been 8 and 3 respectively. In order to obtain more reliable values, we must remember the facts that the sensitivity of the plate differ according to the wave length, and we must also take into account the relations existing between the intensity and the blackness of the photographic record. As the IN-plate used in the previous experiment had a higher sensitivity in the region near the (0–1) band than in that near the (0–0) band, and as the (0–0) bands were very intense and blackened the photographic plate almost to saturation we must estimate the intensity of the (0–1) band to have been very small compared to the (0–0) band. As described in (2) (B) of section 2, the intensity ratio of the (0–0) and (1–1) bands is 20:1 or 100:5 at the temperature $T\sim756$°K and this result agrees closely with the results given in Figs. 6 (a) and 6 (b).

Kaplan[14] was first in observing the atmospheric band in emission in an afterglow of special form. In his paper, it was reported that the (0–0) and (0–1) bands were observed. However, as nothing was mentioned with respect to the intensity distribution, we are not able to discuss his results further.

12) P. A. Fraser, W. R. Jarmain and R. W. Nicholls: loc. cit.
13) M. Shimazu: loc. cit.
14) Kaplan: Phys. Rev., **71** (1947) 274.

(a) Temperature range 200~2000°K

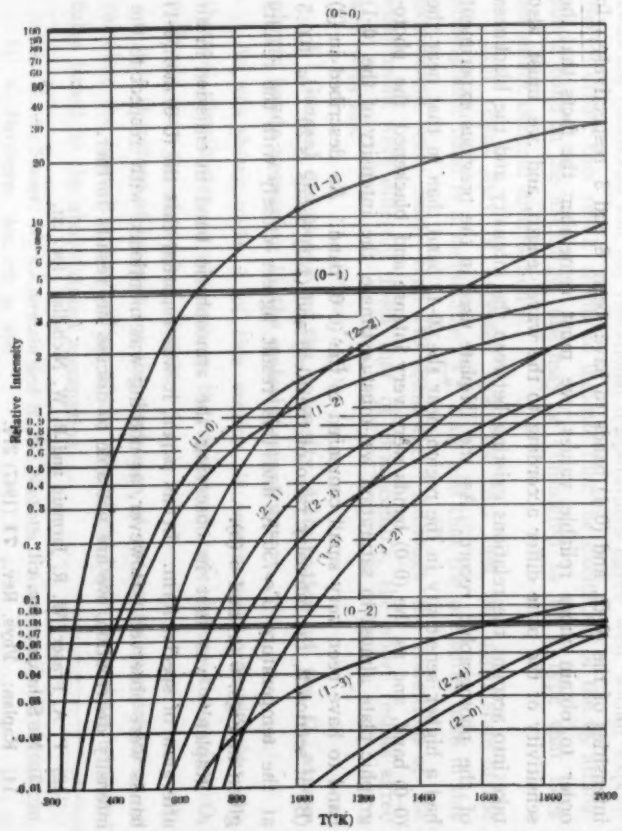

(b) Temperature range 600~6000°K

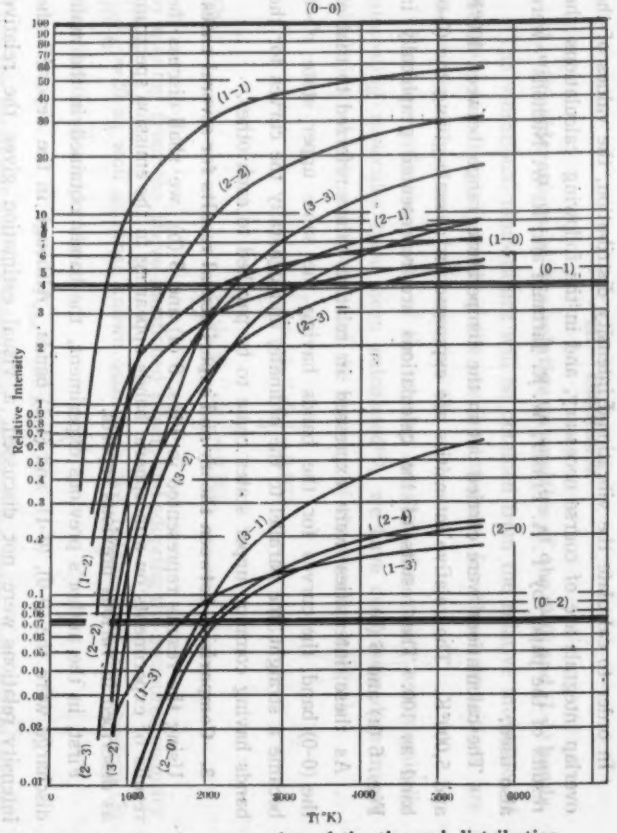

Fig. 6. The relative intensities of various vibrational bands calculated under the assumption of the thermal distribution of the excited molecules.

Branscomb[15] found the (0-0), (0-1), (1-1), (2-2), (3-3) and (4-4) bands of this system in a high frequency electrodeless discharge. Although detailed explanation of the intensity of these bands were not given, Branscomb's data would appear to agree with the results given in Figs. 6 (a) and 6 (b), assuming the temperature 700°K which is the value reported in his paper. It should be noted, however, that according to the results of the present study, the (1-0) and (1-2) bands should be more intense than the (3-3) at this temperature, and nevertheless no mention of these bands appears in his report. The reason for this may be ascribed to the fact that the expected position of these bands is in the region where the plate sensitivity is very poor.

Kvifte[16] photographed the (0-0), (0-1) and (1-1) bands in the emission spectrum by high frequency electrodeless discharge in a mixture of rare gas and oxygen, and gave the relative intensities of the (0-1) and (1-1) bands as 5% and 2% of the (0-0) respectively. Unfortunately nothing is discussed in his paper as regards the temperature, but if we assume fairly low temperature, say $T \leq 500°K$, relative intensities somewhat similar to those given in Fig. 6 (a) will be obtained.

Herman, Hopfield, Hornbeck and Silverman[17] found this system in the CO-O_2 explosion flame and reported the (0-0), (1-1), (2-2), (3-3); (0-1), (1-2) and (2-3) bands. No quantitative data concerning the temperature and intensities are found in their paper, but we are able to estimate the rotational temperature to be about 2200°K from the microphotometer curve which they have given in their paper.

No inconsistency with the present results will be found, namely, if the (2-3) band is observable at 2200°K, other bands that is, the (0-0), (1-1), (2-2), (3-3), (2-1), (3-2), (1-0), (1-2) and the (0-1) should also be observed. But they did not report the (3-2), (2-1) and (1-0) bands, the reason for this probably being that these bands lie approximately at 7059Å, 6969Å and 6883Å repsectively, where the sensitivity of the photographic plate used is poor.

We have discussed the above results from various experiments which have been reported up to the present time. We have seen that these results may be explained without marked inconsistency by the theoretical results from the assumption that the thermal distribution of the upper state of the oxygen molecule is attained before the excited molecule emits the atmospheric bands.

15) L. M. Branscomb: Phys. Rev., **86** (1952) 258.
16) G. Kvifte: Nature **168** (1951) 741.
17) R. C. Herman, H. S. Hopfield, G. A. Hornbeck and S. Silverman: Journ. Chem. Phys., **17** (1949) 220.

According to these conclusions, the unreported bands such as the (1–0), (2–1) and (3–2) might be found if they are photographed under very long exposures so long as they were not interfered by strong lines, by fogging of the photographic plate, or by stray radiation. Observation will be easier if a light source is obtained of higher temperature, emiting atmospheric oxygen bands. It should be most interesting to see developments along these lines in the study of the atmospheric bands.

IV. Summary

In a previous experiment, the author obtained the atmospheric oxygen bands in emission. Afterwards, the relative intensity of the (0–0) and the (1–1) bands was measured using the spectrogram obtained previously.

For the intensity measurement, a simple method of photographic spectral photometry was adopted in which no intensity marks were used for photographic plate calibration, and the procedures are described in detail.

Using the theoretically obtained values of the overlap integrals for these bands and the measured intensity ratio of the (0–0) and the (1–1) bands, we obtained the so-called vibrational temperature. On the other hand, the rotational temperature was measured from the intensity distribution of the rotational lines in the (0–0) bands. These two temperatures agreed closely within experimental error.

Accordingly, it will be concluded that the excited oxygen molecules will be in thermal distribution before they emit the atmospheric bands.

On the basis of this conclusion, we calculated the relative intensities of many bands as measured against the (0–0) bands, for the temperature range 400°K～5000°K, and the results were represented graphically.

The results of experiments on the emission of the atmospheric bands which have been reported up to the present time are discussed on the basis of the present results. These results may be explained fairly well without marked inconsistency.

In conclusion the author wishes to express his sincere gratitude to Prof. Yoshio Fujioka for his kind encouragement and discussions throughout this work.

The Absorption Spectrum of Nitric Oxide in the Far-Ultraviolet Region

Miss Midori UEDA

Institute for Optical Research, Tokyo University of Education

(Received Sep. 30, 1954)

The absorption spectrum of nitric oxide was photographed under various pressures in the far ultraviolet region (1800 A–1300 A), using a 3-meter grazing incidence vacuum spectrograph. The recently found states, i.e. the $E^2\Sigma$, B' and B'' were reinvestigated. Vibrational levels of the $E^2\Sigma$ were confirmed up to $v'=5$ and a formula obtained that conformed with their heads. In order to analyse the pairs of heads that presented aspects similar to the β′-system, a new interpretation of the β″ and an extension of the β′-progression is proposed. A progression, which the author named S, with vibrational constants and an appearance of the head closely resembling the β-system is newly analyzed. A few other progressions are also listed as tentative proposals.

1. Introduction

Since Leifson's[1] pioneer work many reports have been published on the study of the emission and absorption spectra of NO, which have confirmed the existence of the $X^2\Pi$, $A^2\Sigma^+$, $B^2\Pi$, $C^2\Sigma$, $D^2\Sigma^+$ and $E^2\Sigma^+$ electronic states. But there still remain many unanalyzed bands in the emission and absorption spectrum.

Recently Sutcliffe and Walsh[2] have considered the three bands shaded toward the red in the absorption spectrum at 1708 A, 1688 A and 1676 A to be the (14—0), (15—0) and (16—0) of the β-progression. They further suggested that the (4—0) band of the δ-system might be the band which has the four strong heads near 1623 A. This interpretation seems to be plausible at first sight, but upon closer scrutiny several questionable points are revealed, which the author should like to point out in connection with the present study.

Very recently several new electronic states with high excitation energy have been reported by some authors[3)-8)]. As a result of the rotational analysis of

1) S. W. Leifson: Astrophys. Jour. **63** (1926) 73.
2) L. H. Sutcliffe and A. D. Walsh: Proc. Phys. Soc. **A66** (1953) 209.
3) M. W. Feast: Can. Jour. Res. **A28** (1950) 488.
4) P. Baer and E. Miesher: Helv. Phys. Acta. **24** (1951) 331.
5) Y. Tanaka, M. Seya and Mori: Science of Light **1** (1951) 80, J. Chem. Phys. **19** (1951), 979.
6) Y. Tanaka and T. Sai: Science of Light **1** (1951) 85.
7) M. Ogawa: Science of Light **2** (1953) 87.
8) Y. Tanaka: J. Chem. Phys. **21** (1953) 788.

emission bands around 6000 A, Feast discovered a new electronic state $E^2\Sigma^+$, which was also found by Tanaka, Seya and Mori[5] in the absorption spectrum and was named the A-progression. This progression ($E^2\Sigma - X^2\Pi$) shall hereafter be called the γ'-progression, to indicate the similarity of its appearance and vibrational constants to the γ-system. Though in emission the vibrational levels $v'=0$, 1 and 2 only of the $E^2\Sigma$ have been found[3], those up to $v'=5$ have been confirmed in the absorption spectrum, and a formula for the head applicable even to those high levels is here presented.

There are also some other new electronic states. One of them was found in emission by Miescher and Baer[4] as the upper state of the β'-system, and in absorption by Tanaka, Seya and Mori[5] as the upper state of the B-progression. The transition from this state to the $B^2\Pi$ was also observed in the near infrared by Ogawa[7]. In the emission spectrum the vibrational levels of this state has been confirmed only up to $v'=3$, but in the absorption there are several bands whose appearance is quite similar to the β'-system. The transition from the upper level of one of these bands to the $X^2\Pi$ and $B^2\Pi$ was observed by Tanaka[8] and Ogawa[7] respectively. Tanaka[8] has also proposed a new electronic state which closely resembles the upper states of the β'-system in the far ultraviolet region. An interpretation of these states is here presented as a result of observation and consideration by the author regarding the present spectrum.

One of the main purposes of the present work has been to attempt an analysis in the region 1500 A–1300 A, where many bands remain unanalyzed, but the result was the establishment of only one progression, which the author named the *S*-progression. With regard to several other systems to which a tentative analysis was obtained, a table is presented listing them, which we thought might possibly be of some reference value in future studies of the structure of the NO molecule.

2. Experiments

A grazing incident vacuum spectrograph with a 3-meter concave grating was used and a Lyman continuum was employed as light source. To produce nitric oxide gas $NaNO_3$ (64 gr.) and KI (38 gr.) were mixed and dissolved in water (225 gr.), which was then dropped onto concentrated sulphuric acid. The gas was used after being left a whole day to dry in a flask containing P_2O_5. During exposure the NO gas was controlled so as to form a steady flow of gas through the body of the spectrograph. This procedure was necessary in order to avoid the effect of impurities, because as the exposure time was comparatively long, there was some possibility of gas decomposition. Spectrograms were taken under

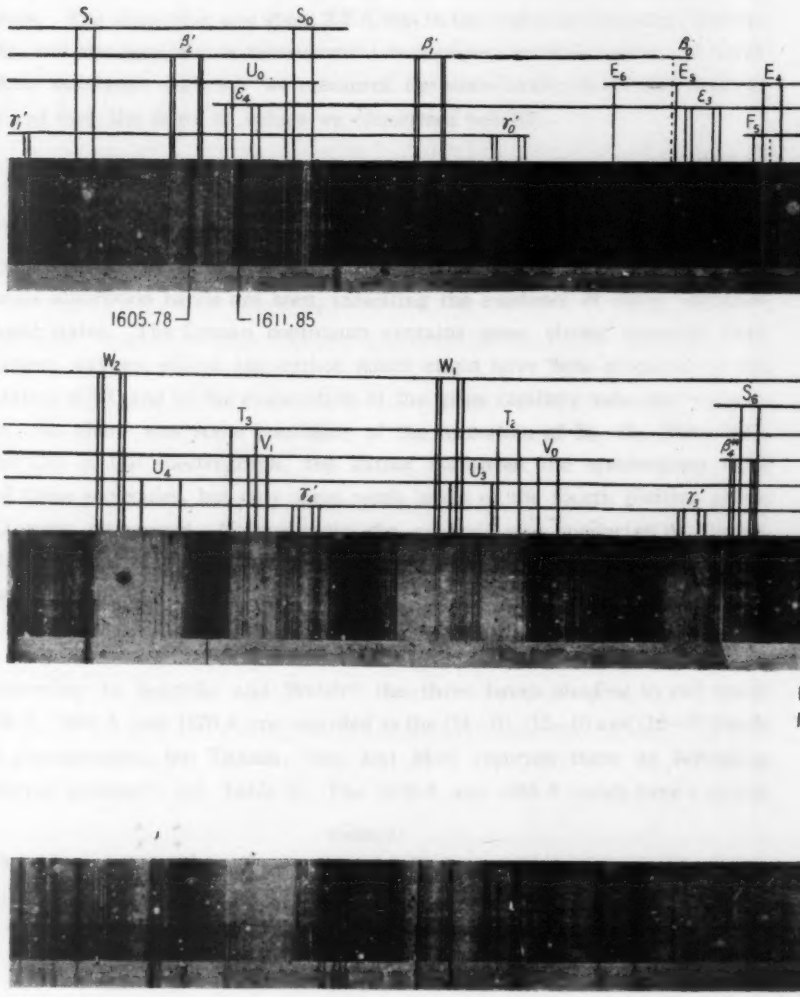

Plate 1. The Ab

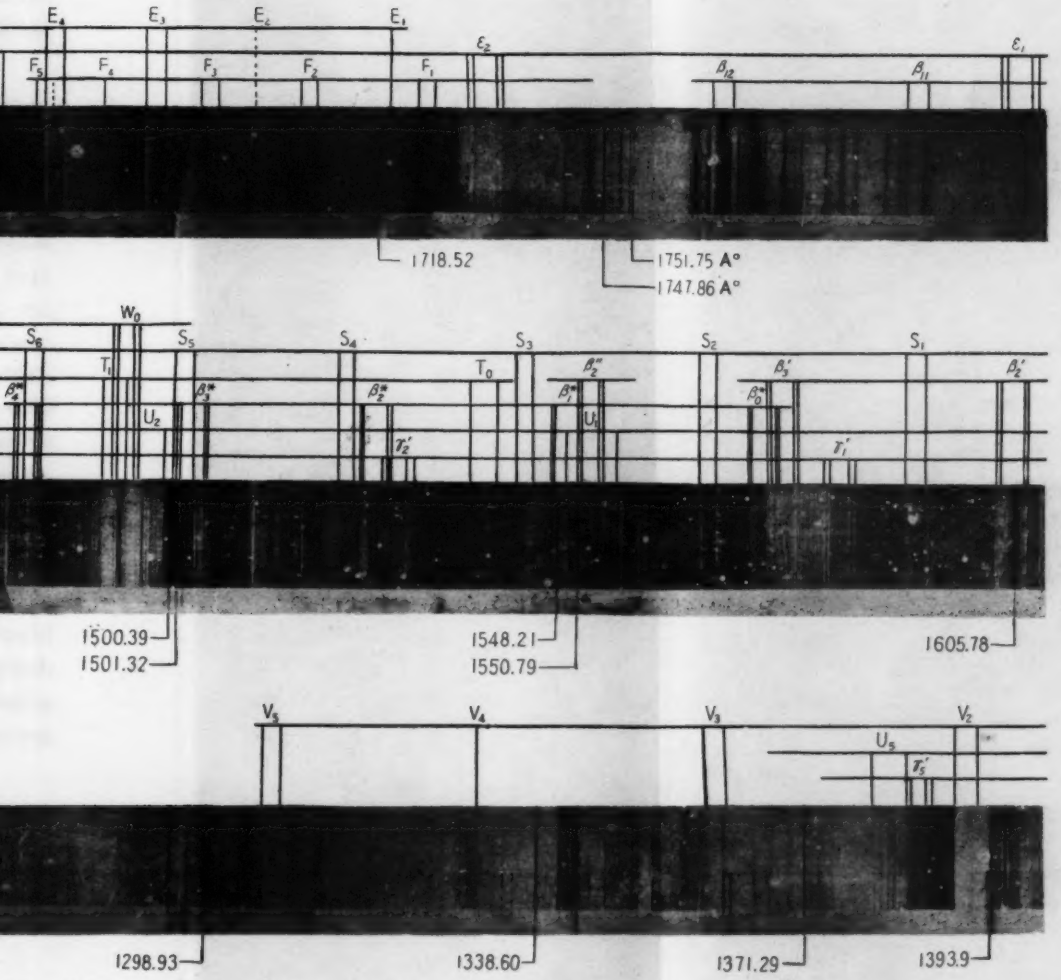

The Absorption Spectrum of Nitric Oxide.

various pressures between 0.1–0.5 mm Hg with Schumann plates prepared by ourselves. The dispersion was about 2.2 A/mm in the region investigated (1800 A–1300 A), and the accuracy of measurement was of the order of cm^{-1}. In order to obtain maximum accuracy we measured the same heads on several different plates and took the mean of values we considered reliable.

3. Results and Discussion

The best parts of the newly photographed spectrograms were picked out and put together to form the complete spectrum shown in Plate I, in which numerous absorption bands are seen, indicating the existence of many unknown electronic states. The Lyman continuum contains some strong emission lines of nitrogen, oxygen, silicon and carbon which might have been produced by the dissociation of NO and by the evaporation of the glass capillary tube and vacuum grease. As there was some possibility of the formation of N_2, O_2, NO_2, N_2O, CO and CO_2 in the spectrograph, the author compared the spectrogram with that of these molecules, but only some weak heads of the fourth positive group of CO were recognized. Consequently the analysis was conducted on the assumption that all of the absorption bands belonged to NO except the fourth positive group of CO.

(*a*) *Sutcliffe and Walsh's β-progression*

According to Sutcliffe and Walsh[3] the three bands shading to red found at 1708 A, 1688 A and 1676 A are regarded as the (14—0), (15—0) and (16—0) bands of the β-progression, but Tanaka, Seya and Mori reported them as belonging to different systems[5]. (cf. Table 1) The 1676 A and 1688 A bands have a strong

Table 1.

Sutcliffe and Walsh[3]		Tanaka, Seya and Mori[5]		Present Measurement	
v'	ν	Name	ν	ν	λ
n	58462	F_2	58466.2	$59469._8$	1710.2_3
	558		534.3	$542._6$	1708.1_8
$n+1$	59135	E_3	59130.7	$59133._8$	1691.0_8
	228		204.2	$214._7$	1688.7_7
$n+2$	59583	E_4	59564.9	$59574._5$	1678.5_7
	663		642.1	$651._6$	76.4_0

intensity and manifest a rotational structure similar to each other, so that these two bands seem to belong to the same system, but the intensity of the 1708 A band is very weak and would appear to have a different structure. The distance between the two R heads coincides with that of the β-system. Although it is very desirable to regard them as the extension of the β-progression, the irregu-

larities which result from this point of view are too great to be attributed merely to the perturbation between $B^3\Pi$ and C, D and $E^1\Sigma$. Further, according to this interpretation the dissociation limit of the $B^3\Pi$ must be lower than $N(^2D)+O(^3P)$. From these considerations it is difficult to regard them as an extension of the β-system. It seems worth while to note that though the 1676 A and 1688 A bands are the clearest and strongest absorption bands in the region 1750–1450 A, in emission they do not seem to make their appearance, at least not so strongly[6]. Further study is called for to investigate the relationship between the intensity of these bands and the gas pressure in a far wider range.

(*b*) *The γ'-Progression*

Each band consists of double-double heads shading to violet. The distance

Table 2. γ'-Progression: Violet shade.

v	Int.	λ obs.	ν obs.	ν calculated from Feast's data	Remarks
0	2	1647.0_5	$60714._5$		
	2	46.3_4	$740._9$		
	2	43.6_5	$840._3$		
	2	43.1_9	$860._7$	60863	
1	3	1585.8_8	$63057._3$		display fine rotational structure
	3	85.1_8	$085._5$		
	4	82.7_1	$182._3$		overlap other band
	4	82.1_5	$205._1$	63205	
2	3	1529.9_5	$65361._6$		
	4	29.2_6	$390._9$		overlap other bands
	3	26.9_8	$489._9$		
	3	26.2_6	$519._6$	65515	
3	5	1478.1_8	$67650._6$		
	5	77.5_5	$679._6$		display no rotational structure and diffuse
	5	75.3_5	$780._5$		
	5	74.8_3	$804._4$	67793	
4	2	1430.8_8	$69887._3$		
	3	30.2_4	$918._3$		
	2	28.2_5	$70015._9$		
	3	27.7_3	$41._1$	70041	
5	2	1386.6_7	$72115._3$		
	3	86.0_1	$149._4$		
	2	84.1_7	$245._4$		
	4	83.6_4	$273._5$	72255	overlap $U(3-0)$ head

between the Q-heads is about 120 cm^{-1}, which is roughly equal to the doublet splitting of $X^2\Pi$. Though all the P-heads appear to be somewhat thick lines, in some bands a fine rotational structure is displayed following the Q-head. In Table 2 are listed the wavelengths and wave numbers. The ΔG curve is shown in Fig. 1, which shows that the vibrational level of $v'=3$ is shifted upwards by about 10 cm^{-1}. The cause of this perturbation may be found in the level appearing in the longer wavelength side of the $\gamma'(3-0)$ and having a structure very similar to it. This level may be one of the higher vibrational levels of $D^2\Sigma$. It seems worth while to note that the $\gamma'(3-0)$ band is rather diffuse and shows no rotational structure, which indicates the possibility of predissociation. The (4—0) band seems to be in a normal position, with heads featuring the usual characteristics of this progression, although its intensity is much weaker than the (3—0). The (5—0) band clearly seems to belong to this system, but it lies about 20 cm^{-1} higher than the position calculated from the vibrational constants of Feast. There must exist some perturbation due to one level or another. Eliminating the effect of perturbation, the following formula for the regular position of the Q-heads is obtained.

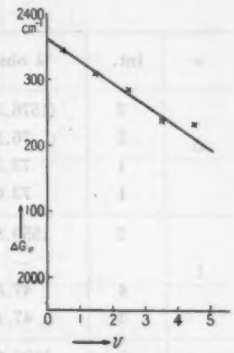

Fig. 1. γ'-progression

$$\nu_{v,0}=\begin{cases}59555.51+2378.53(v+\frac{1}{2})-17.10(v+\frac{1}{2})^2+0.083(v+\frac{1}{2})^3\\ 59675.61\end{cases}$$

The distance between the P and the Q heads calculated with the values of B_v'[3] and B_0''[9),10)] of the $E^2\Sigma$ and $X^2\Pi$ respectively is about 10 cm^{-1} less than the results of the present measurements. This amount far exceeds the order of error entering into measurement of the relative positions of the heads. In every case it is certain that the difference between the heads is larger between P_2 and Q_2 than between P_1 and Q_1 for all bands not only in this progression but also in the γ-and δ-systems. This should indicate that the B_0'' value of the $X^2\Pi_{\frac{3}{2}}$ is larger than that of the $X^2\Pi_{\frac{1}{2}}$.

(c) *The β'-System*

With respect to the β'-system the wave numbers obtained this time are in good agreement with those already reported[2),4)-8)] (cf. Table 4), though the (0—0) band is not clear due to overlapping. The bands for $v'=1$, 2, 3 are so clear that

9) R. H. Gillete and E. H. Eyster: Phys. Rev. **56** (1939) 1113.
10) J. J. Gallagher, F. D. Bedark and C. M. Thomson: Phys. Rev. **93** (1954) 729.

rotational analysis would appear to be possible. Each band has double-double heads shading to red and the separation of the two Q-heads is 120~125 cm^{-1}. The distance between the R- and the Q-heads is around 15 cm^{-1}, the R-heads being quite intense and appearing like lines. Several more pairs of heads are seen possessing appearances with similar characteristics. These are listed in

Table 3. β^*-Progression: Red shade.

v	Int.	λ obs.	ν obs.	ν observed by others	Remarks
0	2	(1576.3_7)	$(63436._8)$		overlap rotational line of $\beta'(v'=3)$ band
	2	$(\ 76.2_1)$	$(\ 443._6)$		
	1	73.2_8	$561._5$		
	1	73.0_1	$572._3$		
1	3	1550.8_6	$64480._3$		
		—	—		overlap atomic C line
	4	47.8_0	$607._6$		
	3	47.4_5	$622._5$		
2	3	1526.6_9	$65502._5$	$65507.6^{7)}$	
	3	26.5_7	$519._6$	$65512.4^{8)}$	
	4	23.7_5	$627._6$	$65630.2^{7)}$	
	4	23.5_5	$636._1$	$65635.8^{8)}$	
3	4	1504.4_1	$66471._1$		
	4	04.1_6	$482._3$		overlap other bands
	5	01.5_8	$596._7$		
		—	—		
4	3	1484.2_1	$67375._8$		
	3	83.9_6	$387._3$		
	3	81.4_6	$501._0$		
	3	81.1_6	$514._5$		
β_2''	2	1553.9_5	$64352._1$		
	2	53.6_4	$364._9$	$64361.3^{8)}$	
	3	50.8_6	$480._3$	$64483.7^{8)}$	
		—	—		overlap atomic C line

Table 3 under the name of β^*-progression. Fig. 2 shows the ΔG curve of the β^*-progression. It is smooth though $\Delta G_{\frac{1}{2}}$ seems slightly smaller than might be normally expected, which shows the possibility of a shift in the $v'=0$ level. Between the (0—0) and the (1—0) bands of this progression, there is another band possessing the same appearance as the β'-progression, though not so intense. This band seems to coincide with the $\beta''(2-0)$ band of Tanaka[5].

Table 4. β'-Progression: Red shade.

v	Int.	λ obs.	ν obs.	observed by others	Remarks
0	2				
	2	1669.1$_5$	59910.$_7$	59906.0[7]	overlap other bands
	3d				
	3d	65.7$_5$	60031.$_8$	60034.2[7]	
1	2	1637.1$_7$	61081.$_1$		
	2	36.7$_9$	095.$_3$		
	3	33.7$_9$	207.$_4$	61205.9[4], 61211[3]	
	2	33.4$_8$	219.$_8$	228[2]	
2	3	1606.9$_3$	62230.$_5$		
	3	06.5$_9$	244.$_6$		
	3	03.7$_1$	355.$_4$	62355.8[4], 62360[3]	
	3	03.3$_9$	367.$_9$	375[2]	
3	3	1578.5$_9$	63348.$_1$		
	3	78.1$_9$	363.$_9$		
	3	75.4$_1$	475.$_5$	63474.7[4], 62476[2]	
	3	75.1$_1$	487.$_6$	488[2]	
4	3	1550.8$_9$	64480.$_3$		
	—	—	—		overlap atomic C line
	4	47.8$_9$	607.$_9$		
	3	47.4$_5$	622.$_5$		
5	3	1526.6$_8$	65502.$_5$	65507.6[7]	
	3	26.5$_7$	519.$_0$	65512.4[8]	
	4	23.7$_5$	627.$_6$	65630.2[7]	
	4	23.5$_5$	636.$_1$	65635.8[8]	
6	4	1504.4$_1$	66471.$_1$		
	4	04.1$_6$	482.$_2$		overlap other heads
	5	01.5$_8$	596.$_7$		
7	3	1484.2$_1$	67375.$_8$		
	3	83.9$_8$	387.$_3$		
	3	81.4$_6$	501.$_0$		
	3	81.1$_8$	514.$_6$		

At the expected position of the (4−0) band of the β'-progression there appear two heads at 64427.$_1$ and 64545.$_1$ cm^{-1}. They are very close to what have been regarded as the heads of the B_5 by Tanaka, Seya and Mori[5]. However as the result of scrutiny of the new spectrograms its heads have been found to appear

quite different from other members. The head on the shorter side shades to violet and that of the longer side, which probably coincides with the head at 64429 cm^{-1} as reported by Leifson[1] appears as a diffuse line.

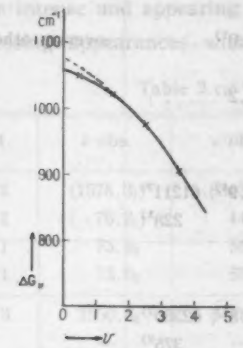

Fig. 2. β*-Progression

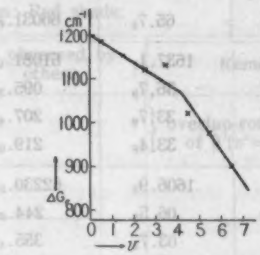

Fig. 3. β'-Progression

It may be possible to consider the β^*-progression as the continuation of the β' and the (1—0), (2—0), (3—0) and (4—0) bands of the β^*-progression should then correspond to the (4—0), (5—0), (6—0) and (7—0) bands respectively of the β'-progression. In this case however the ΔG curve becomes very irregular: $\Delta G_{3\frac{1}{2}}$ comes to be actually larger than $\Delta G_{2\frac{1}{2}}$, as may seen from the curve in Fig. 3. There must be found some reason to explain the great perturbation of the vibrational level $v'=4$. Although the levels $v'=3$ of the β' and $v'=0$ of the β^* lie fairly close to each other, no great perturbation is observed. Therefore a crossing of the potential curves at the $v'=4$ level of the β' state might be expected, against which the non-crossing rule of potential curves of the same species applied, which should explain this irregularity. It is possible that as a consequence of this rule, the potential curve transfers from that of the original β'-state to another curve at a height below the $v'=4$ level, This may be the reason for the slope of the ΔG curve changing abruptly at $v'=4$. In the case above considered, there should exist another progression whose vibrational constants are close to those of the original β'-state and which probably includes the heads around 1550 A[8], which in spite of their characteristics, could not be included in this extension of the β'-progression. The calculated dissociation limit of this state, which owes its potential curve to the non-crossing rule, does exceed $N(^2D)+O(^3P)$, but it is lower than $N(^2P)+O(^3P)$, when $D(NO)=6.48$ eV is adopted. Taking into account that each band consists of four heads this state may be imagined to belong to the $^2\Delta$-type, which dissociates to $N(^2D)+O(^3P)$.

(*d*) *The S-Progression*

This is a newly analysed progression, each member of which has an appearance closely resembling the β-system, that is, each band consists of double heads shading to red, the separation between them being about 80 cm^{-1}. Its

Table 5. *S*-Progression: Red shade.

v'	Int.	λ obs.	ν obs.	Remarks
0	3	1620.9_0	$61694._1$	overlap other band
	1	18.6_7	$779._2$	
1	1	1594.0_9	$62735._1$	
	1	91.8_7	$819._2$	
2	2.5	1568.8_9	$63743._9$	clearly display rotational structure
	2.5	66.7_0	$828._3$	
3	2.5	1544.9_8	$64716._7$	overlap other band
	2.5	43.1_7	$801._8$	
4	1	—	—	
	2	1521.4_9	$65725._2$	
5	2	1502.6_8	$66547._5$	
	2	00.8_1	$630._5$	
6	2	1483.5_2	$67407._1$	overlap β_4* band
	2	81.7_3	$488._5$	

upper state must be the $^1\Pi_r$ whose vibrational constants are very close to those of the $B^1\Pi_r$. None of the members of this progression are very intense, and some of them appear only when the gas pressure is comparatively high. The (2—0) band is superimposed on no other band and clearly shows its rotational structure. The wavelengths and wave numbers of all the heads are listed in Table 5. In Fig. 4 is drawn the ΔG-curve which indicates that the vibrational level $v=4$ is shifted downwards by about 5~6 cm^{-1} on account of perturbation by some level or other. Eliminating the effect of this perturbation the formula to express the wave number of the heads is obtained as follows.

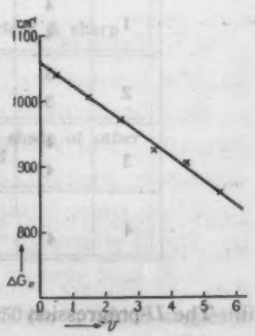

Fig. 4. *S*-progression

$$\nu_{v,0}=\begin{cases}61163.18+1069.4(v+\frac{1}{2})-14.10(v+\frac{1}{2})^3-0.44(v+\frac{1}{2})^5\\ 61248.28\end{cases}$$

Here it is assumed that 61694.$_1$ and 61779.$_2$ cm^{-1} are equal to $\nu_{0,0}$. However the pair of heads appearing on the longest wavelength side of this progression cannot possibly represent the (0−0) band, since the shape and position (except height) of the potential curve of this system seem close to that of the $B^2\Pi_r$, and in the absorption spectrum of the $B^2\Pi \leftarrow X^2\Pi$ the (0−0), (1−0) and (2−0) bands do not appear unless a much higher pressure is used than in the present experiment. The dissociation limit of the upper state may be $N(^3P)+O(^3P)$, from which the $^2\Pi$ state can be obtained with the use of the Wigner-Witmer correlation rule.

(e) *Other Progression*

There still remain a few progressions other than those discussed above, of which mention will be made in spite of some doubtfulness.

i) The *T*-progression

Each band of this progression consists of two heads whose separation is almost equal to that of the $X^2\Pi$. In none of the bands is the rotational structure distinct. The wavelengths and wave numbers of heads are listed in Table 6.

Table 6. *T*-Progression.

v	Int.	λ obs.	ν obs.	Remarks
0	1	1540.6$_5$	64907.$_8$	violet shade
	1	37.7$_8$	5028.$_7$	
1	4	1494.8$_4$	66896.$_7$	red shade
	4	92.0$_9$	7021.$_4$	overlap strong band
2	3	1455.7$_2$	68694.$_7$	red shade
	3	53.1$_4$	8816.$_4$	
3	4	1422.6$_8$	70290.$_6$	red shade
	4	20.2$_3$	0411.$_3$	
4	4	—	—	red shade
		1391.7$_8$	71849.$_9$	in the shade of strong band

ii) The *U*-progression

All heads of this progression are so sharp and intense as to be clearly recognized even in the very crowded region of much overlapping. Each band consists of two heads shading into violet and the rotational structure is not

Table 7. *U*-Progression: Violet shade.

v	Int.	λ obs.	ν obs.	Remarks
0	3	1617.4_7	$61825._1$	
	4	11.0_1	$2072._9$	overlap one of $s(4-0)$ heads
1	2	1555.5_2	$64287._1$	
	3	49.3_1	$4545._1$	
2	5	1499.5_3	$66687._8$	
	5	93.7_8	$6944._4$	
3	5	—	—	in the shade of the other strong band
	4	1447.2_1	$69098._3$	
4	3	1414.1_8	$70712._6$	
	3	09.2_3	$0960._6$	
5	3	1383.6_4	$72273._1$	overlap one of $\gamma'(5-0)$ heads

Table 8. *V*-Progression: Red shade.

v	Int.	λ obs.	ν obs.	Remarks
0	3	1459.8_8	$68498._7$	
	2	57.5_2	$609._7$	
1	4	1424.6_4	$70193._3$	
	4	22.3_9	$304._2$	
2	5	1391.7_8	$71853._0$	
	5	89.4_8	$969._5$	very clear & sharp
3	4	1361.2_6	$73461._1$	
	4	59.1_3	$577._0$	
4	—	—	—	in the shade of other band
	4	1331.3_4	$75112._5$	
5	3	1307.9_8	$76455._0$	
	4	06.0_4	$570._8$	

distinct. The separation of the two heads is about 250 cm^{-1}, which suggests that the upper state of this transition is probably the inverted $^3\Pi$, whose separation is about 130 cm^{-1}. The wavelengths and term values of the heads are listed in Table 7.

Table 9. *W*-Progression: Violet shade.

v	Int.	λ obs.	ν obs.	Remarks
0	5	1496.5_2	$66821._7$	
	5	96.0_2	$844._0$	
	5	93.7_2	$946._9$	
	5	93.3_0	$965._8$	
1	4	1448.0_3	$69060._0$	overlap other bands
	3	47.5_8	$080._8$	
	3	45.2_7	$191._2$	
	3	44.7_7	$215._2$	
2	4	1406.3_7	$71105._0$	
	4	06.0_8	$120._7$	
	4	03.9_1	$229._6$	
	4	03.6_4	$243._3$	

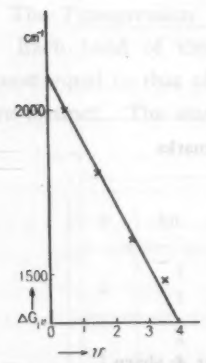

Fig. 5. *T*-progression

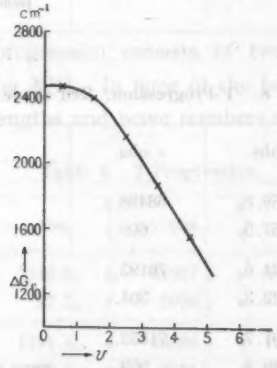

Fig. 6. *U*-progression

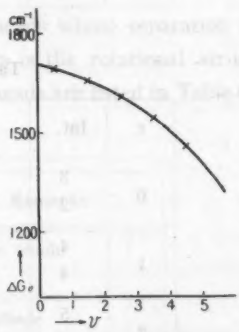

Fig. 7. *V*-progression

iii) The *V*-progression*

Each band consists of two heads shading to red, whose separation is about 110 cm^{-1}. Term values and wavelengths are listed in Table 8. No rotational structure is displayed, although each band extends over a considerably wide range with strong intensity.

iv) The *W*-progression**

Each band consists of double-double heads, the difference between two *Q*-heads being almost equal to the doublet separation of the ground state. All

* The *V*-progression includes some heads which have been picked up as the members of the *C*-progression by Tanaka, Seya and Mori[5].

** The *W*-progression is merely the reinvestigation of what have been reported by Tanaka, Seya and Mori[5] under the name of the *D*-progression.

heads clearly shade to violet with considerable intensity and appear almost as a line. The appearence of the head reveals some similarity to that of the δ-system.

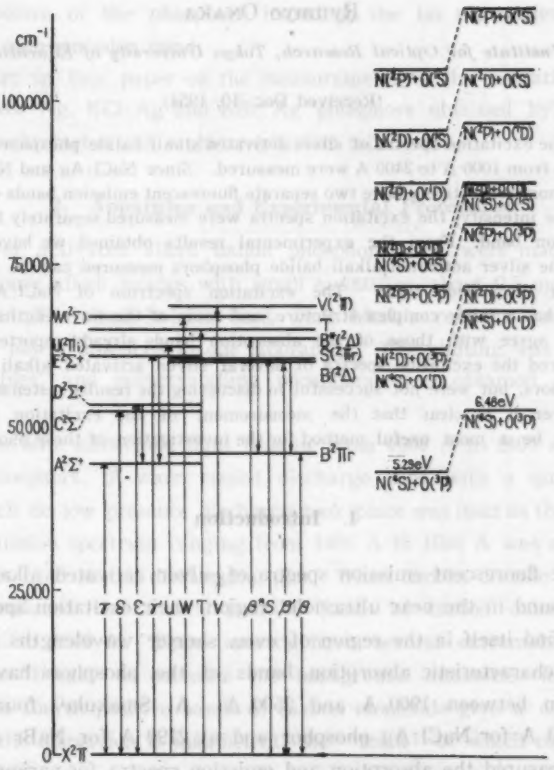

Fig. 8. Energy level diagram of NO molecule.

Acknowledgement

The author wishes to express her sincere thanks to Prof. Y. Fujioka, Dean of the Institute for Optical Research, for his valuable advice and encouragement. Much appreciation is also due to Dr. M. Seya, under whose guidance this work has been carried out. The author is further indebted to Messrs. M. Ogawa and K. Mori for their kind help and discussion.

This research was carried out with the generous financial support of the Ministry of Education.

Excitation Spectra of Silver Activated Alkali Halide Phosphors

Ryumyo ONAKA

Institute for Optical Research, Tokyo University of Education

(Received Dec. 10, 1954)

The excitation spectra of silver activated alkali halide phosphors in the region from 1000 A to 2400 A were measured. Since NaCl:Ag and NaBr:Ag phosphors respectively have two separate fluorescent emission bands of comparable intensity, the excitation spectra were measured separately for each emission band. From the experimental results obtained we have found that the silver activated alkali halide phosphors measured can be excited by far ultraviolet light. The excitation spectrum of NaCl:Ag phosphor has a fairly complex structure, and some of the wavelengths of the peaks agree with those of the absorption bands already reported. We measured the excitation spectra of several silver activated alkali halide phosphors, but were not successful in discussing the results systematically. However it is clear that the measurement of the excitation spectra should be a most useful method for the investigation of these phosphors.

1. Introduction

Since the fluorescent emission spectra of silver activated alkali halide phosphors are found in the near ultraviolet region, their excitation spectra must be expected to find itself in the region of even shorter wavelengths. And in fact some of the characteristic absorption bands of the phosphors have been found in the region between 1900 Å and 2500 A. A. Smakula[1] found absorption bands at 2100 A for NaCl:Ag phosphor and at 2190 A for NaBr:Ag phosphor. M. Kato[2] measured the absorption and emission spectra for various alkali halide phosphors by means of two quartz spectrographs and a photon counter. He found that the luminescence of alkali halide phosphors is to be attributed to the impurity centers. Recently, H. W. Etzel and J. H. Schulman[3] found three characteristic absorption bands each in the spectra of NaCl:Ag, NaBr:Ag, KCl:Ag and KBr:Ag. They also found that the silver activated alkali halide phosphors have two different centers; one attributable to the single, and the other to the paired silver ion.

All measurements above referred to were performed by means of quartz spectrographs, and it was therefore impossible to extend the measurements of

absorption spectra down to the far ultraviolet region in which there might still be some possibility of the silver activated alkali halide phosphors being excited. Furthermore, since there is more than one emission band, it is difficult to know the causal relation between the emission bands and the absorption bands merely from the absorption spectra. The key to this problem must be found in the excitation spectra of the phosphors including the far ultraviolet region to be obtained for each emission band.

We report in this paper on the measurements of the excitation spectra of NaCl:Ag, NaBr:Ag, KCl:Ag and KBr:Ag phosphors obtained by means of a vacuum monochrometer and a photomultiplier tube.

2. Apparatus and Experimental Procedures

The silver activated alkali halide phosphors used were made by melting mixtures of pure alkali halides with small quantities (about 0.5 mole percent) of silver halides. The alkali halides used were Merk's reagents, and the silver halides were newly produced in our laboratory. The melting was done in small quartz crucibles, and polycrystalline phosphors were obtained upon gradual cooling.

Monochromatic ultraviolet light ranging from 1000 A to 2400 A was used to excite the phosphors. A water cooled discharge tube with a quartz capillary through which dc low pressure discharge took place was used as the light source. A strong emission spectrum ranging from 1000 A to 1600 A was obtained when hydrogen was used as the discharging gas. When carbon dioxide was used the discharge produced the fourth positive bands of carbon monoxide ranging from 1300 A to 2500 A. These spectra have several extremely weak parts, which makes it easy to estimate the background intensities included in the spectra. The fourth positive bands of carbon monoxide give a comb-like spectrum when the dispersion is insufficient, the "teeth" of which comb are spaced 15~30 A apart.

The vacuum monochrometer[4] used contains a 20 cm concave grating which moves along the Rowland circle fixed against the body of the instrument. A sharply focused image of the entrance slit is, therefore, maintained at the exit slit for all desired wavelengths of monochromatic light. The dispersion near the exit slit is about 70 A/mm, and the scanning speed used was about 65 A/min. The slit widths were same for both the entrance and exit slits and were about 0.07 mm in most measurements.

The measuring apparatus is shown in Fig. 1. The monochromatic ultraviolet light passing through the exit slit illuminates the phosphor sample. The

samples are prepared by grinding the polycrystals in a quartz mortar and mixing it with a small quantity of pure ethylalcohol and then painting the paste onto a quartz plate mounted on a revolving table. Three samples and a standard phosphor may be mounted at the same time on this revolving table.

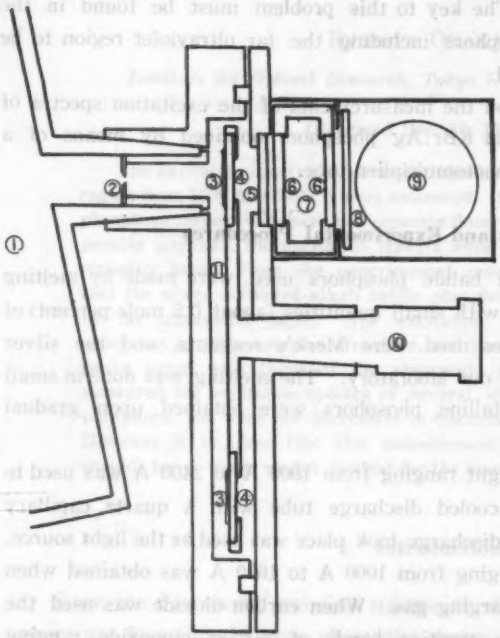

Fig. 1.
Measuring Apparatus.
1. Vacuum monochrometer.
2. Exit slit.
3. Phosphor samples.
4. Quartz plates.
5. Quartz window of the vacuum vessel.
6. Quartz windows of the liquid filter.
7. Filter solution.
8. UV 27 glass filter or ordinary glass plate.
9. 1P28 Photomultiplier tube.
10. Knob of the revolver.
11. Revolving table.

The secondary light from the phosphors is measured by a 1P28 photomultiplier tube after passing through suitable filters, and is recorded automatically by a Hokushin electronic recorder. The NaCl:Ag and NaBr:Ag phosphors each have two emission bands of comparative intensity. The shorter wavelength bands are in the region between 2200 A and 3000 A, and the longer ones between 3500 A and 4500 A in both cases. The shorter wavelength bands can therefore be eliminated by means of an ordinary glass plate. To eliminate the longer wavelength bands we used a $NiSO_4+CoSO_4$ liquid filter having quartz windows. The transmission of this filter is shown in Fig. 2.

In the case of the KCl:Ag and KBr:Ag phosphors single emission bands only were observed. Therefore the liquid filter was not used, and a glass filter (Matsuda UV 27) was inserted. Matsuda UV 27 glass filter cut off the light below 2200 A. The reason for this was that 1P28 photomultiplier tube is sensitive to light down to 1700 A, and there was a possibility of the primary radiation

in the fluorescent light being recorded when excitation by ultraviolet light longer than 1700 A was being measured.

Sodium salicylate was used as the standard phosphor. This is the most useful phosphor for heterochromatic photometry, since it has an almost constant fluorescent quantum yield extending over the wavelength range less than 1000 A to above 2300 A[5].

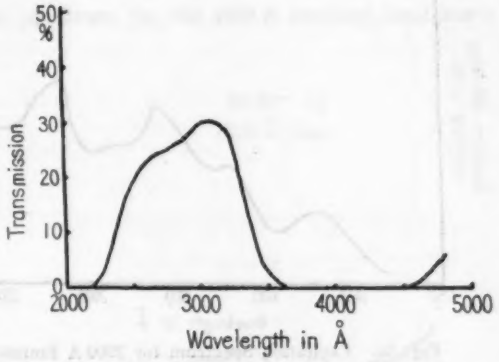

Fig. 2. Transmission of the $NiSO_4+CoSO_4$ Liquid Filter.

The recorded spectrum obtained by scanning the primary light represents the product of the fluorescent efficiency of the phosphor and the intensity of the primary radiation. Therefore, the spectrum of the intensity ratio between a recorded sample phosphor spectrum and a standard phosphor spectrum with constant quantum efficiency obtained would be none other than the excitation spectrum representing the quantum efficiency of the phosphor, if the same source of light is used. In our apparatus, changing the sample phosphors for the standard phosphor be accomplished merely by revolving the table on which the phosphors are mounted, and hence the recording of the spectra may be carried out with a minimum of variation in the measuring conditions.

3. Results and Discussions

NaCl:Ag

NaCl:Ag phosphor has two fluorescent emission bands of comparable intensity, whose maximum intensities are at 2500 A and at 4000 A. The excitation spectrum for the 2500 A emission band is shown in Fig. 3a, and that for the 4000 A emission band in Fig. 3b. These excitation spectra have features so different that we may reasonably conclude that the two emission bands issue from different centers.

The excitation spectrum for the 2500 A emission band has three distinct maxima at 1490 A, 1850 A and 2070 A, and two obscure maxima at 1690 A and at 1950 A. The excitation spectrum for the 4000 A emission band has five distinct maxima at 1510 A, 1770 A, 1910 A, 2100 A and 2300 A.

Etzel *et al*[3] reported that NaCl:Ag phosphor has three characteristic

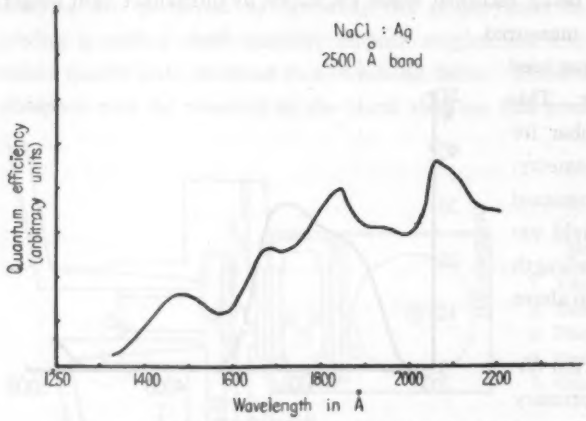

Fig. 3a. Excitation Spectrum for 2500 A Emission Band of NaCl:Ag Phosphor.

absorption bands at 2095 A, 2170 A and 2295 A, and that the 2170 A band absorption results in the emission of the 2500 A band and the 2295 A band absorption in the emission of the 4000 A band. The prominent maximum at 2300 A in the present excitation spectrum for the 4000 A emission band must correspond to the 2295 A absorption band.

The 1500 A peak and the 1580 A depression of the excitation spectra of NaCl:Ag phosphor would appear to be due to the absorption of the host crystal, since these have almost the same wavelengths in both excitation spectra, which agree with the absorption spectrum of NaCl measured by E. G. Schneider and H. M. O'Bryan[6].

It will be hasty to introduce further conclusions merely from the features of the excitation spectra until the absorption of the phosphor in the far ultraviolet region is made clear.

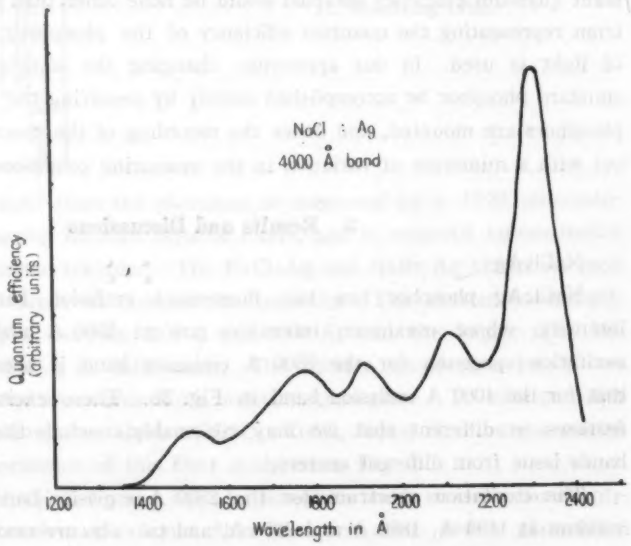

Fig. 3b. Excitation Spectrum for 4000 A Emission Band of NaCl:Ag Phosphor

NaBr:Ag

NaBr:Ag phosphor also has two emission bands at 2600 A and at 4000 A. The excitation spectra for the two emission bands are shown in Figs. 4a, and 4b respectively. The excitation spectrum for the 4000 A emission band has a simple hump around 2000 A. The fluorescent intensity of the 2600 A emission band was so weak that the structure of the excitation spectrum could not be clarified, though it seemed to have some similarities to the excitation spectrum for the 2500 A emission band of NaCl:Ag phosphor.

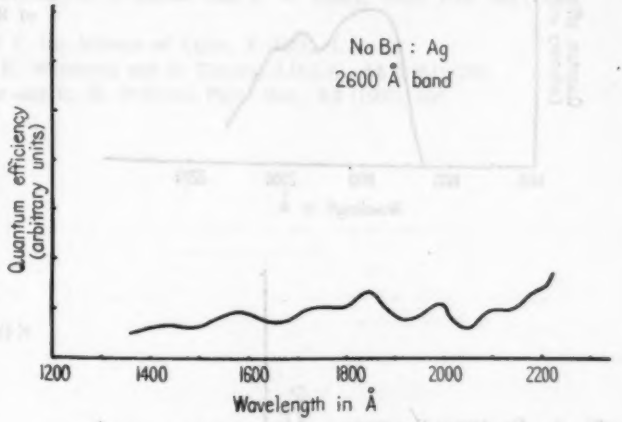

Fig. 4 a. Excitation Spectrum for 2600 A Emission Band of NaBr:Ag Phosphor.

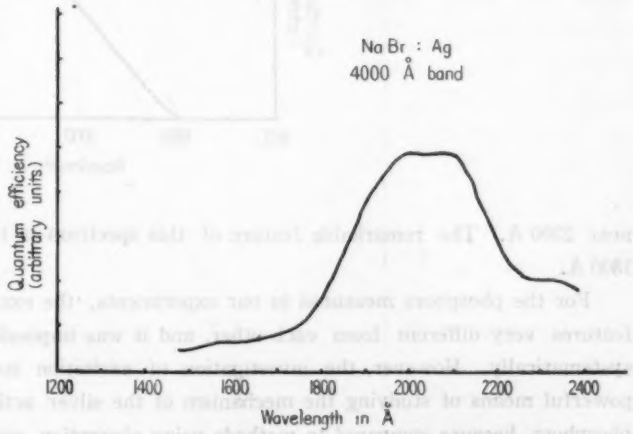

Fig. 4 b. Excitation Spectrum for 4000 A Emission Band of NaBr:Ag Phosphor.

KCl:Ag

KCl:Ag phosphor has a strong emission band at 2700 A. The excitation spectrum is shown in Fig. 5. This has a comparatively simple structure, and has three weak maxima at 1780 A, 1940 A and 2000 A.

KBr:Ag

The excitation spectrum of KBr:Ag phosphor has its intensity maximum

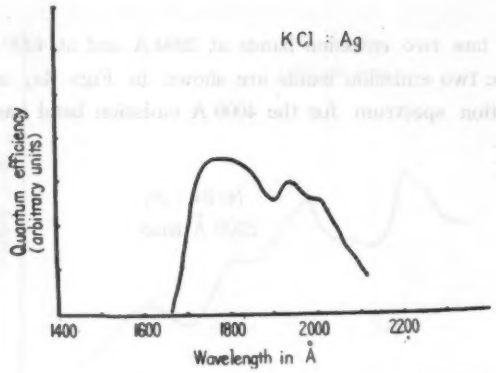

Fig. 5. Excitation Spectrum of KCl:Ag Phosphor.

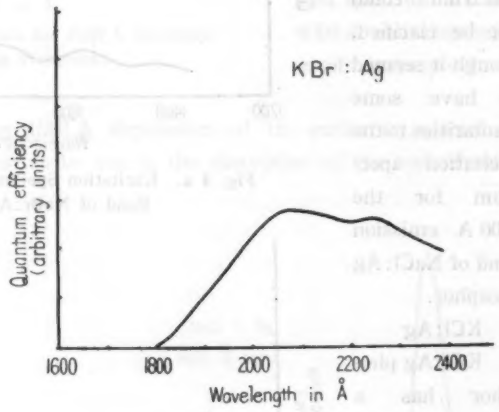

Fig. 6. Excitation Spectrum of KBr:Ag Phosphor

near 2300 A. The remarkable feature of this spectrum is the sharp cut-off at 1800 A.

For the phosphors measured in our experiments, the excitation spectra had features very different from each other, and it was impossible to discuss then systematically. However, the investigation of excitation spectra would be a powerful means of studying the mechanism of the silver activated alkali halide phosphors, because compared to methods using absorption spectra, the investigation of the behaviour of the phosphors by excitation spectra is much easier in the far ultraviolet region, where the host crystals have their strong absorption which renders the measurement of absorption spectra impractical.

The author wishes to express his most sincere thanks to Professor Yoshio Fujioka for his kind suggestions and encouragement upon the present work.

References

1) A. Smakula, ZS. f. Phys., **45** (1927), 1.
2) M. Kato, Sc. Pap. I.P.C.R., **41** (1943), 113.
3) H. W. Etzel and J. H. Schulman, J. Chem. Phys., **22** (1954) 1549; H. W. Etzel, J. H. Schulman, R. J. Ginther and E. W. Claffy, Phys. Rev., **85** (1952), 1063.
4) Y. Fujioka and R. Ito, Science of Light, **1** (1951), 1.
5) F. S. Johnson, K. Watanabe and R. Tousey, J.O.S.A., **41** (1951), 702.
6) E. G. Schneider and H. M. O'Bryan, Phys. Rev., **51** (1937), 293.